UC San Diego

UC San Diego Electronic Theses and Dissertations

Title

Electronic transport in nanoscale structures

Permalink

https://escholarship.org/uc/item/6cz2p6bc

Author

Lagerqvist, Johan

Publication Date

2006

Peer reviewed|Thesis/dissertation

eScholarship.org Powered by the California Digital Library
University of California

UNIVERSITY OF CALIFORNIA, SAN DIEGO

Electronic Transport in Nanoscale Structures

A dissertation submitted in partial satisfaction of the
requirements for the degree
Doctor of Philosophy

in

Physics

by

Johan Lagerqvist

Committee in charge:

Professor Massimiliano Di Ventra, Chair
Professor Prabhakar Bandaru
Professor Dimitri Basov
Professor Clifford Kubiak
Professor Lu Sham

2006

Copyright
Johan Lagerqvist, 2006
All rights reserved.

The dissertation of Johan Lagerqvist is approved, and it is acceptable in quality and form for publication on microfilm:

_____

_____

_____

_____

_____

Chair

University of California, San Diego

2006

To my Mother

TABLE OF CONTENTS

Signature Page . . . iii

Dedication . . . iv

Table of Contents . . . v

List of Figures . . . vii

Acknowledgements . . . ix

Vita and Publications . . . xi

Abstract of the Dissertation . . . xii

1 Introduction . . . 1

2 Electronic Transport in Mesoscopic and Atomic Scale Systems . . . 6
2.1 Single Channel Conductance . . . 7
2.2 Multichannel Conductance . . . 8
2.3 Sources of Electronic Noise . . . 11
2.4 Shot Noise . . . 13
2.4.1 Classical Shot Noise . . . 15
2.4.2 Single Channel Shot Noise . . . 16
2.4.3 Multichannel Shot Noise . . . 16
2.5 Electronic Transport from First Principles . . . 21

3 Shot Noise in Nanoscale Systems . . . 27
3.1 Theoretical Approach . . . 28
3.2 Shot Noise in Parallel Wires . . . 31
3.3 Interference Effects of Transverse Channels . . . 39
3.4 Conclusions . . . 50

4 Fast DNA Sequencing via Transverse Electronic Transport . . . 52
4.1 Theoretical Approach . . . 53
4.2 Results and Discussion . . . 56
4.3 Conclusions . . . 60

5 Fast DNA Sequencing via Transverse Electronic Transport: an In-depth Analysis . . . 62
5.1 Setup and Methods . . . 64
5.2 Results and Discussion . . . 67
5.2.1 Setup . . . 67

5.2.2 Nucleotide Stabilization 72
5.2.3 Influence of the Environment 73
5.3 Conclusions and Future Work 74

6 Charge Screening in Nanopores 77
6.1 Water Sphere 79
6.2 Nanopores 83
6.3 Conclusions and Future Work 85

Bibliography 88

LIST OF FIGURES

2.1 Voltage noise power as a function frequency for a gold point contact at 4.2 K. The curves correspond to an increasing average current, from 0 to 0.9 μA. Figure from Ref.[112]. 14
2.2 Schematic of two electrodes kept at a potential difference, V_B. . . . 24

3.1 Schematic of the system investigated. It consists of two parallel wires, separated by a distance L, between two biased electrodes. . . 33
3.2 Conductance (upper panel), in units of quantum of conductance G_0, and Fano factor (lower panel) as a function of wire separation for two parallel 4-atom wires. 35
3.3 Conductance (upper panel), in units of quantum of conductance G_0, and Fano factor (lower panel) as a function of wire separation for two parallel 5-atom wires. 35
3.4 Contour plot of the charge density for the 4-atom wire system at two different interwire distances. See text for the explicit definition of this density. Vertical black lines correspond to the edges of the jellium model and circles correspond to atomic positions. 38
3.5 Contour plot of the charge density for the 5-atom wire system at interwire distance of 6.5 a.u. See text for the explicit definition of this density. Vertical black lines correspond to the edges of the jellium model and circles correspond to atomic positions. 39
3.6 Schematic of a) a mesoscopic junction and b) a nanoscale junction. 41
3.7 Conductance and Fano factor as a function of number of parallel silicon atoms. The shot noise is calculated with the assumption that channels do interfere with each other as assumed in equation (3.28). 49
3.8 Fano factor as a function of wire separation for two parallel carbon wires. 50

4.1 Transverse current versus time (in arbitrary units) of a highly idealized single strand of DNA translocating through a nanopore with a constant motion. 54
4.2 Currents as a function of time for a poly$(\mathrm{dC})_{15}$ translocating through a nanopore. 58
4.3 Probability distributions of currents at a bias of 1 V for poly$(\mathrm{dX})_{15}$, where X is Adenine/ Thymine/ Cytosine/ Guanine for the black/ blue/ red/ green curve, respectively. 59

5.1 Schematic of a nanopore (purple) with electrodes (gold) attached to the edges of the pore. 63

5.2 Current as a function of time for poly$(dA)_{15}$, as (a) it is propagating through a pore with two electrodes without a stabilizing field, and (b) when the driving field is turned off at a time when a base is aligned in between the electrode pair. 68
5.3 Top graph shows the probability distributions, assuming instantaneous measurements for poly$(dX)_{15}$. The bottom graph again shows the probability distributions, but now with the assumption that each measurement is time averaged in between each sample. 71
5.4 Probability distributions of conductance for varying stabilizing fields for poly$(dA)_{15}$. 74
5.5 Current, at a bias of 0.1 V, as a function of time for poly$(dG)_{15}$, with a single Guanine base stabilized in between the electrodes by the transverse electric field, with (solid red curve) and without (dashed blue curve) water included in the current calculation. 75

6.1 Time averaged radial electric field, E_r, a species would feel at a distance, r, from for a single negatively charged chlorine ion inside a large water sphere. 80
6.2 Schematic view of oscillations in the electric field, as described in the main text. 82
6.3 Total electric field in the radial direction,E_ρ, as a function of distance, ρ, from a negatively charged chlorine ion, in the plane perpendicular to the pore. 85
6.4 Total electric field in the z-direction,E_z, as a function of distance, z, from a negatively charged chlorine, in the center of the pore. . . . 86

ACKNOWLEDGEMENTS

First and foremost I would like to thank my advisor, Professor Massimiliano Di Ventra. Not only has he been deeply involved and closely followed my research, but also provided a wonderful working atmosphere.

I would also like to thank Professor Prabhakar Bandaru, Professor Dimitri Basov, Professor Clifford Kubiak and Professor Lu Sham for their work at my thesis committee.

Special thanks are due to my close collaborators Professor Yu-Chang Chen and Michael Zwolak for many insightful discussions.

I also thank Neil Bushong for many insightful discussions and for proofreading sections of this dissertation.

Chapter 3 is in part a reprint of the material as it appears in Johan Lagerqvist, Yu-Chang Chen and Massimiliano Di Ventra *Shot Noise in Parallel Wires*, Nanotechnology 15, S459(2004), Institute of Physics. The dissertation author is the primary investigator of this paper.

Chapter 3 is in part a reprint of the material as will appear in Yu-Chang Chen, Johan Lagerqvist and Massimiliano Di Ventra *Interference Effects of Transverse Channels on Shot Noise in Atomic Scale Junctions*, in preparation (2006). The dissertation author is a co-author of this paper.

Chapter 4 is in part a reprint of the material as it appears in Johan Lagerqvist, Michael Zwolak and Massimiliano Di Ventra *Fast DNA Sequencing via Transverse Electronic Transport*, Nano Lett. 6, 779(2006), American Chemical Society. The dissertation author is the primary investigator of this paper.

Chapter 5 is in part a reprint of the material as will appear in Johan Lagerqvist, Michael Zwolak and Massimiliano Di Ventra *Influence of Device Operation and the Environment on Rapid DNA Sequencing via Transverse Electronic Transport*, submitted to Proc. Natl. Acad. Sci. U.S.A. (2006). The dissertation author is the primary investigator of this paper.

Chapter 6 is in part a reprint of the material as will appear in Johan Lagerqvist, Michael Zwolak and Massimiliano Di Ventra *Ion Electronics in Nanopores*, in preparation (2006). The dissertation author is the primary investigator of this

paper.

VITA

1977	Born, Luleå, Sweden
2002	M. S. in Engineering Physics, Luleå University of Technology, Sweden
2002	Teaching assistant, Department of Physics, Virginia Polytechnic Institute and State University
2002-2003	Research assistant, Department of Physics, Virginia Polytechnic Institute and State University
2004-2006	Research assistant, Department of Physics, University of California San Diego
2006	Ph. D. in Physics, University of California San Diego

PUBLICATIONS

Johan Lagerqvist, *Design and Analysis of an Electrically Steerable Microstrip Antenna for Ground to Air Use*, Master Thesis (2002)

Johan Lagerqvist, Yu-Chang Chen and Massimiliano Di Ventra *Shot Noise in Parallel Wires*, Nanotechnology 15, S459(2004).

Johan Lagerqvist, Michael Zwolak and Massimiliano Di Ventra *Fast DNA Sequencing via Transverse Electronic Transport*, Nano Lett. 6, 779(2006).

Johan Lagerqvist, Michael Zwolak and Massimiliano Di Ventra *Influence of Device Operation and the Environment on Rapid DNA Sequencing via Transverse Electronic Transport*, submitted to Proc. Natl. Acad. Sci. U.S.A. (2006).

Johan Lagerqvist, Michael Zwolak and Massimiliano Di Ventra *Ion Electronics in Nanopores*, to be published (2006).

Yu-Chang Chen, Johan Lagerqvist and Massimiliano Di Ventra *Interference Effects of Transverse Channels on Shot Noise in Atomic Scale Junctions*, to be published (2006).

Johan Lagerqvist, Michael Zwolak and Massimiliano Di Ventra *Comment on: Characterization of the tunneling conductance across DNA bases*, to be published (2006).

ABSTRACT OF THE DISSERTATION

Electronic Transport in Nanoscale Structures

by

Johan Lagerqvist
Doctor of Philosophy in Physics
University of California San Diego, 2006
Professor Massimiliano Di Ventra, Chair

In this dissertation electronic transport in nanoscale structures is discussed. An expression for the shot noise, a fluctuation in current due to the discreteness of charge, is derived directly from the wave functions of a nanoscale system. Investigation of shot noise is of particular interest due to the rich fundamental physics involved. For example, the study of shot noise can provide fundamental insight on the nature of electron transport in a nanoscale junction. We report calculations of the shot noise properties of parallel wires in the regime in which the interwire distance is much smaller than the inelastic mean free path. The validity of quantized transverse momenta in a nanoscale structure and its effect on shot noise is also discussed.

We theoretically propose and show the feasibility of a novel protocol for DNA sequencing based on the electronic signature of single-stranded DNA while it translocates through a nanopore. We find that the currents for the bases are sufficiently different to allow for efficient sequencing. Our estimates reveal that sequencing of an entire human genome could be done with very high accuracy in a matter of hours, e.g., orders of magnitude faster than present techniques. We also find that although the overall magnitude of the current may change dramatically with different detection conditions, the intrinsic distinguishability of the bases is not significantly affected by pore size and transverse field strength.

Finally, we study the ability of water to screen charges in nanopores by using all-

atom molecular dynamics simulations coupled to electrostatic calculations. Due to the short length scales of the nanopore geometry and the large local field gradient of a single ion, the energetics of transporting an ion through the pore is strongly dependent on the microscopic details of the electric field. We show that as long as the pore allows the first hydration shell to stay intact, e.g., $\sim$6 nearby water molecules, the electric field of the ion can be well screened. We also discuss the consequences of the formation of hydration layers and of the discrete nature of polarization at atomic length scales for the applicability of continuum dielectric models.

1

Introduction

With the current trend of down-scaling witnessed in the semiconductor industry, one can envision that devices used in the industry soon will reach dimensions of the same order of magnitude as the size of atoms themselves. In order to pave the road for future nanoscale engineering, it is essential to understand the underlying physics at these length scales.

This dissertation focuses on a specific aspect of nanoscale structures: electronic transport through these structures. Because one of the driving forces behind the tremendous growth seen in this field is the development of smaller and faster transistors, the understanding of how electrons propagate through nanoscale structures is highly relevant. The understanding of electronic transport in nanoscale devices has applications beyond the design of better transistors; for example, in Chapters 4 and 5 a method for rapid DNA sequencing is suggested based on electronic transport through each individual base.

One of many fundamental questions under investigation in the field of electronic transport is the so-called shot noise, a quantum fluctuation in current due to the discreteness of charge. [8] Investigation of shot noise is of particular interest due to the rich physics involved. For example, the study of shot noise can provide fundamental insight on the nature of electron transport in a nanoscale junction, such as the role of the Pauli exclusion principle. [8] Measurement of shot noise also provides an additional dimension to exploring the change in local temperature caused by the coupling between propagating electrons and ionic

vibrations. [20, 19] Since shot noise depends on the detailed electronic distributions, it also provides a sensitive tool in probing nanoscale junctions, where the electronic properties can be affected by the exact arrangement of each and every individual atom. [64, 18] As shot noise originates from charge quantization, and hence is sensitive to the statistics of quantized electrons, it is a more effective tool than current in probing fundamental transport related quantities such as energy distribution, kinetics, and interactions due to Coulomb repulsion and the Pauli exclusion principle. [72, 83, 11] Measurement of shot noise can also reveal information about the underlying quantum statistics of correlated electrons beyond the scope of what can be understood by measuring the current only. The first half of this dissertation focuses on shot noise in nanoscale devices.

The second half of this dissertation discusses the feasibility of using transverse electronic transport within a nanopore as an accurate and rapid DNA sequencing technology. With the sequencing of the full human genome and the rapidly decreasing costs of sequencing, the prospect of genome-based medicine is now on the forefront of scientific research. A low-cost and rapid method to sequence DNA would dramatically change the way we look at medicine and give us a new tool for use in biological and physical sciences.

Several intriguing sequencing methods [58, 10, 128, 44, 66] have been proposed which would lead us closer to achieving the goal of fast DNA sequencing. Many of these methods are based on the idea of translocating DNA through a nanopore. [58, 1, 28, 91, 117, 92, 29, 90, 79, 95, 2, 17, 38, 48, 80, 108, 46, 81, 78] In their pioneering work Kasianowicz et *al.* demonstrated that DNA can be pulled through a biological nanopore roughly the size of the DNA itself. [58] The translocation of the DNA can be detected by measuring a blockade current when ions are partially prevented from entering the pore. More recent experiments are based on solid state pores made of silicon-based materials. [80, 108, 46, 81, 78, 86, 6, 54] The advantage of solid state pores is that it may be possible to embed single molecule sensors in the pore to measure various physical properties of the DNA during translocation, allowing the DNA to be directly sequenced by detecting specific signatures of individual bases. In our idea, we envision a nanopore device with embedded nanoscale electrodes. As

a single-stranded DNA molecule is driven through the pore, an electrical current can be injected transversely through each base to detect which of the DNA/RNA bases are present.

In Chapter 2 the reader is first introduced to electronic transport in mesoscopic devices. The dimensions of these devices are small enough that the assumptions required for Ohm's law to be valid are broken. A mesoscopic device is however still large enough such that individual atoms do not have to be taken into account, but their potential can be smoothed out. Both theories for calculating the average current through such a device and theories describing the shot noise are covered. The last section of this chapter covers electronic transport in devices small enough such that each individual atom in the system has to be taken into account. More specifically, this section discusses a first-principles method based on Density Functional Theory, which can be used to calculate the electronic wave functions of a nanoscale system.

In Chapter 3 we develop a theory for calculating the shot noise directly from the wave functions of a nanoscale system. We then report first-principles calculations of shot noise properties of parallel carbon wires in the regime in which the interwire distance is much smaller than the inelastic mean free path. As future nanoscale electronic devices are likely to be made up in parallel, with distances in between functional elements smaller than the inelastic mean free path, it is important to understand this system. We find that, with increasing interwire distance, the current approaches rapidly a value close to twice the current of each wire, while the Fano factor, for the same distances, is still larger than the Fano factor of a single wire.

We also discuss how the shot noise is affected by the quantum nature of transverse momenta. In mesoscopic systems, quantum channels are formed via leads acting as waveguides. However, the validity of this assumption may be questioned in a device where a nanoscale junction is immediately adjacent to two large electrodes. Due to the lack of proper waveguides in this system, the transverse momentum is not quantized. This may introduce mixing effects of transverse channels in the reservoirs, which can affect the shot noise.

Chapter 4 introduces a novel idea for DNA sequencing based on electronic transport. We propose and theoretically show the feasibility of a protocol for sequencing based on the distributions of transverse electrical currents of single-stranded DNA while it translocates through a nanopore. Our estimates, based on the statistics of these distributions, reveal that sequencing of an entire human genome could be done with very high accuracy in a matter of hours without parallelization, that is, orders of magnitude faster than present techniques.

In Chapter 5 the sequencing method proposed in Chapter 4 is analyzed in further detail. We examine the effects of the environment and detection probes on the distinguishability of the DNA bases. We find that the intrinsic measurement bandwidth of the electrodes helps the detection of single bases by averaging over the current distributions of each base. We also find that although the overall magnitude of the current may change dramatically with different detection conditions, the intrinsic distinguishability of the bases is not significantly affected by pore size and transverse field strength. The latter is the result of very effective stabilization of the DNA by the transverse field induced by the probes, so long as that field is much larger than the field that drives DNA through the pore. In addition, the ions and water together effectively screen the charge on the nucleotides, so that the electron states participating in the transport properties of the latter ones resemble those of the uncharged species. Finally, water in the environment has negligible direct influence on the transverse electrical current.

In Chapter 6, we study the ability of water to screen charges in nanopores by using all-atom molecular dynamics simulations coupled to electrostatic calculations. Due to the short length scales of the nanopore geometry and the large local field gradient of a single ion, the energetics of transporting an ion through the pore is strongly dependent on the microscopic details of the electric field. These details are determined by the atomic configurations of species around the ion. We show that as long as the pore allows the first hydration shell to stay intact, e.g., $\sim$6 nearby water molecules, the electric field of the ion is well screened. We also discuss the consequences of the formation of hydration layers and of the discrete nature of polarization at atomic length scales for the applicability of continuum

dielectric models.

2

Electronic Transport in Mesoscopic and Atomic Scale Systems

In macroscopic physics we are used to calculating the resistance of a conductor with the help of the familiar Ohm's law [97]. However, as the dimensions of the object in question are reduced, it is not certain that Ohm's law is still valid. [4, 60] A fundamental assumption used when deriving Ohm's law is that the system is diffusive, meaning the conductor has to be much larger than the electron mean free path. Then, as an electron is propagating through the conductor, it continuously relaxes and changes direction (that is, diffuses through the system), while driven by an external electric field. Thus as the scale of the system becomes of the same order of magnitude as the mean free path of the electron, Ohm's law falls apart and new physics governs the electronic transport.

In the first two sections of this chapter, the reader is introduced to the fundamentals of electronic transport in mesoscopic systems, where the dimensions of the device are small enough that Ohm's law is not valid. Sources of electronic noise is discussed with emphasis on shot noise. Next, previous results are re-derived in a more rigorous way, based on second quantization. Finally, the last section describes a method for calculating the wave functions of a system with scattering boundary conditions, small enough such that each and every atom has to be taken

into account, based on first principles.

2.1 Single Channel Conductance

For a system with dimensions smaller than the mean free path (in the so-called ballistic limit), electrons propagate through the system without experiencing the diffusive scattering described above. [26] Instead of viewing electron transport as a response to an external electric field, one can then see the process as electrons injected at one side of the system with a given probability of reaching the other side, as discussed in for example Refs. [67, 68, 69, 70, 71, 52, 26, 51].

Assume we have two large electrodes connected together with a junction, with the electrodes coupled to a battery. Then if the electrodes are sufficiently large, a chemical potential, $\mu_{R(L)}$, can be associated with the right(left) electrode far from the edge of the electrode. If we for simplicity assume the left electrode has a positive potential and the bias of the battery is V, the chemical potential of the left electrode is raised such that the difference in Fermi level between the two electrodes is $E_{FL} - E_{FR} = eV$, where $E_{FL/FR}$ is the fermi level of the left/right electrode. As the electrons in the system obeys Fermi-Dirac statistics, the current through the system can now be written as

$$I = -e \int dE \mathcal{D}(E) v(E) \Big[T(E) f(E - \mu_L) + R'(E) f(E - \mu_R) - f(E - \mu_R) \Big], \quad (2.1)$$

where $\mathcal{D}$ is the density of states and f is the Fermi-Dirac distribution. $T(E)$ is probability that an electron, with energy E, originating in the left electrode is transmitted to the right electrode, while $R'(E)$ is the probability that and electron originating from the right electrode is reflected back.

By assuming the bias to be within the linear regime (that is the difference in chemical potential between the two electrodes is small), $f(E-\mu_R)$ can be expressed as a Taylor series such that [3]

$$f(E - \mu_r) \approx f(E - \mu_L) + \frac{df(E - \mu_L)}{dE}(\mu_L - \mu_R), \quad (2.2)$$

which when inserted in 2.1 results in

$$I = e(\mu_R - \mu_L) \int dE \mathcal{D}(E) v(E) (-\frac{df}{dE}) T(E). \quad (2.3)$$

The one dimensional density of states is however

$$\mathcal{D}(E) = 2\frac{dk}{2\pi dE} = \frac{2}{hv(E)}, \tag{2.4}$$

where a factor of two is included as we assume the system is spin unpolarized. Invoking this, the current can now be expressed as

$$I = \frac{2e}{h}(\mu_R - \mu_L)\int dE(-\frac{\delta f}{\delta E})T(E), \tag{2.5}$$

or for zero temperature

$$I = \frac{2e}{h}(\mu_R - \mu_L)T(E_F) = \frac{2e^2V}{h}T(E_F). \tag{2.6}$$

Similarly, the zero temperature conductance, G, equals

$$G = \frac{I}{V} = G_0T(E_F), \tag{2.7}$$

where $G_0 = 2e^2/h$ is the so called quantum of conductance and corresponds to the conductance of a fully transmitted wave and E_F is the Fermi energy. Equation 2.7 is usually called the single channel Landauer formula. This is a somewhat surprising result. One might, at first sight, believe that a fully transmitted wave should have zero resistance. Instead here we find the conductance instead is G_0 when $T = 1$. The conductance is however calculated in between the two reservoirs, such that not only the resistance of the junction itself is taken into account for, but also the contact resistance resulting from that large reservoirs are injecting electrons into a narrow constriction. The resistance due to the barrier is zero when $T = 1$, but as the contact resistance still is present, the total conductance is finite. A more rigorous derivation follows later in this chapter.

2.2 Multichannel Conductance

Due to the dimensions of the system it is reasonable to assume that the region in between the two electrodes acts as two wave guides connecting a scatterer to the two electrodes, where the wave guides are adiabatically coupled to the reservoirs. For wave guides large enough such that the potential of the individual atoms

can be smoothed out, the potential profile of the wave guide is constant(or vary very slowly) in the direction of electron flow (z-direction). The solutions of this Hamiltonian then assume standing waves in x- and y-directions and traveling wave form in the z-direction, with eigenvalues

$$E_F = E_n + \frac{\hbar^2 k_n^2}{2m}. \tag{2.8}$$

The first term on the right hand side of the equation is the energy of mode n of the standing wave. The second term is the energy of the traveling wave. In mesoscopic physics, mode n is also referred to as channel n. The total number of channels of the system is of the order of $Ak_F^2/2\pi$, where A is the cross sectional area and k_F is the Fermi wavevector. Note however that the system has wave guides connecting it to both electrodes, where the junction acts as a scatterer connecting the two wave guides together. Hence the junction can mix the channels in the two wave guides together.

The probability of a wave incoming from the left channel n is going to transmit through the junction to right channel m is given by

$$T_{mn} = |t_{mn}|^2 \tag{2.9}$$

and similarly the probability the same wave would reflect back into left channel m is

$$R_{mn} = |r_{mn}|^2. \tag{2.10}$$

However waves can also originate from the right side. In similar fashion the transmission and reflection probability for these waves are given by

$$T'_{mn} = |t'_{mn}|^2 \tag{2.11}$$

and

$$R'_{mn} = |r'_{mn}|^2. \tag{2.12}$$

Here t_{mn} and t'_{mn} are the transmission amplitudes and r_{mn} and r'_{mn} are the reflection amplitudes. This scattering process can be described in matrix form with the so called scattering matrix, s, defined as

$$\begin{pmatrix} o' \\ o \end{pmatrix} = s \begin{pmatrix} i \\ i' \end{pmatrix} = \begin{pmatrix} r & t' \\ t & r' \end{pmatrix} \begin{pmatrix} i \\ i' \end{pmatrix}, \tag{2.13}$$

where i and i' are the incoming flux amplitudes and o and o' are the outgoing flux amplitudes. For a single channel system, each transmission and reflection amplitude in the scattering matrix would be a scalar. However, for a multi channel system r, t, r' and t' themselves assumes the from of a matrix, as each channel has their own incoming and outgoing flux amplitudes.

Due to current conservation, the scattering matrix must be unitary such that $ss^\dagger = 1$, or

$$rr^\dagger + t't'^\dagger = tt'^\dagger + r'r'^\dagger = 1 \tag{2.14}$$

and

$$rt^\dagger + t'r'^\dagger = r^\dagger t' + t^\dagger r' = 0. \tag{2.15}$$

The total transmission probability from all channels on the left side to right channel n can now be defined as

$$T_n = \sum_n |t_{mn}|^2, \tag{2.16}$$

where t_{mn} is the element in the scattering matrix connecting incoming channel m with outgoing channel n. The square comes from the fact that we wish to obtain the probability of transmission. Similarly, the reflection probability is given by

$$R_n = \sum_n |r_{mn}|^2. \tag{2.17}$$

For waves incoming from the right waveguide we can define

$$T'_n = \sum_n |t'_{mn}|^2, \tag{2.18}$$

and

$$R'_n = \sum_n |r'_{mn}|^2, \tag{2.19}$$

with similar notation. Combining these equations with the requirements originating from the unitary of the scattering matrix we find that

$$R'_n + T_n = 1 \tag{2.20}$$

and

$$R_n + T'_n = 1. \tag{2.21}$$

In similar fashion as for the single channel case discussed in the previous section, the current can be written as

$$I = -e \sum_n \int dE \mathcal{D}_n(E) v_n(E) \Big[T_n(E) f(E - \mu_L) + R'_n(E) f(E - \mu_R) - f(E - \mu_R) \Big]. \tag{2.22}$$

By following the same arguments as for the single channel case, the zero temperature current expression is simplified to

$$I = \frac{2e^2 V}{h} \sum_n T_n(E_F), \tag{2.23}$$

and the conductance to

$$G = G_0 \sum_n T_n(E_F), \tag{2.24}$$

where again $G_0 = 2e^2/h$ is the is the conductance of a single fully transmitted channel. A more rigorous derivation follows later in this chapter.

The perhaps most significant verification of this, so called multi channel Landauer equation, is the quantum point contact experiment, [115, 114] where a gate causes a constriction in a two dimensional electron gas. By varying the gate bias, the width of the constriction can be changed such that the conductance of the two dimensional electron gas shows clear quantization in units of G_0. The explanation of this is that, as the width of the constriction is opened up, more channels starts to conduct.

2.3 Sources of Electronic Noise

The currents derived above are time averaged quantities. In a real experiment the current is fluctuating around its average value. This fluctuation is called "noise". Perhaps the most famous source of noise is the so-called *thermal noise*, or Johnson-Nyquist noise, resulting from thermal excitation of the conducting electrons.

The power spectral density of a resistor is given by [98]

$$\Phi(f) = \frac{2Rhf}{e^{\frac{hf}{k_B T}} - 1}, \tag{2.25}$$

where R is the resistance, h is Planck's constant, f is the frequency, k_B is Boltzmann's constant and finally T is the temperature. For $f << \frac{k_B}{h}$, $\Phi(f)$ can be expanded as a first order Taylor series and

$$\Phi(f) \approx 2Rk_BT. \tag{2.26}$$

If R is assumed to be frequency independent, the root mean square voltage fluctuation is then calculated as

$$v_n = \sqrt{4k_bTR\Delta f}, \tag{2.27}$$

where Δf is the bandwidth of the measurement and a factor of two comes from the fact that we have to integrate over both positive and negative frequencies. Similarly the root mean quare current noise is given by

$$i_n = \sqrt{\frac{4k_BT\Delta f}{R}}. \tag{2.28}$$

It is worth noticing that, as the thermal noise is temperature dependent, it can be suppressed by operating at low enough temperatures.

Deviations from the average current can also be caused in a system which fluctuates between configurations with nearly identical energy, but different currents; this is called *telegraph noise*. This noise characteristically follows a Lorentzian power spectrum. For a gold point contact experiment [124] this could for example be caused by an atom fluctuating between two different states, with almost identical energy but different current.

Yet another source of noise is the so called *1/f-noise*, named after its power spectrum which is inversely proportional to the frequency. The 1/f-noise is is observed in many systems, ranging from the water level in the Nile(the world's longest data set) [94] to the current through a nano-scale gold point contact. [112] Despite the common occurrence of 1/f-noise, it is still not fully understood and is believed to have many different sources. For a gold point contact, it is suggested to be caused by a superposition of telegraph noise, created by defect motions. [112]

As charge is quantized, the current experiences a noise since, at two given times, the number of electrons passing through the junction may not be identical.

One can compare this with rain through a cross-sectional surface. As the water is quantized into drops, the flow of water at different times through a cross-sectional surface may very well be different and the drops pass through the surface more or less uncorrelated from each other. This so called *shot noise* has a power spectrum which is frequency independent and is discussed in much more detail later in this, and subsequent, chapters. [112]

As an example of these sources of noise, Figure 2.1 shows the noise power as a function of frequency in a nano-scale point contact, consisting of just one, or a few, gold atoms. The point contact is constructed by using a mechanically controllable break-junction technique and has a conductance of 1.53 G_0. Each curve corresponds to an increasing average current of 0, 0.1, 0.2 ... 0.9 μA and all measurements are performed at a temperature of 4.2 K. First and foremost, we see that even the zero average current case(lowest curve) experience noise. This is the thermal noise and is frequency independent up until a cutoff frequency of about 50 kHz, caused by the capacitance of surrounding setup. The sharp peaks are caused by electromagnetic interference from the outside world. As the average current is increased, we see both 1/f-noise and shot noise emerging in the data. For low frequencies the 1/f-noise is dominant, but rapidly decays as the frequency is increased. Since the shot noise power is independent of frequency, the shot noise is visible along with the thermal noise, which is also frequency-independent. However, since the shot noise is directly proportional to the average current, unlike the thermal noise which is independent of the average current, the two sources of noise can easily be separated out.

2.4 Shot Noise

In the past decade research regarding the electronic transport properties of nanoscale devices has received increased attention, due to the the vast improvements made in the down-scaling of electronic devices. This interest not only covers the design and integration of practical nanoscale electronic device, but also fundamental understanding of transport properties in nanoscale systems. [25, 119, 36,

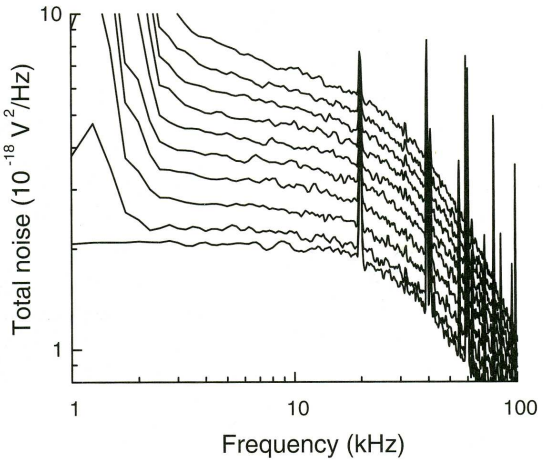


Figure 2.1: Voltage noise power as a function frequency for a gold point contact at 4.2 K. The curves correspond to an increasing average current, from 0 to 0.9 μA. Figure from Ref.[112].

111, 27, 93, 102, 127, 63, 101, 118, 16, 96, 20, 21, 19, 121] One of these fundamental questions under investigation is the shot noise, a zero temperature quantum fluctuation in current due to the discreteness of charge, [8] as introduced to to the reader in the previous section.

Investigation of shot noise is of particular interest due to the rich fundamental physics is involved. For example, the study of shot noise can provide fundamental insight on the nature of electron transport in a nanoscale junction, such as the role of the Pauli exclusion principle and the statistics of quantized charge which is highly relevant in transport. Measurement of shot noise also provides an additional dimension to exploring the local temperatures of nano-structures caused by the coupling between propagating electrons and ionic vibrations. [22] Since shot noise depends on the detailed electronic distributions, it also provides a sensitive tool in probing nano-junctions, where the electronic structures can be affected by the exact arrangement of each and every individual atom. As shot noise originates from charge quantization, and hence is sensitive to the statistics of quantized electrons, shot noise is a more effective tool than current in probing fundamental transport related quantities such as energy distribution, kinetics, and interaction due to Coulomb repulsion and the Pauli exclusion principle. [11, 72, 83] Measurement

of shot noise can reveal information about the underlying quantum statistics of correlated electrons beyond the scope of what can be understood by measuring the current only.

2.4.1 Classical Shot Noise

First predicted by Schottky in his groundbreaking paper from 1918 [105], where he demonstrated that as electrons are emitted randomly from the cathode, there should be a fluctuation in the current in between the anode and cathode. If the electrons are emitted completely uncorrelated from each other they obey Poisson statistics such that the mean-square fluctuation of the number of emitted electrons, N is

$$< \Delta N^2 >=< (N- < N >)^2 >=< N > . \tag{2.29}$$

The average current during the time interval considered, t, is

$$I = e\frac{N}{t}. \tag{2.30}$$

By combining these two equations we find that the mean square fluctuation of the current itself is

$$< \Delta I^2 >= \frac{eI}{t}. \tag{2.31}$$

Here $\Delta I(t)$ is the excess current, at time t, compared to the average current. In general the noise power spectrum of a current is given by [112]

$$S(f) = 2\int_{-\infty}^{\infty} < \Delta V(0)\Delta V(t) > e^{i\omega t}dt, \tag{2.32}$$

where f is the frequency and $\omega = 2\pi f$. As we in our example with the vacuum tube assume the electrons are emitted completely uncorrelated, $< I(t)I(t') >= 0$ must hold for all $t \neq t'$. Then, in the limit of $\omega \to 0$, we find that

$$S = 2\int_0^t < \Delta I(t')^2 > dt' = 2eI. \tag{2.33}$$

This is the so-called Poisson limit of the shot noise. For most systems correlations between the electrons reduce the shot noise such that the shot noise is lower than that of the uncorrelated case. It is however worth pointing out that this is not the case for all systems. In certain specific cases one can have so-called super-Poissonian noise. [7, 8]

2.4.2 Single Channel Shot Noise

In the case where electrons are emitted in vacuum tubes, the electrons either have to be emitted via thermal excitation or by tunneling through a barrier. Thus the probability of transmission is very low. [8] If instead each electron is transmitted with a probability T and reflected with a probability R, such that $T + R = 1$, the above result does not hold. The occupation numbers for incoming, reflected and transmitted states can then be labeled as n_i, n_t and n_r, respectively. If the incoming state is on average occupied with a probability f, then the time average of the various states must be $< n_i >= f$, $< n_t >= fT$ and $< n_r >= fR$. Fluctuations away from each time averaged quantity can then be defined as $\Delta n_t = n_t - < n_t >$ and $\Delta n_r = n_r - < n_r >$ for the transmitted and reflected occupation numbers. The mean square fluctuations are then

$$\begin{aligned} < (\Delta n_t)^2 >=< n_t > - < n_t >^2 = fT(1 - fT), \\ < (\Delta n_r)^2 >=< n_r > - < n_r >^2 = fR(1 - fR), \\ < (\Delta n_t)(\Delta n_r) >= - < n_t >< n_r >= -TRf^2, \end{aligned} \tag{2.34}$$

where we have used the fact that $< n_t n_r >= 0$, since each measured electron is either transmitted or reflected. For the zero temperature case, where $f = 1$, these equations reduces to

$$< (\Delta n_t)^2 >=< (\Delta n_r)^2 >= - < (\Delta n_t)(\Delta n_r) >= TR = T(1 - T). \tag{2.35}$$

Similarly to the average current derived above, we also find that in the zero temperature and zero frequency limit, the shot noise spectrum is

$$S = 2eV\frac{2e^2}{h}TR = 2eV\frac{2e^2}{h}T(1 - T) \tag{2.36}$$

for biases small enough such that the expansion in equation 2.2 is still valid. For small T, where $(1-T) \approx 1$, we recover equation 2.33, as expected. A more rigorous derivation of the shot noise follows in the next section.

2.4.3 Multichannel Shot Noise

In the above calculation it is assumed the system only has a single channel. However when the conductance given in equation 2.24 is derived, we argue that a

mesoscopic system may have multiple channels, each contributing to its conductance. In this section we derive the shot noise for a multichannel system via second quantization.

Following Ref. [8], we begin by defining the creation and annihilation operators, $\hat{a}^\dagger_{Ln}(E)$ and $\hat{a}_{Ln}(E)$, which create and annihilate incoming electrons with energy E, in channel n of the left lead. Similarly, creation and annihilation operators $\hat{b}^\dagger_{Ln}(E)$ and $\hat{b}_{Ln}(E)$ describes the electrons in the outgoing states. These operators obey the anticommutation relations

$$\begin{aligned} \hat{a}^\dagger_{Ln}(E)\hat{a}_{Ln'}(E') + \hat{a}_{Ln'}(E')\hat{a}^\dagger_{Ln}(E) &= \delta_{nn'}\delta E - E', \\ \hat{a}_{Ln}(E)\hat{a}_{Ln'}(E') + \hat{a}_{Ln'}(E')\hat{a}_{Ln}(E) &= 0, \\ \hat{a}^\dagger_{Ln}(E)\hat{a}^\dagger_{Ln'}(E') + \hat{a}^\dagger_{Ln'}(E')\hat{a}^\dagger_{Ln}(E) &= 0. \end{aligned} \tag{2.37}$$

The creation and annihilation operators for the right lead, $\hat{a}^\dagger_{Rn}(E)$, $\hat{a}_{Rn}(E)$,$\hat{b}^\dagger_{Rn}(E)$ and $\hat{b}_{Rn}(E)$ are similarly defined.

The standard current operator for the left lead is then given by [8]

$$\hat{I}_L(z,t) = \frac{\hbar e}{2im}\int d\mathbf{r}_\parallel \left[\hat{\Psi}^\dagger_L(\mathbf{r},t)\frac{\delta}{\delta z}\hat{\Psi}_L(\mathbf{r},t) - (\frac{\delta}{\delta z}\hat{\Psi}^\dagger_L(\mathbf{r},t))\hat{\Psi}_L(\mathbf{r},t)\right], \tag{2.38}$$

where

$$\hat{\Psi}_L(\mathbf{r},t) = \int dE e^{-iEt/\hbar}\sum_{n=1}^{N_L(E)}\frac{\xi_{Ln}(\mathbf{r}_\parallel)}{(2\pi\hbar v_{Ln}(E))^{1/2}}[\hat{a}_{Ln}e^{ik_{Ln}z} + \hat{b}_{Ln}e^{-ik_{Ln}z}] \tag{2.39}$$

and

$$\hat{\Psi}^\dagger_L(\mathbf{r},t) = \int dE e^{-iEt/\hbar}\sum_{n=1}^{N_L(E)}\frac{\xi^*_{Ln}(\mathbf{r}_\parallel)}{(2\pi\hbar v_{Ln}(E))^{1/2}}[\hat{a}^\dagger_{Ln}e^{-ik_{Ln}z} + \hat{b}^\dagger_{Ln}e^{ik_{Ln}z}], \tag{2.40}$$

where z is the coordinate of the electron flow and $\mathbf{r}_\parallel$ is the coordinate parallel to the electrode surface, or perpendicular to the z-axis. ξ^L_n is the wave function in the plane of $\mathbf{r}_\parallel$.

$$k_{Ln} = \frac{\sqrt{2m}}{\hbar}\sqrt{E - E_{Ln}} \tag{2.41}$$

is the wave vector and $v_n(E) = \hbar k_{Ln}/m$ is the velocity of channel n.

By inserting equations 2.39 and 2.40 in 2.38 we now find that the current can be expressed as

$$\begin{aligned}\hat{I}_L(z,t) =& \frac{e}{4\pi\hbar}\sum_n \int dE dE' e^{i(E-E')t/\hbar} \frac{1}{\sqrt{v_{Ln}(E)v_{Ln}(E')}} \\ & \{[v_{Ln}(E)+v_{Ln}(E')][exp[i(k_{Ln}(E')-k_{Ln}(E))z]\hat{a}^\dagger_{Ln}(E)\hat{a}_{Ln}(E') \\ & - exp[i(k_{Ln}(E)-k_{Ln}(E'))z]\hat{b}^\dagger_{Ln}(E)\hat{b}_{Ln}(E')] \\ & + [v_{Ln}(E)-v_{Ln}(E')][exp[-i(k_{Ln}(E)+k_{Ln}(E'))z]\hat{a}^\dagger_{Ln}(E)\hat{b}_{Ln}(E') \\ & - exp[i(k_{Ln}(E)+k_{Ln}(E'))z]\hat{b}^\dagger_{Ln}(E)\hat{a}_{Ln}(E')]\},\end{aligned} \tag{2.42}$$

which reduces to

$$\hat{I}_L(t) = \frac{e}{2\pi\hbar}\sum_n \int dE dE' e^{i(E-E')t/\hbar}[\hat{a}^\dagger_{Ln}(E)\hat{a}_{Ln}(E') - \hat{b}^\dagger_{Ln}(E)\hat{b}_{Ln}(E')] \tag{2.43}$$

if one assumes that $v_n(E)$ is energy independent. Since $v_n(E)$ typically varies at the order of the Fermi energy and E and E' are relatively close to each other, this assumption is, for most cases, valid. Next, by letting $E' = E + \hbar\omega$ and integrating over ω one finds that

$$\hat{I}_L(t) = \frac{e}{2\pi\hbar}\sum_n \int dE[\hat{n}^+_{Ln}(E,t) - \hat{n}^-_{Ln}(E,t)], \tag{2.44}$$

where $\hat{n}^+_{Ln}(E) = \hat{a}^\dagger_{Ln}(E)\hat{a}_{Ln}(E)$ and $\hat{n}^-_{Ln}(E) = \hat{b}^\dagger_{Ln}(E)\hat{b}_{Ln}(E)$ are the usual occupation number operators. We here see the current is calculated by comparing the occupation number of right and left moving waves.

Now we define the scattering matrix, s, with dimensions $(N_L+N_R)\times(N_L+N_R)$, similarly to before, as

$$\begin{pmatrix} \hat{b}_{L1} \\ \cdots \\ \hat{b}_{LN_L} \\ \hat{b}_{R1} \\ \cdots \\ \hat{b}_{RN_R} \end{pmatrix} = s \begin{pmatrix} \hat{a}_{L1} \\ \cdots \\ \hat{a}_{LN_L} \\ \hat{a}_{R1} \\ \cdots \\ \hat{a}_{RN_R} \end{pmatrix}. \tag{2.45}$$

Again, the top left elements in the scattering matrix describe electrons emitted from the left electrode which are reflected back; the bottom left elements describe

electrons transmitted from left to right electrode; the top right elements describe electrons transmitted from right to left electrode; while the bottom right elements describe electrons originating from the right electrode which are reflected back to the right electrode. As the scattering matrix describes four different physical scenarios, it can be split into four smaller matrices

$$s = \begin{pmatrix} r & t' \\ t & r' \end{pmatrix}, \tag{2.46}$$

each describing the scenarios above.

With the help of the scattering matrix, equation 2.44 can now be rewritten as

$$\hat{I}_L(t) = \frac{e}{2\pi\hbar} \sum_{\alpha\beta} \sum_{mn} \int dE dE' e^{i(E-E')t/\hbar} \hat{a}^\dagger_{\alpha m}(E) A^{mn}_{\alpha\beta}(L; E, E') \hat{a}_{\beta n}(E'), \tag{2.47}$$

where $\alpha, \beta = L, R$.

$$A^{mn}_{\alpha\beta}(L; E, E') = \delta_{mn}\delta_{\alpha L}\delta_{\beta L} - \sum_k s^\dagger_{L\alpha;mk}(E) s_{L\beta;kn}(E') \tag{2.48}$$

and $s_{L\alpha;mk}(E)$ is the scalar from the scattering matrix defining the coupling between $\hat{b}_{Lm}(E)$ and $\hat{a}_{\alpha k}(E)$.

Similarly we can express the current in lead $\alpha = L, R$ as

$$\hat{I}_\alpha(t) = \frac{e}{2\pi\hbar} \sum_{\beta\gamma} \sum_{mn} \int dE dE' e^{i(E-E')t/\hbar} \hat{a}^\dagger_{\beta m}(E) A^{mn}_{\beta\gamma}(\alpha; E, E') \hat{a}_{\gamma n}(E'), \tag{2.49}$$

with

$$A^{mn}_{\beta\gamma}(\alpha; E, E') = \delta_{mn}\delta_{\alpha\beta}\delta_{\alpha\gamma} - \sum_k s^\dagger_{\alpha\beta;mk}(E) s_{\alpha\gamma;kn}(E'). \tag{2.50}$$

As we wish to derive an equation for the shot noise, we now define the correlation function of the current of electrode α and the current of electrode β as

$$S_{\alpha\beta}(t - t') = \frac{1}{2} < \Delta\hat{I}_\alpha(t)\Delta\hat{I}_\beta(t') + \Delta\hat{I}_\beta(t')\Delta\hat{I}_\alpha(t) >, \tag{2.51}$$

where $\Delta\hat{I}_i(t) = \hat{I}_i(t) - < I_i >$ is the deviation from the the average current in lead i, at time t. If we instead express it in Fourier space, we find that

$$2\pi\delta(\omega - \omega')S_{\alpha\beta} = < \Delta\hat{I}_\alpha(\omega)\Delta\hat{I}_\beta(\omega') + \Delta\hat{I}_\beta(\omega')\Delta\hat{I}_\alpha(\omega) > . \tag{2.52}$$

In the last step we use that equation 2.51 must be a function of $t-t'$ only. Bloch-De Dominicis theorem [62] gives us that for a Fermi gas

$$\begin{aligned} &< \hat{a}^{\dagger}_{\alpha k}(E_1)\hat{a}_{\beta l}(E_2)\hat{a}^{\dagger}_{\gamma m}(E_3)\hat{a}_{\delta n}(E_4) > - \\ &< \hat{a}^{\dagger}_{\alpha k}(E_1)\hat{a}_{\beta l}(E_2) >< \hat{a}^{\dagger}_{\gamma m}(E_3)\hat{a}_{\delta n}(E_4) >= \\ &\delta_{\alpha\delta}\delta_{\beta\gamma}\delta_{kn}\delta_{ml}\delta(E_1-E_4)\delta(E_2-E_3)f_{\alpha}(E_1)(1-f_{\beta}(E_2)). \end{aligned} \tag{2.53}$$

Utilizing this, equation 2.47 and equation 2.49, the noise power can now be written as

$$\begin{aligned} S_{\alpha\beta}(\omega) =& \frac{e^2}{2\pi\hbar}\sum_{\gamma\delta}\sum_{mn}\int dE A^{mn}_{\gamma\delta}(\alpha;E,E+\hbar\omega)A^{nm}_{\delta\gamma}(\beta;E+\hbar\omega,E)\times \\ &\{f_{\gamma}(E)[1-f_{\delta}(E+\hbar\omega)]+[1-f_{\gamma}(E)]f_{\delta}(E+\hbar\omega)\}, \end{aligned} \tag{2.54}$$

or in the zero frequency limit

$$\begin{aligned} S_{\alpha\beta}(0) =& \frac{e^2}{2\pi\hbar}\sum_{\gamma\delta}\sum_{mn}\int dE A^{mn}_{\gamma\delta}(\alpha;E,E)A^{nm}_{\delta\gamma}(\beta;E,E)\times \\ &\{f_{\gamma}(E)[1-f_{\delta}(E)]+[1-f_{\gamma}(E)]f_{\delta}(E)\}. \end{aligned} \tag{2.55}$$

For zero temperature this expression can further be reduced to

$$\begin{aligned} S_{\alpha\beta} =& \frac{e^2}{2\pi\hbar}\sum_{\gamma\neq\delta}\int dE\ Tr\left[s^{\dagger}_{\alpha\gamma}s_{\alpha\delta}s^{\dagger}_{\beta\delta}s_{\beta\gamma}\right]\times \\ &\left[\Theta(\mu_{\gamma}-E)\{1-\Theta(\mu_{\delta}-E)\}+\Theta(\mu_{\delta}-E)\{1-\Theta(\mu_{\gamma}-E)\}\right], \end{aligned} \tag{2.56}$$

where Θ is the Heaviside step function. In the linear regime this expression can be even further reduced to

$$S \equiv S_{LL} = S_{RR} = -S_{LR} = -S_{RL} = \frac{e^2}{\pi\hbar}Tr(r^{\dagger}rt^{\dagger}t)e|V| \tag{2.57}$$

since the scattering matrix is unitary and should be calculated at the Fermi level. In eigen-channel basis set

$$S = \frac{e^3|V|}{\pi\hbar}\sum_n T_n R_n = \frac{e^3|V|}{\pi\hbar}\sum_n T_n(1-T_n), \tag{2.58}$$

where $T_n + R_n = 1$. When all transmission probabilities are small, the Poisson value of the shot noise is recovered

$$S_P = \frac{e^3|V|}{\pi\hbar}\sum_n T_n = 2e < I > . \tag{2.59}$$

As the noise given by equation 2.58 is always smaller than, or equal to, its Poisson value, it is convenient to define the Fano factor as

$$F = S/S_P. \tag{2.60}$$

For a system in the linear regime, with n channels, the Fano factor then is

$$F = \frac{\sum_n T_n(1-T_n)}{\sum_n T_n}. \tag{2.61}$$

For sake of completeness, we now re-derive the expression for the average current for a multi-channel system. From equation 2.47 the time averaged current can be expressed as

$$< I_L >= \frac{e}{2\pi\hbar}\int dE\ Tr[t^\dagger(E)t(E)][f_L(E) - f_R(E)], \tag{2.62}$$

where we have used that the scattering matrix must be unitary. The fact that

$$< \hat{a}^\dagger_{\alpha m}(E)\hat{a}_{\beta n}(E') >= \delta_{\alpha\beta}\delta_{mn}\delta(E-E')f_\alpha(E) \tag{2.63}$$

for a Fermi gas at thermal equilibrium is also used. For a small bias at zero temperature the conductance is then

$$G = \frac{e^2}{2\pi\hbar}Tr[t^\dagger t] = \frac{e^2}{2\pi\hbar}\sum_n T_n, \tag{2.64}$$

where in the last step the conductance is expressed in eigen-channel basis set. This is identical to equation 2.24, if one take into account that the here derived equation is for a single spin channel.

2.5 Electronic Transport from First Principles

In the previous sections we assumed the junction is coupled to two leads, which in turn are adiabatically coupled to reservoirs. While these assumptions are reasonable in a mesoscopic system where all the details of the system are much larger than the the atoms themselves, one should be careful about making these assumptions in a nanoscale system. Here we define a nanoscale system as a system

small enough such that the potential of the individual atoms should be taken into account.

Take, for example, a break junction experiment [102], where the goal is to create a nanoscale junction consisting of just a few atoms. A macroscopic wire is attached to a beam which can bend. Then a notch is made in the wire and the beam is gradually bent such that the wire is slowly stretched. As the stretching continues, the wire eventually breaks at the notch. Now by reducing the bending slightly, the two newly created tips merge into a single junction hopefully consisting of just one, or few, atoms. The entire process can be monitored by applying a current through the wire. As the current stops flowing, one knows the wire is broken and the beam bending should be slightly reduced until current starts flowing again [112].

In this experiment the junction rapidly opens up into electrodes(wires) with dimensions larger than the inelastic mean free path for the electrons. One can very well then imagine that the nanoscale junction is directly coupled to the reservoirs without the leads introduced in the previous section. If this is the case the wire does not act as wave guides causing standing waves in directions transverse to the current flow, unlike a mesoscopic system. Instead one would see incoming propagating waves from all directions towards the wire [77, 74, 33, 32, 31].

Similarly to before, we see this system as two bulk electrodes kept at fixed chemical potential difference, $V_B = E_{FR} - E_{FL}$, with the help of an external battery. E_{FL} and E_{FR} are the Fermi levels of left and right electrodes. In this section we assume E_{FR} is always larger than E_{FL}. Atomic units are also used throughout this section. See Figure 2.2 for a schematic of the electrodes. The nanoscale junction is then sandwiched in between these two electrodes and, as the two electrodes have different chemical potential, a current flow through the junction in conjunction with a tunneling current in between the electrodes. By ignoring any dynamical effects, the system can now be described as a static many body scattering problem, [77, 74, 33, 32, 31, 12] with a total Hamiltonian $H = H_0 + V$, where H_0 is the Hamiltonian of the bare electrodes only and V is the potential of the junction[1]. The wave functions of the total Hamiltonian, with scattering

[1]This thesis only approaches electronic transport in nanoscale systems via static scattering theory. Novel methods for treating the transport from a dynamical picture are currently under

boundary conditions, can be found by recasting the Schrodinger equation into so-called Lippman-Schwinger [77] form. The solution of the Lippman-Schwinger equation requires that the solution of the system with Hamiltonian H_0 is known. Thus before analyzing the entire problem, we first focus on the bare electrodes only. Then, once the solution of the bare electrodes is found the total problem, including the scattering potential of the junction, is discussed.

By assuming that the electrodes are semi-infinite, and that they can be represented by a uniform background(jellium) model [4], the total effective potential of the electrodes, v_{eff}, can be reduced to a one dimensional parameter, $v_{eff}(z)$, where z is the position coordinate in the direction of the electron flow. [77, 74, 33, 32, 31, 12] $v_{eff}(z)$ contains both the electrostatic and exchange-correlation potential. The assumption of semi-infinite electrodes is reasonable since the electrodes are larger than the mean free path of the electrons and many orders of magnitude larger than the junction itself. For simplicity, let us assume zero temperature such that the Fermi-Dirac distributions describing the statistics of the electrons in the electrodes assume step function shapes. Further, let us assume that the potential deep inside the right/left electrode is constant at $V_{eff}(\infty)$ / $V_{eff}(-\infty)$. The wave functions can then develop three different forms, depending on the energy of the states of H_0. If the energy falls within $V_{eff}(\infty)$ and $V_{eff}(-\infty)$ (region 1 in Figure 2.2), the solutions consist of sine waves deep inside an electrode, which exponentially decay as they approach the edge of the electrode. For energies in between $V_{eff}(\infty)$ and E_{FL} (region 2 in Figure 2.2), the solutions are formed by plane waves incident from left and right electrodes, with transmitted and reflected waves from both incident waves. The final case, for energies, E, between E_{FL} and E_{FR} (region 3 in Figure 2.2), has wave functions made up of waves traveling from right to left electrode and their transmitted and reflected parts. [77, 74, 33, 32, 31, 12] This is the region giving rise to the current flow, and the states are of the form

$$\Psi^0_{E\mathbf{K}_\parallel}(\mathbf{r}) = e^{i\mathbf{K}_\parallel\cdot\mathbf{R}} u_{E\mathbf{K}_\parallel}(\mathbf{z}), \tag{2.65}$$

development, but are outside the scoop of this thesis [34, 13, 103].

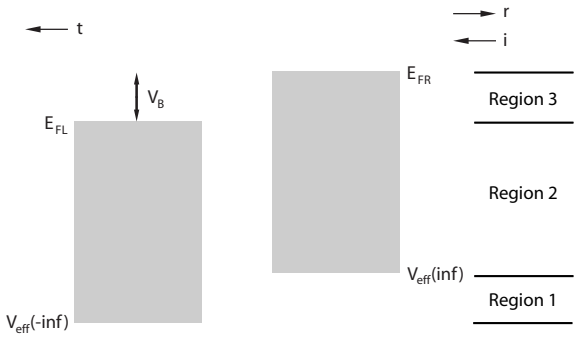


Figure 2.2: Schematic of two electrodes kept at a potential difference, V_B. Electrons incident from right are either reflected back with probability r or transmitted though with probability t. Regions 1 through 3 correspond to different solutions of this system, as discussed in further detail in the text.

satisfying the boundary conditions

$$u_{E\mathbf{K}_\parallel}(z) = (2\pi)^{3/2} k_R^{-1/2} \times \begin{cases} e^{-ik_R z} + Re^{ik_R z} & z \to \infty \\ Te^{-ik_L z} & z \to -\infty, \end{cases} \tag{2.66}$$

where $\mathbf{K}_\parallel$ is the momentum parallel to the electrode surface, $k_R^2 = 2E - |\mathbf{K}_\parallel|^2 - 2v_{eff}(\infty)$, $k_L^2 = 2E - |\mathbf{K}_\parallel|^2 - 2v_{eff}(-\infty)$ and $\mathbf{R}$ is the position perpendicular to z. Further Ψ^0 has to satisfy the continuum normalization condition

$$\int d^3\mathbf{r} \Psi^0_{E'\mathbf{K'}_\parallel}(\mathbf{r}) \cdot \mathbf{r} \Psi^0_{E_\parallel^{\mathbf{K}}}(\mathbf{r}) = \delta(E' - E)\delta(\mathbf{K'}_\parallel - \mathbf{K}_\parallel). \tag{2.67}$$

The electron density and potential can now be solved for self consistently using potentials from density functional theory [49, 61] within local density approximation [61].

Once the solution of the bare electrodes is known, we can focus on the total scattering problem, including the junction with the scattering potential V. By representing the atoms in the junction with pseudopotentials [5] and using density functional theory [49, 61] within local density approximation, [61] V can be written as

$$V(\mathbf{r}, \mathbf{r}') = v_{ps}(\mathbf{r}, \mathbf{r}') + \left[v_{xc}[n(\mathbf{r})] - v_{xc}[n^0(\mathbf{r})] + \int d^3\mathbf{r}'' \frac{\delta n(\mathbf{r}'')}{|\mathbf{r} - \mathbf{r}''|} \right] \delta(\mathbf{r} - \mathbf{r}'). \tag{2.68}$$

v_{ps} is the potential the electrons feel from the ions in the junction, represented with nonlocal pseudopotentials, [5] v_{xc} is the exchange-correlation potential, $n(\mathbf{r})$ is the

electronic density for the total system, $n^0(\mathbf{r})$ is the electronic density for the bare electrodes only and finally $\delta n(\mathbf{r}) = n(\mathbf{r}) - n^0(\mathbf{r})$. [77, 74, 33, 32, 31] While it is true that static density functional theory is derived for ground state calculations only, it has been shown that the dynamical correction to the conductance of a metallic junction is negligible and of the order of a few tenths of percent for a molecular junction. [103] Care should however be taken if the bias is large enough such that the system is outside the linear regime.

We wish to find the solutions to the Schrodinger equation $H\Psi_E = E\Psi_E$ with scattering boundary conditions. We write the Schrodinger equation with scattering boundary conditions in Lippman-Schwinger form [77, 74, 33, 32, 31]

$$\Psi_{E\mathbf{K}_\parallel}(\mathbf{r}) = \Psi^0_{E\mathbf{K}_\parallel}(\mathbf{r}) + \int d^3\mathbf{r}' d^3\mathbf{r}'' G^0_E(\mathbf{r},\mathbf{r}') V(\mathbf{r},\mathbf{r}') \Psi_{E\mathbf{K}_\parallel}(\mathbf{r}''), \tag{2.69}$$

which can be solved self consistently. [77, 74, 33, 32, 31] $\Psi_{E\mathbf{K}_\parallel}$ are the wave functions for the total systems and are, for sake of simplicity, labeled in same manner as $\Psi^0_{E\mathbf{K}_\parallel}$ despite that $\mathbf{K}_\parallel$ is not a good quantum number anymore. G^0_E is the Green's function for the bare electrodes and can be calculated from

$$[E + \frac{1}{2}\Delta^2 - v^0_{eff}(z)] G^0_E(\mathbf{r},\mathbf{r}') = \delta(\mathbf{r} - \mathbf{r}'). \tag{2.70}$$

The total electron density is finally given by [77, 74, 33, 32, 31]

$$n(\mathbf{r}) = 2\sum_i |\Psi_i(\mathbf{r})|^2 + 2\int dE \int d^2\mathbf{K}_\parallel |\Psi_{E\mathbf{K}_\parallel}(\mathbf{r})|^2, \tag{2.71}$$

where a factor of 2 is included due to spin degeneracy and Ψ_i are the wave functions of any bound states, which are found by direct diagonalization of H. The solution to this problem is then found by solving equations 2.68, 2.69 and 2.71 self-consistently.

Once the wave functions of the problem are known, a multitude of physical effects can be studied. These include, for example, the time averaged current over the junction [77, 74, 33, 32, 31], the shot noise of this current [18, 64], current induced forces [31, 122, 30] and local heating heating due to electron-phonon interactions [20, 121]. This dissertation however only cover the time averaged current and its noise due to charge quantization(shot noise).

The total, time averaged, current density of the system is given by [74, 33, 32, 31]

$$\mathbf{j}(\mathbf{r}) = -2\int_{E_{FL}}^{E_{FR}} dE \int d^2\mathbf{K}_{\|} Im\{[\Psi_{E\mathbf{K}_{\|}}(\mathbf{r})] * \Delta\Psi_{E\mathbf{K}_{\|}}(\mathbf{r})\}, \tag{2.72}$$

where the integral over $\mathbf{K}_{\|}$ is limited by $|\mathbf{K}_{\|}| \leq \sqrt{2[E - v_{eff}(\infty)]}$. However as the electrodes are semi-infinite, the total current for the system would be infinite due to tunneling in between the electrodes. Instead a more useful quantity to calculate is the *extra* current introduced to the system by the junction, as given by

$$\delta J = \int d^2\mathbf{R}\hat{z} \cdot [\mathbf{j}(\mathbf{r}) - \mathbf{j}^0(\mathbf{r})]. \tag{2.73}$$

It is worth noticing that the current has not been calculated using the Landauer formula introduced previously, but instead is calculated directly from the wave functions of the system via the current operator.

In this section we have developed a powerful tool which can be used to obtain the wave functions of an atomic scale system with open boundary conditions. Based on these wave functions, an expression for the shot noise is derived in the next chapter.

3

Shot Noise in Nanoscale Systems

In this chapter we first derive an expression for the shot noise of a nanoscale system directly from the wavefunctions of the system. We then report first-principles calculations of shot noise properties of parallel carbon wires in the regime in which the interwire distance is much smaller than the inelastic mean free path. We find that, with increasing interwire distance, the current approaches rapidly a value close to twice the current of each wire, while the Fano factor, for the same distances, is still larger than the Fano factor of a single wire. This enhanced Fano factor is the signature of the correlation between electron waves traveling along the two different wires. In addition, we find that the Fano factor is very sensitive to bonding between the wires, and can vary by orders of magnitudes by changing the interwire spacing by less than 0.5 Å. While these findings confirm that shot noise is a very sensitive tool to probe electron transport properties in nanoscale conductors, they also suggest that a considerable experimental control of these structures is required to employ them in electronics.

Finally, the validity of quantized transverse momenta in a nanoscale structure is discussed. In mesoscopic systems the quantum channels, which require a smooth matching of the electron gas in the reservoirs to the narrow region connected in between, are formed via leads. However, the validity of this assumption may be questioned in an atomic scale junction where an abrupt constriction is formed since the nanoscale junction is immediately adjacent to two large electrodes. Due to the lack of proper waveguides, the transverse momenta may not be quantized,

which can introduce mixing effects of the channels in the reservoirs. We discuss how the shot noise is affected by the quantum nature of the transverse momenta in ballistic regime. We demonstrate that the Fano factor may increase linearly with the number of well-separated parallel wires by interference effects through the reservoirs. This is in sharp contrast to the case of mesoscopic system, where the Fano factor is independent of the number of well-separated parallel wires.

3.1 Theoretical Approach

In the theory of mesoscopic systems, shot noise is generally expressed in terms of the transmission probabilities T_n of each conducting channel n. Instead of discussing shot noise in a system that carries an average current I, it is customary to report on the ratio (called Fano factor) between the shot noise and its Poisson (uncorrelated electrons) limit $2eI$, where e is the electron charge. For a two-terminal conductor the Fano factor can then be expressed, in linear response, as

$$F = \sum_n T_n \left(1 - T_n\right) / \sum_n T_n \tag{3.1}$$

as derived in the previous chapter.

However, we will not use the above expression (or its generalization to the non-linear case [8]). Instead, we will derive an expression of shot noise in terms of single-particle wavefunctions. [20] This choice is a convenient one: we calculate the latter quantities directly from the integral form of the Schrödinger equation within the density-functional theory of many-electron systems, [74, 32, 123] as shown in the previous chapter. We here derive such an expression [20] and demonstrate that it reduces to Eq. (3.1) when the transmission probabilities are extracted from the single-particle wavefunctions.

We start by introducing the field operator of propagating electrons for a sample connected to a left (L) and right (R) electrode in terms of single-particle wavefunctions $\Psi_E^{L(R)}\left(\mathbf{r}, \mathbf{K}_\parallel\right)$ with energy E (atomic units are used throughout this chapter) and component of the momentum parallel to the electrode surface $\mathbf{K}_\parallel$ [74, 32, 123]

$$\hat{\Psi} = \hat{\Psi}^L + \hat{\Psi}^R, \tag{3.2}$$

where

$$\hat{\Psi}^{L(R)} = \sum_{E} a_{E}^{L(R)}(t)\,\Psi_{E}^{L(R)}\left(\mathbf{r},\mathbf{K}_{\parallel}\right). \tag{3.3}$$

In this expression $a_{E}^{L(R)}(t) = \exp(-i\omega t)a_{E}^{L(R)}$, where $a_{E}^{L(R)}$ are the annihilation operators for electrons incident from the left (right) electrode, satisfying the usual anticommutation relations: $\{a_{E}^{i\dagger}, a_{E'}^{j}\} = \delta_{ij}\delta(E-E')$. We assume that the electrons coming from the left (right) electrode thermalize completely far away from the sample, i.e., the statistics of electrons coming from left (right) is determined by the equilibrium Fermi-Dirac distribution function $f_{E}^{L(R)}$ deep into the left (right) electrode, i.e.,

$$< a_{E}^{i\dagger} a_{E'}^{j} >= \delta_{ij}\delta(E-E')\,f_{E}^{i}, \tag{3.4}$$

with i, j=R, L.

In order to obtain the wave functions, $\Psi_{E}^{L(R)}(\mathbf{r},\mathbf{K}_{\parallel})$, we solve the Lippman-Schwinger equation self-consistently

$$\begin{aligned}\Psi_{E}^{L(R)}(\mathbf{r},\mathbf{K}_{\parallel}) &= \Psi_{0,E,\mathbf{K}_{\parallel}}^{L(R)}(\mathbf{r}) \\ &+ \int d\mathbf{r}_1 \int d\mathbf{r}_2 G(\mathbf{r},\mathbf{r_1}) V(\mathbf{r_1},\mathbf{r_2}) \Psi_{E}^{L(R)}(\mathbf{r_2},\mathbf{K}_{\parallel}).\end{aligned} \tag{3.5}$$

$\Psi_{0,E,\mathbf{K}_{\parallel}}^{L(R)}$ are the wave functions incident from the left (right) bare biased electrodes, and G is the corresponding Green's function. V is the difference between the potential of the total system and the one of the bare biased electrodes. It includes the sum of the nuclear, Hartree and exchange-correlation potentials. [74, 32, 123]

From the field operator Eq. (3.3) we can define the current operator

$$\hat{I}(z,t) = -i\int d\mathbf{R}\int d\mathbf{K}_{\parallel}\left(\hat{\Psi}^{\dagger}\partial_{z}\hat{\Psi} - \partial_{z}\hat{\Psi}^{\dagger}\hat{\Psi}\right). \tag{3.6}$$

The ensemble average current at zero temperature is thus

$$< \hat{I} >= -i\int_{E_{FL}}^{E_{FR}} dE \int d\mathbf{R}\int d\mathbf{K}_{\parallel}\left(\tilde{I}_{E,E}^{R,R}\right), \tag{3.7}$$

where

$$\tilde{I}_{E,E'}^{ij} = \left(\Psi_{E}^{i}\right)^{*}\nabla\Psi_{E'}^{j} - \nabla\left(\Psi_{E}^{i}\right)^{*}\Psi_{E'}^{j}, \tag{3.8}$$

with i, j=R, L. We have also assumed the right chemical potential to be higher than the left one.

The shot noise spectral density is defined as the Fourier transform of the current autocorrelation function

$$2\pi S(\omega) = \int dt e^{i\omega t} \left\langle \Delta\hat{I}(t)\, \Delta\hat{I}(0) \right\rangle, \tag{3.9}$$

where $\Delta\hat{I}(t)$ is the excess current operator with respect to the average current defined above. Using the Bloch-De Dominicis theorem [20] we can express $S(\omega)$ as

$$S(\omega) = \sum_{i,j=L,R} \int dE f^i_{E+\omega} \left(1 - f^j_E\right) \cdot \int d\mathbf{R}_1 \int d\mathbf{K}_1 \tilde{I}^{ij}_{E+\omega,E} \int d\mathbf{R}_2 \int d\mathbf{K}_2 \tilde{I}^{ji}_{E,E+\omega}. \tag{3.10}$$

Taking the zero frequency and zero temperature limit, the shot noise, S, can finally be written as [20]

$$S = \int_{E_{FL}}^{E_{FR}} dE \left| \int d\mathbf{R} \int d\mathbf{K} \tilde{I}^{LR}_{E,E} \right|^2, \tag{3.11}$$

where $\tilde{I}^{LR}_{E,E}$ is defined in Eq. (3.8).

In order to demonstrate that Eq. (3.11) reduces to Eq. (3.1) we consider only a single one-dimensional scattering channel. In this case the right- and left-moving waves satisfy the boundary conditions (with obvious notation)

$$\Psi^R_E = (2\pi)^{3/2} k_L^{-1/2} \times \begin{cases} e^{ik_L x} + R_L e^{-ik_L x} & x < -\infty \\ T_R e^{ik_R x} & x > \infty \end{cases} \tag{3.12}$$

and

$$\Psi^L_E = (2\pi)^{3/2} k_R^{-1/2} \times \begin{cases} T_L e^{-ik_L x} & x < -\infty \\ e^{-ik_R x} + R_R e^{ik_R x} & x > \infty, \end{cases} \tag{3.13}$$

respectively.

Introducing the above expressions into Eq. (3.8) and re-writing Eq. (3.11) as

$$S(x_1, x_2) = \int_{E_{FL}}^{E_{FR}} dE \hat{I}^{RL}_{EE}(x_1) \hat{I}^{LR}_{EE}(x_2), \tag{3.14}$$

we can define $S^{ij} = S(x_1 \to \pm\infty, x_2 \to \pm\infty)$, with i, j=R, L. We thus obtain that (with $T_R = T_L = T$)

$$S^{LL} = \frac{V_0}{\pi} T(1 - T), \tag{3.15}$$

where we have implicitly assumed that $E_{FR} - E_{FL} = eV_0$, where V_0 is the external bias, and T is independent of energy. For $T \ll 1$ we obtain the Poisson limit of shot noise $S^P = \frac{V_0}{\pi}T$. Taking the ratio of Eq. (3.15) with S^P leads to Eq. (3.1). Similarly we can prove that the following relations are valid [8]

$$S^{LL} = S^{RR} = -S^{RL} = -S^{LR}, \tag{3.16}$$

as a direct consequence of current conservation.

As a test of Eq. (3.11) we have calculated the noise for a single gold atom between two bulk electrodes modeled by jellium with $r_s = 3$. The gold atom is placed at 2.2 a.u. from each jellium edge. For a bias of $0.1V$ we obtain a conductance of $1.1G_0$ ($G_0 = 2e^2/h$) and a Fano factor of 0.14. Experimental results on gold point contacts indicate that to such value of conductance corresponds a Fano factor of 0.16 ± 0.03, [113] indicating a good agreement between theory and experiment in the present case.

3.2 Shot Noise in Parallel Wires

In recent years we have witnessed an increased interest in the transport properties of molecules sandwiched between two bulk electrodes. [119, 63, 25, 36, 101, 118, 16, 111, 27, 93, 102, 127, 96, 32, 42] This interest is partly motivated by the possible use of such structures in future electronic applications, and partly by the desire to understand electronic transport in atomic scale conductors. In most of the experiments reported so far the number of molecules sandwiched between two bulk electrodes is unknown. [119, 25, 36, 111, 27, 93, 102, 127, 63, 101, 118, 16] Even in experiments where this number is supposedly very small [119, 25, 36, 111, 27, 93, 102, 127] it is still unclear whether a single molecule is responsible for the reported current-voltage (I-V) characteristics or if many molecules contribute. [33, 37] Irrespective of this issue, future electronic applications of molecular wires will likely require assembly of many components with interwire separations at the nanometer scale. At these distances electrons are less likely to experience inelastic scattering events so that quantum interference between electron waves traveling in adjacent

wires dominates. We can therefore expect that the transport properties of an ensemble of coupled wires are not necessarily a simple superposition of the transport properties of each isolated wire. [75] Past work has indeed addressed this issue by studying the electric current in parallel atomic-scale wires as a function of their separation. [120, 85, 75] For instance, Lang and Avouris have found large variations of the low-bias conductance of two carbon wires connected in parallel to bulk electrodes as a function of their separation. [75] These variations have been attributed to both a direct bonding between the wires and an indirect interaction due to the presence of the metal electrodes. [75]

In this section we want to build on the knowledge gained from these earlier studies and investigate a related transport property: steady-state current fluctuations (shot noise) in parallel wires. Our motivation is twofold: for one, current fluctuations need to be small for nanoscale components to have practical applications. Understanding the magnitude of these fluctuations in single wires and to what extent interference effects between coupled wires modify shot noise is therefore paramount to progress in nanoscale electronics. Secondly, shot noise contains more information on the transport properties of particles than the average current.[8] In the case of electrons, for instance, shot noise provides information on their energy distribution [11], kinetics, [72] and interactions due to the Coulomb repulsion and the Pauli exclusion principle [83]. Shot noise has also been found to depend on the atomic details of nanoscale wires like their length and coupling to bulk electrodes. [20] All these studies suggest that shot noise is a very sensitive tool to study electron transport properties in nanoscale conductors and we hope that our work will motivate further experimental work in this direction.

To the best of our knowledge very few reports have appeared in literature on the shot noise properties of parallel conductors connected to bulk electrodes. [50, 41, 59] All of them employ simple models of the electronic structure of the system and/or of the current correlations on each electrode. [50, 41, 59] For instance, Iannaccone *et al.* have shown that if an electron transmitted from one wire in a given lead does not enter the adjacent wire on the same lead, then the shot noise of each wire adds classically to give a Fano factor equal to the Fano factor of one wire. [50]

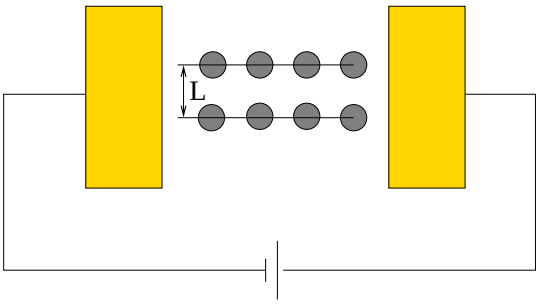


Figure 3.1: Schematic of the system investigated. It consists of two parallel wires, separated by a distance L, between two biased electrodes.

We call this case an "uncoupled-wire" situation. However, when the distance between the wires is few nanometers it is unlikely that the above case can occur: any phase-breaking process (whether it is due to inelastic scattering, quasi-elastic dephasing or electron-electron scattering) would not be enough to break completely the correlation between waves traveling along the two distinct wires. The shot noise of the total system, therefore, should not be a simple classical summation of noise of each individual component. This is precisely the physical situation we want to investigate here.

Following the work of Lang and Avouris [75] we study the transport properties of a system comprising two carbon wires of different lengths (also known as cumulene carbon atom chains) between two bulk electrodes (see schematic in Fig. 3.1). The bulk electrodes are modeled with a semi-infinite uniform-background model (jellium model). [74, 32, 123] The interior electron density of the electrodes is taken close to the value for metallic gold ($r_s \approx 3$). Note that in the work reported in Ref. [75] the interior electron density of the electrodes has been chosen to have $r_s \approx 2$. Therefore, the actual shape of the conductance as a function of inter-wire distance is different than the one reported in the present work. However, the physical trends are similar.

The cumulene-chain system is structurally and electronically quite simple, such that the first-principles calculations reported here can be done with a relatively high level of accuracy. In addition, cumulene atom chains can be loosely identified as the smallest "carbon nanotubes" possible. The results presented in this work

can thus bear some relevance in nanotube electronics. We find, in agreement with previous reports, [75] that the current varies with interwire distance and saturates to a value close to twice the current of each wire with increasing wire separation. On the other hand, the Fano factor can vary by orders of magnitudes by changing the interwire spacing by less than 0.5 Å. Furthermore, when the current is very close to the value of twice the current of each wire, the Fano factor is still larger than the Fano factor of a single wire. This enhanced Fano factor is the signature of the correlation between electron waves traveling along the two different wires. At the distances considered here, this correlation is unlikely to be destroyed by inelastic scattering effects, therefore this effect should be observed in parallel nanoscale wires.

We will consider two different wire lengths: 4-atom chains and 5-atom chains. In each wire, the C-C distance has been fixed at 2.5 a.u. and, due to the construction of the jellium model, [76] the end carbon atoms of the chains are 1.4 a.u. inside the positive background edge of jellium. [75] The value of the external bias is $V = 0.01V$. The conductance in units of G_0 (top) and Fano factor (bottom) for these two systems as a function of the interwire distance are plotted in Figs. 3.2 and 3.3. In order to keep the same numerical error in the calculation of current and noise for all interwire distances, and due to computational limits, we could not evaluate these quantities for distances larger than about 6.5 a.u. In these figures we report both the actual data points (filled squares) calculated from first principles and an interpolation in between the data points (solid line). We also indicate in the figures the "uncoupled-wire" case for both the current (twice the current of each independent wire, i.e. without any wire-wire interaction) and Fano factor (equal to the Fano factor of each wire - the current doubles as well the noise, leaving the ratio unchanged). It is immediately evident from both figures that both the current and the Fano factor change in a non-linear way with interwire distance. However, the variation of noise is even more dramatic. We discuss the current first.

It is clear from Figs. 3.2 and 3.3 that the conductance variation depends on the length of the carbon wires. For instance, the conductance reaches a value of about

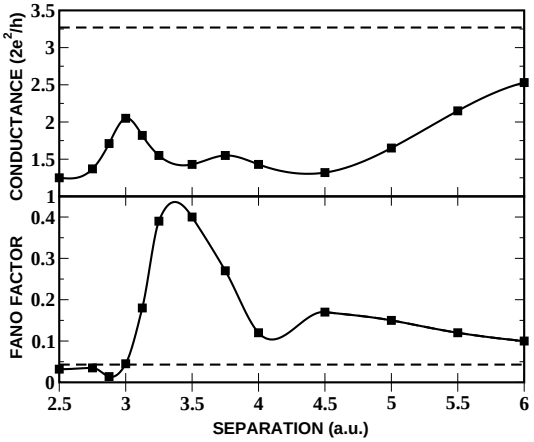


Figure 3.2: Conductance (upper panel), in units of quantum of conductance G_0, and Fano factor (lower panel) as a function of wire separation for two parallel 4-atom wires. Filled squares correspond to calculated values. Horizontal broken lines correspond to twice the conductance of a single wire (upper panel) and the Fano factor of a single wire (lower panel).

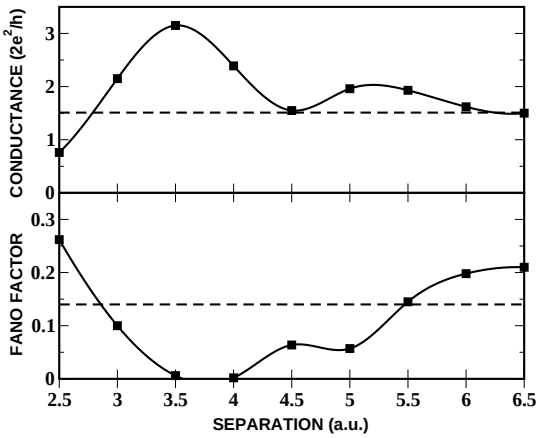


Figure 3.3: Conductance (upper panel), in units of quantum of conductance G_0, and Fano factor (lower panel) as a function of wire separation for two parallel 5-atom wires. Filled squares correspond to calculated values. Horizontal broken lines correspond to twice the conductance of a single wire (upper panel) and the Fano factor of a single wire (lower panel).

twice the conductance of each independent wire at about 6.5 a.u. for the 5-atom chain, while this is not the case for the 4-atom chain. In addition, the conductance of the system at infinite distance (i.e. in the absence of wire-wire interactions) is larger for the 4-atom wire than for the 5-atom wire. This difference is related to the fact that even-atom-number wires have fully occupied π states, while the odd-atom-number wires have a half-filled π state at the Fermi level. [75, 20] Note, however, that the band width of the metal electrodes (determined by the value of r_s) is much smaller in the present case than the one used in Ref. [75]. This implies that the extra σ and π states introduced by the coupling of the wires to the electrodes are truly bound states in our case, thus effectively reverting the trend of the change of conductance as a function of wire length: in the present case, the conductance (for large interwire separations) is larger for even number of carbon atoms than for odd number of carbon atoms. Finally, the change in conductance is related to the detailed bonding properties of the parallel wires. [75]

It is evident in Fig. 3.2 and Fig. 3.3 that there is a correlation between the change in conductance as a function of interwire distance and the corresponding change in Fano factor. In general, whenever the conductance increases the Fano factor decreases, as can be understood intuitively from Eq. (3.1). However, the Fano factor is more affected by the interwire interaction than the conductance. We therefore discuss the bonding properties in connection to the Fano factor. In order to do so we show contour plots of the charge density. The charge density we consider is the one due to the populated global current-carrying states originating from the right electrode for the system with the carbon atoms, minus the same quantity for the electrode-electrode system without the atoms. For the 4-carbon wire this quantity is plotted in Fig. 3.4 for a wire distance of about 2.9 a.u. (top) and 3.3 a.u. (bottom), i.e. for the case in which the noise is minimum (even lower than the value for the "uncoupled-wire" case) and maximum, respectively (see also Fig. 3.2). It is evident from Fig. 3.4 (top) that at 2.9 a.u. the wires form two symmetric σ bonds from each carbon p orbital oriented parallel to the electrode surface and in the plane where the centers of all C atoms lie. These two σ bonds link the four carbon atoms between the jellium edges as shown in

Fig. 3.4 (top). In this configuration, electron waves travel from one electrode to the other as if the structure had two perfectly (degenerate) open channels (the value of the conductance in this case is also close to two, see Fig 3.2). We stress however that this is only an analogy and does not necessarily imply that the number of open global channels in the structure is exactly two. On the other hand, at a distance of 3.3 a.u. (bottom of Fig. 3.4), there is more redistribution of charge from the interchain σ bonds to the π bonds along each wire, thus increasing backscattering and the correlation between electron waves on each side of the structure. This feature is also present (even if at different distances) for the 5-atom chain. In this case, the formation of three quasi-degenerate σ bonds extends from about 3.5 a.u. to about 3.7 a.u. giving rise to a conductance of about $3G_0$ and a (almost) zero Fano factor in the same range (see Fig. 3.3). The Fano factor is thus very sensitive to wire-wire interactions, and in particular to the charge redistribution between bonds. Since even small charge redistributions can increase or reduce backscattering, the Fano factor can change by simply changing the interwire distance by less than 0.5Å.

When the two wires are separated by a relatively large distance, the wire-wire interaction is negligible and the current reaches a value close to twice the value of the current of each wire. However, correlations between waves traveling in the two different wires do not necessarily go to zero, and this would affect the noise. This can be understood by looking at the contour plot of the charge density (as defined above) for a 5-C wire at interwire distance of 6.5 a.u. (Fig. 3.5). At this distance the conductance is almost exactly twice the value of the conductance of each wire (see Fig. 3.2). However, the Fano factor is still *larger* than the Fano factor of each wire. This is because, even though there is essentially no bonding between the carbon atoms of the two wires (see Fig. 3.5), there is still some probability for a wave that gets out of a wire on one side of the junction to travel *along* the surface of the electrode and get reflected back into the other wire from the same side of the junction. In other words, the global current-carrying wavefunctions have finite extension in the surface region between the wires. Indeed, for large wire separations, the lateral component of the scattering wavefunctions resembles

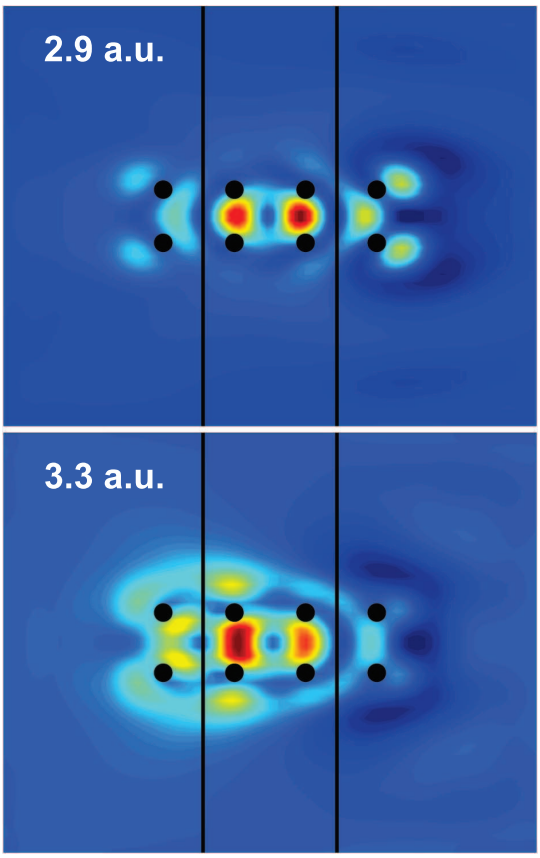


Figure 3.4: Contour plot of the charge density for the 4-atom wire system at two different interwire distances. See text for the explicit definition of this density. Vertical black lines correspond to the edges of the jellium model and circles correspond to atomic positions.

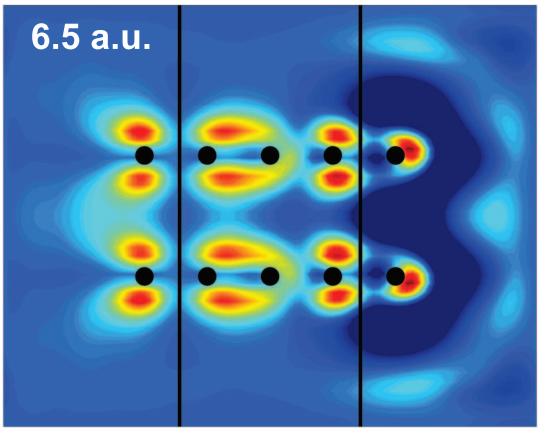


Figure 3.5: Contour plot of the charge density for the 5-atom wire system at inter-wire distance of 6.5 a.u. See text for the explicit definition of this density. Vertical black lines correspond to the edges of the jellium model and circles correspond to atomic positions.

closely a Bloch wave within few atomic units from the surface region in between the wires. This wavefunction extension thus generates extra noise compared to the "uncoupled-wire" case. An alternative and intuitive way of thinking about this point is the following: at large wire separations, the different paths along which an electron is carried from one lead to the other across either one of the two single wires, have energies that are quasi-degenerate. The system thus fluctuates fast between these quasi-degenerate states and additional noise is generated (in a manner similar to the generation of telegraph noise). Clearly, such correlations would be destroyed if inelastic effects were into play. However, as explained above, for the distances considered here these effects are less likely to contribute.

3.3 Interference Effects of Transverse Channels

In mesoscopic systems, it is assumed that the scattering structure itself is connected to reservoirs via wave guides, or leads, as schematically shown in Figure 3.6a. The reservoirs are assumed to be large enough that inelastic scattering occurs within them and are also assumed to be connected to the leads adiabatically. Then all modes, or channels, generated by the wave guides are incoherent with

each other. Thus, interference effects between different input channels can be neglected. [14] Under these assumptions, electrons relevant in transport can adjust themselves in the ideal leads and restore their quantized momentum. In this case the shot noise, S, can be expressed, in terms of the transmission probabilities of each channel, T_n, as $S \propto \sum_n T_n (1 - T_n)$ which is derived in the previous chapter. The above expression requires incoherent electrons in the leads and is generally valid for a mesoscopic system with a smooth matching of the electrodes to the narrow region of the quantum point contact. However, the validity of this assumption may be questioned in an atomic scale junction(shown in Figure 3.6b) where the electrodes are immediately adjacent to the junction. Due to the lack of wave guides which can quantize the momenta in the direction transverse to electron flow, energy would be the only quantum number. As a consequence, interference effects between different input channels may be important.

In this section we discuss the validity of these assumptions and derive equations for the shot noise for cases both when the probes are close to the junction, so that no restoration of transverse momenta can occur (as in previous section), and when the electrodes are further away, so that transverse momenta can be restored via physical effects in the electrodes. We also show that interference effects of transverse modes will cause drastic change in the nature of shot noise, while the current will not significantly be affected. Finally, we discuss the effect these assumptions have on the shot noise in nanoscale devices built in parallel.

The effective single-particle wave functions are calculated self-consistantly within the framework of density-functional theory of many-electron systems utilizing local density approximation, [74, 33, 32, 123] as in previous sections. The wave functions of the total system including any atoms sandwiched in between two planar electrodes, modeled jellium, are then calculated self-consistently in Lippman-Schwinger form:

$$\begin{aligned} \Psi_{E\mathbf{K}}^{L(R)}(\mathbf{r}) &= \Psi_{0,E,\mathbf{K}}^{L(R)}(\mathbf{r}) \\ &\quad + \int d\mathbf{r}_1 \int d\mathbf{r}_2 G(\mathbf{r},\mathbf{r}_1)\, V(\mathbf{r}_1,\mathbf{r}_2)\, \Psi_{E\mathbf{K}}^{L(R)}(\mathbf{r}_2), \end{aligned} \tag{3.17}$$

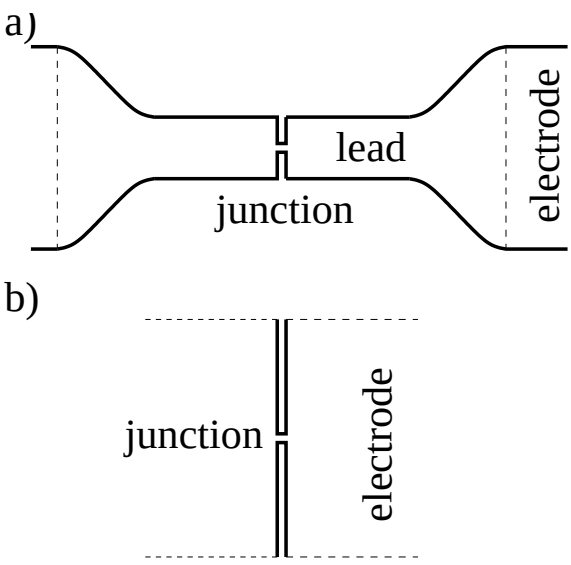


Figure 3.6: Schematic of a) a mesoscopic junction and b) a nanoscale junction. The mesoscopic junction in constructed by a junction connected to the electrodes via well defined leads, which act as wave guides. The nano-scale junction lacks the leads as the junction rapidly opens up into the electrodes. This causes the junction to be connected directly to the leads.

where $\Psi^{L(R)}_{0,E,\mathbf{K}}(\mathbf{r}) = \chi_{\mathbf{K}}(\mathbf{R})\, u^{L(R)}_{E\mathbf{K}}(z)$ are the scattering wave functions, for the electrodes corresponding to propagating electrons incident from the left (right) electrode in the absence of the scattering potential $V(\mathbf{r}_1, \mathbf{r}_2)$. G is the corresponding Green's function, and $\mathbf{R}$ and z are the coordinates parallel and perpendicular to the electrode surface, respectively.

For a nanoscale junction sandwiched in between two large electrodes, one may assume that energy is the only eigenstate of the system. Since the system is lacking a well-defined wave guide between electrodes and junction, when probes are immediately adjacent to junction, the propagating electrons would not be able to self-adjust themselves and restore the quantization of momentum in the direction transverse to the electron flow. In such case transverse momentum $\mathbf{K}$ is no longer a conserved quantity and should be treated as an argument in the wave function to be integrated out. Identical to the previous section, we can thus introduce a field operator describing propagating electrons incident from the left and right electrodes in terms of the effective single-particle wave functions $\Psi^{L(R)}_{E}(\mathbf{r}, \mathbf{K})$ with

energy E and $\mathbf{K}$ as the eigenstate and the component of momentum parallel to the electrode surface as the argument in the wave function

$$\hat{\Psi} = \sum_{\alpha,E} a_E^{\alpha}(t)\, \Psi_E^{\alpha}(\mathbf{r}, \mathbf{K}), \tag{3.18}$$

where $a_E^{L(R)}(t) = \exp(-i\omega t) a_E^{L(R)}$. The vector $\mathbf{K}$ as level in wave function is absent in the annihilation operators $a_E^{L(R)}$, representing the destruction of an electron with eigenenergy E incident from the left (right) electrode. The creation and annihilation operators satisfy the usual anticommutation relations

$$\{a_{E_1}^{\alpha\dagger}, a_{E_2}^{\beta}\} = \delta_{\alpha\beta}\delta(E_1 - E_2), \tag{3.19}$$

and the statistical expectation value of the product of creation and annihilation operator is given by

$$< a_{E_1}^{\alpha\dagger} a_{E_2}^{\beta} >= \delta_{\alpha\beta}\delta(E_1 - E_2)\, f_E^{\alpha}, \tag{3.20}$$

where we assume that the statistics of electrons coming from the left (right) electrodes is determined by the equilibrium Fermi-Dirac distribution function $f_E^{L(R)}$ in the left (right) reservoir. The current operator can be expressed in a standard way,

$$\hat{I}(z,t) = \frac{e\hbar}{mi} \int d\mathbf{R} \int d\mathbf{K} \left[\hat{\Psi}^{\dagger}\partial_z\hat{\Psi} - \partial_z\hat{\Psi}^{\dagger}\hat{\Psi}\right], \tag{3.21}$$

where $\hat{\Psi}$ is the field operator as described in equation (3.18); the transverse momenta $\mathbf{K}$ has already been integrated out in equation (3.21). The current operator can be expressed alternatively in the following form

$$\begin{aligned} \hat{I}(z,t) &= \frac{e\hbar}{mi} \sum_{E_1 E_2} \sum_{\alpha\beta} \int d\mathbf{R} \int d\mathbf{K} \\ &\quad e^{i(E_1 - E_2)t/\hbar} a_{E_1}^{\alpha\dagger} a_{E_2}^{\beta} \tilde{I}_{E_1,E_2}^{\alpha\beta}(\mathbf{r}, \mathbf{K}), \end{aligned} \tag{3.22}$$

where

$$\tilde{I}_{E_1,E_2}^{\alpha\beta}(\mathbf{r}, \mathbf{K}) = \left(\Psi_{E_1}^{\alpha}\right)^* \nabla\Psi_{E_2}^{\beta} - \nabla\left(\Psi_{E_1}^{\alpha}\right)^* \Psi_{E_2}^{\beta},$$

and $\Psi_E^{L(R)}$ are the effective single-particle wave functions. By using the quantum statistical average of the product of electron creation and annihilation operator given by equation (3.20), the average current at zero temperature is

$$< \hat{I} >= \frac{e\hbar}{mi} \int_{E_{FL}}^{E_{FR}} dE \int d\mathbf{R} \int d\mathbf{K} \tilde{I}_{E,E}^{RR}(\mathbf{r}, \mathbf{K}) \,. \tag{3.23}$$

We now proceed further to consider the autocorrelation of the current operator. In case with probes immediately adjacent to the nanostructure such that no well-defined wave guide is available, the current-current correlation operator can be expressed as

$$\begin{aligned} \hat{I}(z_1, t_1)\hat{I}(z_2, t_2) = \left(\frac{e\hbar}{mi}\right)^2 \sum_{E_1,\ldots,E_4} e^{i(E_1-E_2)t_1/\hbar + i(E_3-E_4)t_2/\hbar} \\ \cdot \left[\sum_{i,j=L,R} a_{E_1}^{i\dagger} a_{E_2}^{j} \int d\mathbf{R}_1 \int d\mathbf{K}_1 \tilde{I}_{E_1,E_2}^{ij}(\mathbf{r}_1, \mathbf{K}_1)\right] \\ \cdot \left[\sum_{k,l=L,R} a_{E_3}^{k\dagger} a_{E_4}^{l} \int d\mathbf{R}_2 \int d\mathbf{K}_2 \tilde{I}_{E_3,E_4}^{kl}(\mathbf{r}_2, \mathbf{K}_2)\right] . \end{aligned} \tag{3.24}$$

In order to consider the fluctuations of current away from their averaged value, we introduce the operator $\triangle\hat{I}(t) = \hat{I}(t) - \left\langle \hat{I} \right\rangle$ and consider the noise spectral function

$$S(\omega) = \int d(t_1 - t_2) e^{i\omega(t_1-t_2)} \left\langle \triangle\hat{I}(t_1)\triangle\hat{I}(t_2) \right\rangle . \tag{3.25}$$

To explicitly carry out the average of current-current correlation, we need the quantum statistical expectation value of products of $a_{E_1}^{i\dagger} a_{E_2}^{j} a_{E_3}^{k\dagger} a_{E_4}^{l}$. For a Fermi electron gas at equilibrium the quantum statistical expectation values of products of four operators are given by Bloch-De Dominicis theorem:

$$\begin{aligned} \left\langle a_{E_1}^{i\dagger} a_{E_2}^{j} a_{E_3}^{k\dagger} a_{E_4}^{l} \right\rangle &= \left\langle a_{E_1}^{i\dagger} a_{E_2}^{j} \right\rangle \left\langle a_{E_3}^{k\dagger} a_{E_4}^{l} \right\rangle \\ &\quad - \left\langle a_{E_1}^{i\dagger} a_{E_4}^{l} \right\rangle \left\langle a_{E_2}^{j} a_{E_3}^{k\dagger} \right\rangle . \end{aligned} \tag{3.26}$$

From Bloch-De Dominicis theorem together with the current autocorrelation operators given by equation 3.24, we can derive the shot noise spectral function:

$$S(\omega) = 2\pi\hbar \left(\frac{e\hbar}{mi}\right)^2 \sum_{\alpha,\beta=L,R} \int dE f^{\alpha}_{E+\hbar\omega} \left(1 - f^{\beta}_{E}\right)$$
$$\cdot \int d\mathbf{R}_1 \int d\mathbf{R}_2 \int d\mathbf{K}_1 \int d\mathbf{K}_2$$
$$\cdot \tilde{I}^{\alpha\beta}_{E+\hbar\omega,E}(\mathbf{r}_1, \mathbf{K}_1)\, \tilde{I}^{\beta\alpha}_{E,E+\hbar\omega}(\mathbf{r}_2, \mathbf{K}_2). \tag{3.27}$$

For the shot noise spectral function at $\omega = 0$ we obtain the shot noise

$$S = 2\pi\hbar \left(\frac{e\hbar}{mi}\right)^2 \int_{E_{FL}}^{E_{FR}} dE \left| \int d\mathbf{R} \int d\mathbf{K} \tilde{I}^{LR}_{E,E}(\mathbf{r}, \mathbf{K}) \right|^2, \tag{3.28}$$

following by the symmetry of $\tilde{I}^{\alpha\beta}_{E+\hbar\omega,E} = -\tilde{I}^{\beta\alpha}_{E,E+\hbar\omega}$.

The shot noise formula given by equation (3.28) is derived within the assumption that transverse momentum $\mathbf{K}$ is not a good quantum number describing the electrons relevant in the transport. In contrast to the above assumption for atomic scale junction with the probes located nearby the nanostructure, the quantization of the transverse momentum $\mathbf{K}$ can be restored within an adiabatic constriction where electrons can adjust themselves to restore quantization in transverse direction in the smooth connection between nano-structure and reservoirs. In this case, the field operators assume the form

$$\hat{\Psi} = \sum_{\alpha,E,\mathbf{K}} a^{\alpha}_{E\mathbf{K}}(t)\, \Psi^{\alpha}_{E\mathbf{K}}(\mathbf{r}), \tag{3.29}$$

where $a^{L(R)}_{E\mathbf{K}}(t) = \exp(-i\omega t) a^{L(R)}_{E\mathbf{K}}$ and $a^{L(R)}_{E\mathbf{K}}$ is the annihilation operators representing the destruction of an electron with eigenenergy E and momentum $\mathbf{K}$ incident from the left (right) reservoir, satisfying the anticommutation relations

$$\{a^{\alpha}_{E_1\mathbf{K}_1}, a^{\beta\dagger}_{E_2\mathbf{K}_2}\} = \delta_{\alpha\beta}\delta(E_1 - E_2)\,\delta(\mathbf{K}_1 - \mathbf{K}_2). \tag{3.30}$$

The expectation value of the product of electron creation and annihilation operator at thermal equilibrium is given by

$$< a^{\alpha\dagger}_{E_1\mathbf{K}_1} a^{\beta}_{E_2\mathbf{K}_2} >= \delta_{\alpha\beta}\delta(E_1 - E_2)\,\delta(\mathbf{K}_1 - \mathbf{K}_2) f^{\alpha}_{E}, \tag{3.31}$$

where we have assumed that the statistics of electrons coming from the left (right) electrodes is determined by the equilibrium Fermi-Dirac distribution function $f_E^{L(R)}$ in the left (right) reservoir. The interference effects of transverse channels are disabled by the orthonormality in momentum $\mathbf{K}$. It follows that the current operator can be expressed as

$$\begin{aligned}\hat{I}(z,t) &= \frac{e\hbar}{mi}\sum_{E_1E_2}\sum_{\alpha\beta}\int d\mathbf{R}\int d\mathbf{K}_1\int d\mathbf{K}_2 \\ &\quad \cdot e^{i(E_1-E_2)t/\hbar}a^{\alpha\dagger}_{E_1\mathbf{K}_1}a^{\beta}_{E_2\mathbf{K}_2}\tilde{I}^{\alpha\beta}_{E_1\mathbf{K}_1,E_2\mathbf{K}_2}(\mathbf{r}),\end{aligned} \tag{3.32}$$

where

$$\tilde{I}^{\alpha\beta}_{E_1\mathbf{K}_1,E_2\mathbf{K}_2}(\mathbf{r}) = \left(\Psi^{\alpha}_{E_1\mathbf{K}_1}\right)^* \nabla\Psi^{\beta}_{E_2\mathbf{K}_2} - \nabla\left(\Psi^{\alpha}_{E_1\mathbf{K}_1}\right)^*\Psi^{\beta}_{E_2\mathbf{K}_2}.$$

Applying the quantum expectation value of the product of electron creation and annihilation operator in equation (3.31), the average of current at zero temperature is then given by

$$<\hat{I}>=\frac{e\hbar}{mi}\int_{E_{FL}}^{E_{FR}}dE\int d\mathbf{R}\int d\mathbf{K}\tilde{I}^{R,R}_{E\mathbf{K},E\mathbf{K}}(\mathbf{r}), \tag{3.33}$$

which is exactly the same as the averaged current described by equation (3.20). Hence, whether the transverse momentum, $\mathbf{K}$, is a good quantum number in the creation and annihilation operators does not affect the current.

In sharp contrast to the averaged current, which is not modified by the quantum statistics of electrons, shot noise is sensitive to whether the transverse momentum, $\mathbf{K}$, involves the quantum statistics expectation value. If the system consists of a well-defined wave guide, it will restore the transverse modes as good quantum number before reaching the probes detecting shot noise. In this case the quantum statistical expectation value at equilibrium for the products of four operators is given by

$$\begin{aligned}\left\langle a^{i\dagger}_{E_1\mathbf{K}_1}a^{j}_{E_2\mathbf{K}_2}a^{k\dagger}_{E_3\mathbf{K}_3}a^{l}_{E_4\mathbf{K}_4}\right\rangle &= \left\langle a^{i\dagger}_{E_1\mathbf{K}_1}a^{j}_{E_2\mathbf{K}_2}\right\rangle\left\langle a^{k\dagger}_{E_3\mathbf{K}_3}a^{l}_{E_4\mathbf{K}_4}\right\rangle \\ &\quad -\left\langle a^{i\dagger}_{E_1\mathbf{K}_1}a^{l}_{E_4\mathbf{K}_4}\right\rangle\left\langle a^{j}_{E_2\mathbf{K}_2}a^{k\dagger}_{E_3\mathbf{K}_3}\right\rangle.\end{aligned} \tag{3.34}$$

Applying the above quantum statistics expectation value, we can derive the shot noise spectral function which has the following form:

$$S(\omega) = 2\pi\hbar \left(\frac{e\hbar}{mi}\right)^2 \sum_{\alpha,\beta=L,R} \int dE f^{\alpha}_{E+\hbar\omega} \left(1 - f^{\beta}_{E}\right) \cdot \int d\mathbf{R}_1 \int d\mathbf{R}_2 \int d\mathbf{K}_1 \int d\mathbf{K}_2 \tilde{I}^{\alpha\beta}_{E+\hbar\omega\mathbf{K}_1, E\mathbf{K}_2}(\mathbf{r}_1)\, \tilde{I}^{\beta\alpha}_{E\mathbf{K}_1, E+\hbar\omega\mathbf{K}_2}(\mathbf{r}_2). \tag{3.35}$$

For DC steady state current at zero temperatures the quantum fluctuation of current is given by the shot noise spectral function at $\omega = 0$:

$$S = 2\pi\hbar \left(\frac{e\hbar}{mi}\right)^2 \int_{E_{FL}}^{E_{FR}} dE \int d\mathbf{K}_1 \int d\mathbf{K}_2 \left| \int d\mathbf{R} \tilde{I}^{LR}_{E\mathbf{K}_1, E\mathbf{K}_2}(\mathbf{r}) \right|^2, \tag{3.36}$$

following by the symmetry of $\tilde{I}^{\alpha\beta}_{E+\hbar\omega,E} = -\tilde{I}^{\beta\alpha}_{E,E+\hbar\omega}$.

The role of the transverse momenta, $\mathbf{K}$, in the quantum expectation value of discrete electrons leads to two different type of shot noise formulas, given by equation (3.28) and equation (3.36). When the system lacks wave guides such that the transverse momentum, $\mathbf{K}$, is not a good quantum number, shot noise is affected by the interference effects between transverse momentum formula due to channel mixing. In the following example we illustrate the role of interference effect and how it affects shot noise. For simplicity we consider wave functions which are presumedly separable in transverse and longitudinal component with the form of $\Psi^{\alpha}_{E,\mathbf{K}}(\mathbf{r}) = \chi_{\mathbf{K}}(\mathbf{R})\, u^{\alpha}_{E\mathbf{K}}(z)$, where $\chi_{\mathbf{K}}(\mathbf{R})$ is the transverse wave functions satisfying orthonormal conditions

$$\int d\mathbf{R} \chi^{*}_{\mathbf{K}_1}(\mathbf{R})\, \chi_{\mathbf{K}_2}(\mathbf{R}) = \delta(\mathbf{K}_1 - \mathbf{K}_2), \tag{3.37}$$

and $u^{\alpha}_{E\mathbf{K}}(z)$ is the wave function along z-direction. Deep inside the electrodes ($z \to \pm\infty$), the right- and left- moving waves satisfy scattering boundary conditions

$$u^{L}_{E\mathbf{K}}(z) = \sqrt{\frac{m}{2\pi\hbar^2 k_L}} \times \begin{cases} e^{ik_L x} + R_L e^{-ik_L x} & x < -\infty \\ T_L e^{ik_R x} & x > \infty \end{cases} \tag{3.38}$$

and

$$u^R_{E\mathbf{K}}(z) = \sqrt{\frac{m}{2\pi\hbar^2 k_R}} \times \begin{cases} T_R e^{-ik_L x} & x < -\infty \\ e^{-ik_R x} + R_R e^{ik_R x} & x > \infty, \end{cases} \tag{3.39}$$

where $\frac{\hbar^2 k_R^2}{2m} = E - \frac{\hbar^2 \mathbf{K}^2}{2m} - v_{eff}(\infty)$ and $\frac{\hbar^2 k_L^2}{2m} = E - \frac{\hbar^2 \mathbf{K}^2}{2m} - v_{eff}(-\infty)$. $v_{eff}(\pm\infty)$ is the bottom of band deep inside right/left electrodes. The above wave functions lead to different expressions for the shot noise, depending on if calculated with equation (3.28) or (3.36). In the case where $\mathbf{K}$ is not a good quantum number, the Fano factor, defined as $F = S/2eI$, is given by

$$F = \frac{\int_{E_{FL}}^{E_{FR}} dE \left| \int d\mathbf{K} T_L^* R_R \right|^2}{\int_{E_{FL}}^{E_{FR}} dE \int d\mathbf{K} \left| T_R \right|^2}, \tag{3.40}$$

where the integration of the transverse momenta $\mathbf{K}$ are performed before the square which lead to interference between parallel channels. The interference effects are due to the absence of wave guides. The quantization of the transverse momentum is not restored and $\mathbf{K}$ does not appear in the quantum expectation value of four operators. Interference effects between transverse channels may lead to enhancement, or suppression, of the Fano factor, as will be shown with first principles calculations later in this section. In contrast to the possible existence of interference effects in atomic scale junction, one could, if a well defined wave-guide exists, have quantization of transverse modes as described above. In such case the shot noise is given by

$$F = \frac{\int_{E_{FL}}^{E_{FR}} dE \int d\mathbf{K} \left| T_L^* R_R \right|^2}{\int_{E_{FL}}^{E_{FR}} dE \int d\mathbf{K} \left| T_R \right|^2}, \tag{3.41}$$

where the transmission (reflection) probability are related to transmission (refection) coefficient by $T = \left|T_L\right|^2, R = \left|T_R\right|^2 = 1 - T$. The shot noise essentially restores the Büttiker type formula

$$F = \sum_n T_n(1 - T_n) / \sum_n T_n. \tag{3.42}$$

Shot noise exceeding the Poisson value may be possible due to interference effects. To demonstrate possibility of super Poissonian noise we assume, for simplicity, that a system of N identical parallel wires, which are well separated, and

sandwiched by two planar electrodes. We further assume that the system is in linear response regime and each wire carries a single channel such that the current is

$$I = \frac{2e}{\hbar} \sum_{n=1}^{N} T_n, \tag{3.43}$$

where $T_n = |T_{R,n}|^2$ is the transmission probability of n-th wire. The Fano factor given by equation (3.40) is then

$$F = \frac{\left| \sum_{n=1}^{N} T_{L,n}^{*} R_{R,n} \right|^2}{\sum_{n=1}^{N} |T_{R,n}|^2}, \tag{3.44}$$

where $T_{L,n}$ (and $R_{R,n}$) are identical for all n. Following by Cauchy-Schwarz inequality (equal sign holds in this particular case), equation (3.44) becomes

$$F = \sum_{n=1}^{N} (1 - T_n) = N(1 - T_n), \tag{3.45}$$

which predicts that the Fano factor increases linearly with the the number of parallel wires, when the wires are well separated, but still experience interference effects through the reservoirs. A lack of quantization of **K** channels may then, in this case, cause the shot noise to exceed the Poisson limit via interference of **K** channels inside the planar electrodes. This is in contrast to the Fano factor of completely uncoupled wires, $F = 1 - T_n$ as given by equation (3.41), which is independent of the number of wires in parallel. Hence, the Fano factor without channel mixing equals the Fano factor of a single wire when identical parallel wires are well separated, which is also found in Ref. [50].

To further analyze this effect, first principles calculations of parallel silicon atoms sandwiched in between two gold electrodes have been performed with a bias of 10 mV. Once the wave functions of the systems are known, the current and shot noise for the case of interfering channels can be calculated with the help of equation (3.33) and (3.28), respectively. These quantities have been calculated for one to six parallel silicon atoms, placed on a square lattice with a spacing of 7 a.u. Figure 3.7 shows the current and Fano factor, for interfering channels, as a function

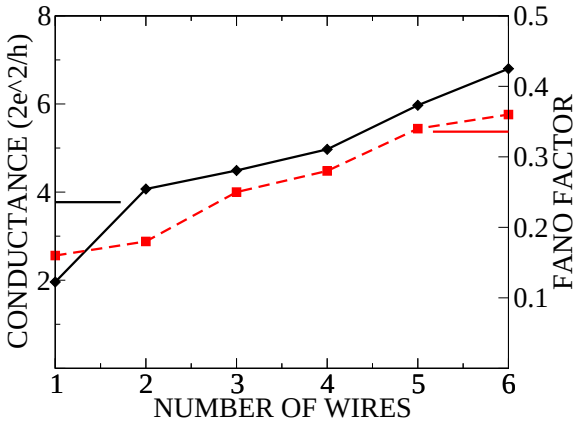


Figure 3.7: Conductance(black diamonds) in units of quantum of conductance and Fano factor(red squares) as a function of number of parallel silicon atoms. The shot noise is calculated with the assumption that channels do interfere with each other as assumed in equation (3.28). Sold black and dashed red lines are guides for eye only.

of number of parallel silicon atoms. We can see that both the conductance and Fano factor increases roughly linearly with increasing number of atoms in parallel. The Fano factor is however not increased by a factor of two when the number of parallel atoms is doubled, as expected from equation (3.45). This is due to the fact that the atomic spacing is not large enough such that the atoms do not see each other and can best be seen from the conductance. For completely separated wires, the conductance should also be proportional with the number of atoms in parallel. In Figure 3.7 the conductance is however only increased by a factor of three when the number of parallel silicon atoms is increased from one to six. Due to numerical reasons we have not been able to analyze systems with larger atomic spacing. Still we have been able to show that the Fano factor increases with the number of atoms in parallel as expected from equation (3.45).

As a final example, the shot noise of two parallel carbon chains, each with four atoms, have been calculated using both equation (3.28) and equation (3.36). The details of this geometry are identical to those of previous section, where the shot noise assuming interfering channels already is calculated. The main finding is that, for this system, the shot noise is always larger for the case of non-interfering

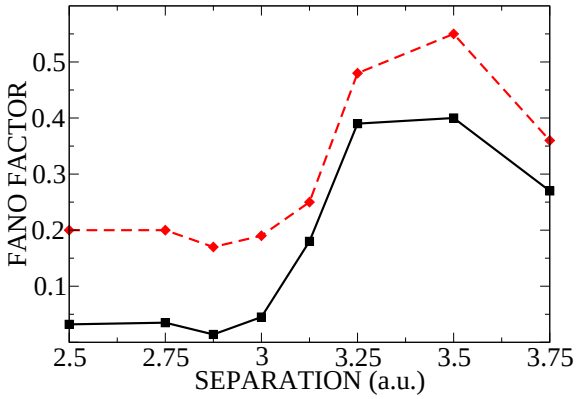


Figure 3.8: Fano factor as a function of wire separation for two parallel carbon wires. Black squares corresponds to the shot noise calculated assuming interference in between channels, while red diamonds assume non-interference as described by equations (3.28) and (3.36) respectively. Sold black and dashed red lines are guides for eye only.

channels. For example, the lowest calculated Fano factor for interfering channels is 0.014, while for non-interfering channels 0.17, or more than 10 times larger. It can be explained by comparing equation 3.28 and 3.36 with each other. In equation 3.28 the complex quantity $\tilde{I}^{LR}_{E,E}$, describing the interference between right and left moving waves, is integrated over momentum before the absolute value is taken, which allows for phase cancelation, unlike the corresponding case in equation (3.36). We would however like stress that this is not a universal result as the shot noise is a highly complex quantity caused by interference of both right and left moving waves. For other systems it is possible that the shot noise may be larger for non-interfering channels.

3.4 Conclusions

In summary, in this chapter we have investigated how the size of the electrodes affects the average current and shot noise in a nano-junction. Depending on the distance between the probes and the junction itself, the electrodes may be able to restore the transverse momenta of each conductance channel. If the probes are located in close proximity to the electrodes, the electrodes do not have time to

restore the transverse momenta and hence one may observe interference effects in between the different channels. While this does not affect the average current, the shot noise is highly sensitive to these interference effects. For example, the Fano factor of well-separated atomic wires is directly proportional to the number of wires in parallel in the case of interfering channels, while it is independent of the number of wires for non-interfering channels.

We conclude this chapter by stressing that, as the present work also shows, shot noise is a very sensitive tool to probe electron transport properties. Therefore, in order to increase our understanding of transport in atomic-scale structures, it would be very desirable to have experimental results of noise properties of molecular wires. We hope our work will inspire future studies in this direction. However, we note that the extreme sensitivity of noise to bonding properties between parallel wires can actually constitute a limitation in electronic applications of nanoscale structures.

The text of this chapter is in part a reprint of the material as it appears in Johan Lagerqvist, Yu-Chang Chen and Massimiliano Di Ventra *Shot Noise in Parallel Wires*, Nanotechnology 15, S459(2004), Institute of Physics. The dissertation author is the primary investigator of this paper. The text of this chapter 3 is also in part a reprint of the material as will appear in Yu-Chang Chen, Johan Lagerqvist and Massimiliano Di Ventra *Interference Effects of Transverse Channels on Shot Noise in Atomic Scale Junctions*, in preparation (2006). The dissertation author is a co-author of this paper.

4

Fast DNA Sequencing via Transverse Electronic Transport

Now that the first full human genome has been sequenced [73, 116], new uses of sequencing in medicine seem to be on the horizon. One of the most ambitious goals is to able to sequence an entire human genome in less than an hour for about 1,000 USD, allowing for every-day sequencing in medicine. [23] With the ability to rapidly sequence an individual's genome, we could study diseases like never before from the perspective of the genetic makeup of each individual. We could thus specifically tailor drugs and treatments to remedy illnesses and predict likely future conditions of a person. This goal of personalized medicine is hampered today by the high costs and slow speeds of DNA sequencing methods. Currently, it costs many millions of US dollars and takes months to sequence one human genome of about three billion base pairs. [15]

Recent innovations in manufacturing processes have made it possible to fabricate devices with pores at the nanometer scale [80, 108, 46, 81, 78], i.e., the scale of individual nucleotides. This opens up fascinating new venues for sequencing DNA. For instance, one suggested method is to measure the so called blockade current [58, 1, 28, 91, 117, 92, 29, 90, 79, 95, 2, 17, 38, 39, 48]. In this method, a longitudinal electric field is applied to pull DNA through a pore. As the DNA goes through, a significant fraction of ions is blocked from simultaneously entering the pore. By continuously measuring the ionic current, single molecules of DNA can

be detected. Other methods using different detection schemes, ranging from optical [10] to capacitive [44], have also been suggested. Despite much effort, however, single nucleotide resolution has not yet been achieved [15].

In this chapter, we explore an alternative idea which would allow single-base resolution by measuring the electrical current perpendicular to the DNA backbone while a single strand immersed in a solution translocates through a pore. To do this, we envision embedding electrodes in the walls of a nanopore as schematically shown in the inset of Figure 1. The realization of such a configuration, while difficult to achieve in practice, is within reach of present experimental capabilities [80, 108, 46, 81, 78]. The DNA is sequenced by using the measured current as an electronic signature of the bases as they pass through the pore. We couple molecular dynamics simulations and quantum mechanical current calculations to examine the feasibility of this approach. We find that if some control is exerted over the DNA dynamics, the *distributions* of current values for each nucleotide will be sufficiently different to allow for rapid sequencing. We show that a transverse field of the same magnitude as that driving the current provides sufficient control.

4.1 Theoretical Approach

We first discuss an idealized case of DNA dynamics which sets the foundations for the approach we describe. Second, we look at the distributions of transverse currents through the nucleotides in a realistic setting using a combination of quantum-mechanical calculations of current and molecular dynamics simulations of DNA translocation through the pore. We use a Green's function method to calculate the current across the electrodes embedded in the nanopore, as described in Ref. [128]. A tight-binding model is used to represent the molecule and electrode gold atoms. For each carbon, nitrogen, oxygen, and phosphorus atom $s-, p_x-, p_y-$, and p_z- orbitals are used, while s-orbitals are used for hydrogen and gold. The retarded Green's function, $\mathcal{G}_{DNA}$, of the system can then be written as

$$\mathcal{G}_{DNA}(E) = [E\mathcal{S}_{DNA} - \mathcal{H}_{DNA} - \Sigma_t - \Sigma_b]^{-1}, \tag{4.1}$$

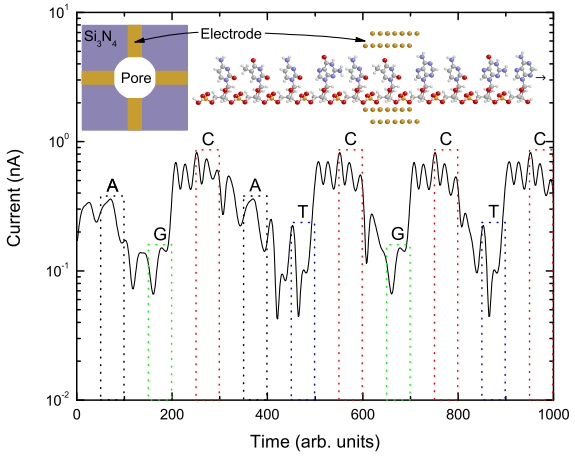


Figure 4.1: Transverse current versus time (in arbitrary units) of a highly idealized single strand of DNA translocating through a nanopore with a constant motion. The sequence of the single strand is AGCATCGCTC. The left inset shows a top-view schematic of the pore cross section with four electrodes (represented by gold rectangles). The right inset shows an atomistic side view of the idealized single strand of DNA and one set of gold electrodes across which electrical current is calculated. The boxes show half the time each nucleotide spends in the junction. Within each box, a unique signal from each of the bases can be seen.

where $\mathcal{S}_{DNA}$ and $\mathcal{H}_{DNA}$ are the overlap and the Hamiltonian matrices[1]. $\Sigma_{t(b)}$ are the self energy terms describing the coupling between the electrodes and the DNA. The total current can then be expressed as

$$I = \frac{2e}{h} \int_{-\infty}^{\infty} dE T(E)[f_t(E) - f_b(E)], \tag{4.2}$$

where $T(E)$ is the transmission coefficient and is given by

$$T(E) = \mathrm{Tr}[\Gamma_t \mathcal{G}_{DNA} \Gamma_b \mathcal{G}_{DNA}^{\dagger}]. \tag{4.3}$$

$f_{t(b)}$ is the Fermi-Dirac function of top (bottom) electrode, and $\Gamma_{t(b)} = i(\Sigma_{t(b)} - \Sigma_{t(b)}^{\dagger})$. The electrodes are comprised of 3x3 gold atoms arranged as a (111) surface two layers deep, and are biased at 1 V. The electrode spacing is 12.5 Å. Room temperature has been used for all calculations throughout the paper.

The first question is whether it is at all possible, in the best case scenario, to see differences in the transverse current between the different nucleotides in the absence of structural fluctuations, ions, and water. We address this by studying a highly idealized case of DNA translocation dynamics. The transverse current of a random sequence of single-stranded DNA (ss-DNA) moving through the junction with a constant motion is shown in Figure 1. This figure shows that the different nucleotides do indeed have unique electronic signals in this ideal case. Similar results have been obtained for static configurations of nucleotides in a previous theoretical work by two of the present authors [128], where, in addition, it was shown that neighboring bases do not affect the electronic signature of a given base so long as the electrode widths are of nanometer scale, i.e., of the order of the base spacing. These results provide a good indication that DNA can be sequenced if its dynamics through the pore can be controlled. As we show below, such control is provided by a transverse field of the same magnitude as that driving the current.

[1]We have used the program YAeHMOP (http://yaehmop.sourceforge.net/) to generate the tight-binding parameters used in this work. These parameters reproduce the states near the highest occupied and the lowest unoccupied molecular orbitals quite well compared to density-functional (DFT) calculations on the passivated nucleotide. In solution though, the nucleotides are charged. We have performed DFT calculations on charged nucleotides and found that the complex chemical environment with water molecules, counter-ions, and the gold electrodes effectively passivates the charge on the nucleotides. This finding allows us to use the same tight-binding parameters as in the passivated case. On the other hand, water only lowers the electrical current by a few percent on average, and its effect on the distributions is negligible. We will discuss these issues in more detail in a future publication.

Obviously, in a real device there will always be fluctuations of the current. These fluctuations are mainly due to two sources: 1) structural fluctuations of the DNA, ions and water, and 2) noise associated with the electrical current itself, like thermal, shot and 1/f noise [64]. Apart from 1/f noise, which can be overcome by operating slightly away from the zero-frequency limit, we estimate that, for the case at hand, shot noise and thermal noise are negligibly small, giving rise to less than 0.1% of error in the current[2]. [64] The most significant source of noise is thus due the structural motion of the DNA and its environment [3].

4.2 Results and Discussion

We have explored this structural noise by coupling molecular dynamics simulations with electronic transport calculations (described above) to obtain the real-time transverse current of the ss-DNA translocating through a Si_3N_4 nanopore [4]. The Si_3N_4 making up the membrane is assumed to be in the β-phase [45] with funnel-like shape (see Figure 2), while the electrodes are described above. A larger distance only reduces the current, while a shorter distance does not allow easy translocation of the DNA. As we describe below, the actual geometry of the electrodes and pore does not change the protocol we suggest for sequencing. The positions of the atoms of the nanopore and electrodes are assumed to be frozen throughout the simulation. The electric field generated by the electrodes is not included when the ss-DNA translocates through the pore, since the driving field is much larger in magnitude. Its effect will be analyzed later. A large driving field of 10 kcal/(mol Å e) is used to achieve feasible simulation times. In experiments such a large field would not be necessary.

[2]For instance, for a typical current of 1nA and the bias of 1V we consider in this work, if we assume a frequency bandwidth Δf of 10 kHz, the thermal noise can be estimated to be $i_n = \sqrt{\frac{4k_BT\Delta f}{R}} = 0.4$pA at room temperature. The effect of shot noise is comparable or less.

[3]These effects are also very important for charge transport in DNA along the longitudinal direction, see, e.g., Ref. [35]

[4]The dynamics of ss-DNA in the pore was calculated using the classical molecular dynamics package NAMD2 [56]. For the DNA, TIP3 water, and ions (1 M KCl) the CHARMM27 [40, 84] force field was used. UFF parameters [100] were used for the interaction between the device itself and other elements.

For convenience we choose to study the current that flows across two pairs of mutually-opposite electrodes (see inset of Figure 1). The four electrodes are not necessary for the conclusions we draw (in an experiment two are enough [109]). However, analyzing the current in two perpendicular directions gives us additional information on the orientation of a nucleotide inside the pore. For instance, if the ratio between the two currents is large, we know the nucleotide is aligned in the direction of the electrodes with the larger current. If the two currents are about equal in both directions, it is likely that the base is aligned at a 45 degree angle, and so forth. This is illustrated by the snapshots in Figure 2 where we see the expected behavior of the current for an ss-DNA with fifteen consecutive Cytosine bases translocating between the two pairs of electrodes [5].

We have found similar curves for all other bases as well, making it difficult to sequence DNA on the basis of just a simple read-out of the current, like what these curves show. In other words, due to structural fluctuations and the irregular dynamics of the ss-DNA, a single measurement of the current for each base is not enough to distinguish the different bases with high precision. We thus conclude that a *distribution* of electrical current values for each base needs to be obtained. This can be done by slowing the DNA translocation in the pore [39] so that each base spends a larger amount of time aligned with the electrodes. Most importantly, we find that when the field that drives the DNA through the pore is smaller than the transverse field that generates the current, one base at a time can align with a pair of electrodes quite easily. This is due to the fact that the DNA backbone is charged in solution, so that its position can be controlled by the transverse field.

Figure 3 shows the main results of this Letter. It shows the calculated distribution of transverse currents for each base in a realistic setting when the driving field is much smaller than the transverse field. We obtain these distributions by turning off the driving field and sampling the current while one base fluctuates between the electrodes [6]. The distributions for each base are indeed different. Note that

[5] We stress again that for the conclusions of our paper we are only interested in the current of mutually-opposite electrodes. In any case, the current in between two neighboring electrodes would require inelastic scattering events, and hence is expected to be small.

[6] While collecting these distributions, the transverse field of strength 1.84 kcal/(mol Å e) which generates the current is on during the molecular dynamics simulations. During a time span of

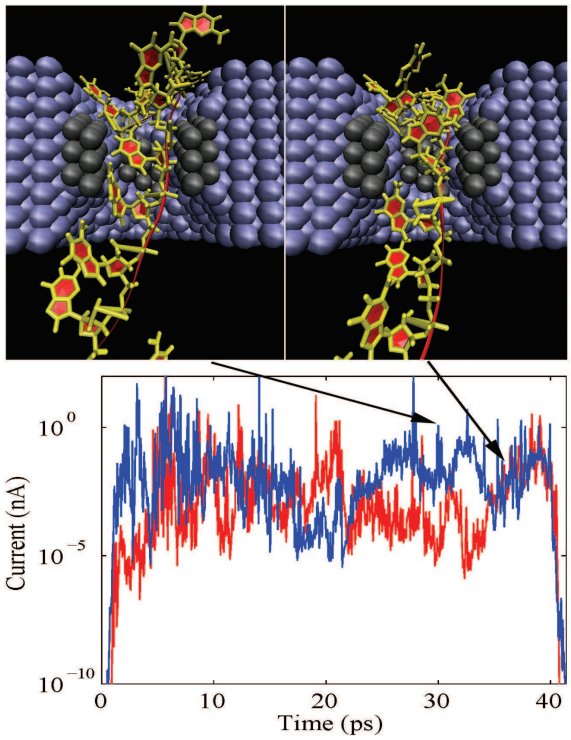


Figure 4.2: Currents as a function of time for a poly$(dC)_{15}$ translocating through a nanopore. Blue (red) curve indicates the current, for a bias of 1 V, between the right and left (front and back) electrodes represented in gray in the snapshots (the fourth electrode is located behind the field of view and is hence not visible in the snapshots). During approximately the first half of the translocation, the two currents follow each other, indicating no bases are aligned with either electrode pair. Left snapshot indicates the case in which a nucleotide is aligned with a pair of electrodes; the right snapshot when the nucleotide is not aligned between either pair of electrodes. In the snapshots, solution atoms are not shown and red colors are a guide for the eye only.

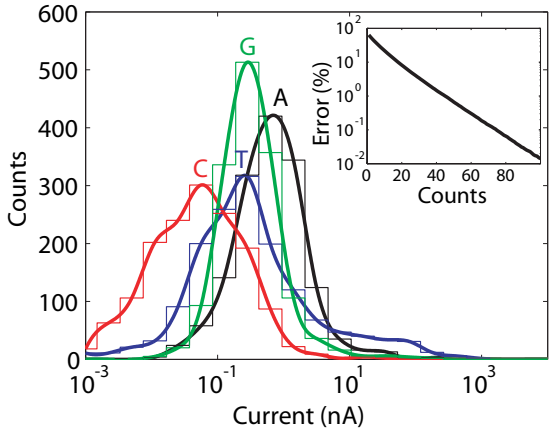


Figure 4.3: Probability distributions of currents at a bias of 1 V for poly$(dX)_{15}$, where X is Adenine/Thymine/Cytosine/Guanine for the black/blue/red/green curve, respectively. The thin lines show the actual current intervals used for the count, while the thick lines are an interpolation. The inset shows the exponentially decaying ratio of falsely identified bases versus number of independent counts (measurements) of the current averaged over the four bases.

these distributions may vary according to the microscopic geometry of the pore and electrodes, but our suggested protocol to sequence via transverse transport remains the same. *First*, one needs to "calibrate" a given nanopore device by obtaining the distributions of current with, say, short homogeneous polynucleotides, one for each base. *Second*, once these "target" distributions are obtained, a given sequence can be extracted with the *same* device by comparing the various currents with these "target" distributions, and thus assigning a base to each measurement within a certain statistical accuracy. Both the target and sequencing distributions need to be obtained under the conditions we have discussed above, i.e. the driving field smaller than the transverse field, which allow the transverse field to control the nucleotides alignment with respect to the electrodes.

Finally, given these distributions and the accuracy with which we want to sequence DNA, we can answer the question of how many independent electrical current measurements one needs to do in order to sequence DNA within that accu-

75 ps, we record 1500 values of the current. The switch-off of the driving field is dictated by the molecular dynamics timescales: we cannot slow down the translocation to an experimentally accessible regime.

racy. The number of current measurements will dictate how fast we can sequence. We can easily estimate this speed from the distributions of Figure 3 by calculating the statistical likelihood for all configurations of a given base in the junction region and multiplying it by the probability that we can tell this base from all other bases for the value of the current at that specific configuration. The average probability that we can correctly sequence a base after N measurements is then given by

$$< P > = \sum_{X=A,T,C,G} \frac{1}{4} \sum_{\{I_n\}} \frac{\prod_{n=1}^{N} P_X^n}{\prod_{n=1}^{N} P_A^n + \prod_{n=1}^{N} P_T^n + \prod_{n=1}^{N} P_C^n + \prod_{n=1}^{N} P_G^n} \tag{4.4}$$

where A, T, C and G are the distributions, as shown in Figure 3, for the four bases. P_X^n is the probability that a base is X considering only the current for measurement n. It can be found by comparing the ratios of the four distributions. Finally, the sum over $\{I_n\}$ is a sum over all possible sets of measurements of size N. The inset of Figure 3 shows $1- < P >$, the exponentially decaying ratio of falsely identified bases versus number of independent counts (measurements) of the current averaged over the four bases, where the ensemble average is performed using Monte-Carlo methods. From this inset we see that if, for instance, we want to sequence DNA with an error of 0.1%, we need about 80 electrical current measurements to distinguish the four bases. If we are able to collect, say, 10^7 measurements of the current per second (a typical rate of electrical current measurements) we can sequence the whole genome in less than seven hours without parallelization. Note that it is mainly the rate at which electrical current measurements can be done that sets an upper limit for the sequencing speed, not the DNA translocation speed. Clearly, these estimates may vary with different device structures but are representative of the speeds attainable with this sequencing method.

4.3 Conclusions

In this chapter we proposed and theoretically showed the feasibility of a protocol for sequencing based on the distributions of transverse electrical currents of

single-stranded DNA while it translocates through a nanopore. Our estimates, based on the statistics of these distributions, reveal that sequencing of an entire human genome could be done with very high accuracy in a matter of hours without parallelization, e.g., orders of magnitude faster than present techniques. The practical implementation of our approach would represent a substantial advancement in our ability to study, predict and cure diseases from the perspective of the genetic makeup of each individual. If successfully implemented, DNA sequencing could be performed orders of magnitude faster than currently available methods and still much faster than other pre-production approaches recently suggested [23, 106, 87].

The text of this chapter is in part a reprint of the material as it appears in Johan Lagerqvist, Michael Zwolak and Massimiliano Di Ventra *Fast DNA Sequencing via Transverse Electronic Transport*, Nano Lett. 6, 779(2006), American Chemical Society. The dissertation author is the primary investigator of this paper.

5

Fast DNA Sequencing via Transverse Electronic Transport: an In-depth Analysis

Previous chapter shows the potential for sequencing DNA by measuring a transverse electronic current [128] as single-stranded DNA (ss-DNA) translocates through a nanopore. The concept envisions a nanopore device with embedded nanoscale electrodes, as schematically shown in Figure 5.1. Operating such a device with a transverse field, $\mathbf{E}_{\perp}$, (the field that drives the electronic current) greater than the longitudinal pulling field, $\mathbf{E}_{\parallel}$, (i.e. the field that drives DNA translocation) stabilizes the motion of the nucleotide between the electrodes. [66] This creates a very desirable situation where structural fluctuations (the most important source of intrinsic noise [66]) are reduced to such a level that *distributions* of currents for each base, while still overlapping, are different enough to allow for high statistical distinguishability between the different bases. In previous work, however, it was assumed that each measurement could be performed almost instantaneously. This is just a theoretical assumption, and a more realistic treatment of the measurement probes needs to be taken into account.

In this chapter we will show that, contrary to naive expectation, the measurement bandwidth of the electrical probes reduces these overlapping distributions into sharply peaked and disjoint distributions. Therefore, assuming that no exter-

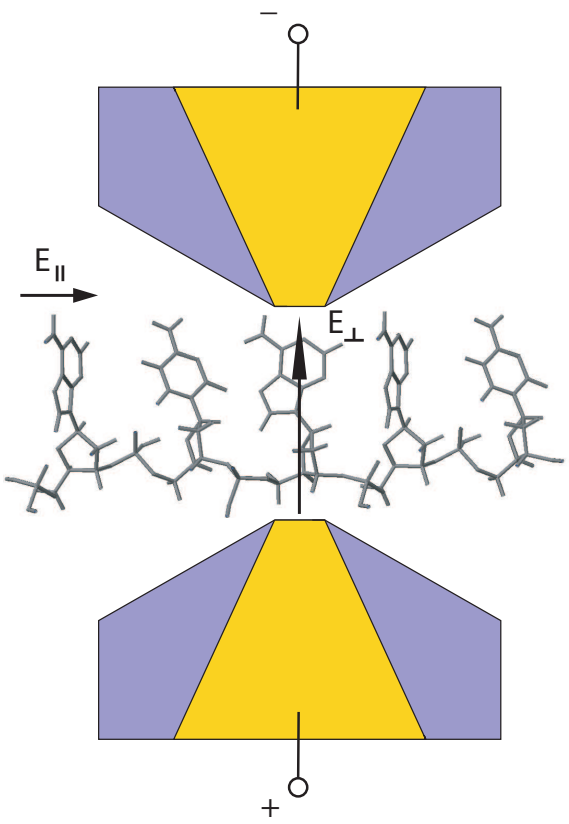


Figure 5.1: Schematic of a nanopore (purple) with electrodes (gold) attached to the edges of the pore. The electrodes are used to inject a current through the nucleotides (gray) in the direction transverse to the backbone. The electronic signature can then be used to sequence the DNA.

nal sources of noise are present other than shot, thermal and structural fluctuation noise, a single current measurement may be sufficient to distinguish each individual base. Thus by measuring the current as the nucleotides translocate through the pore, the DNA can be accurately sequenced in extremely short time scales.

In Chapter4 it is estimated that the raw sequencing throughput of a single 12.5 Å pore, operating with a 1V transverse bias, could be as high as 3 billion bases in 7 hours. In a real device, however, the pore diameter will not be easy to control and it may not be possible to operate the device at high transverse biases. Also, ions and water in the pore are additional sources of noise on top of the structural fluctuations of the ss-DNA. In this chapter we will examine in

detail these effects on the distinguishability of the bases. To do this, we use all-atom molecular dynamics simulations coupled with quantum mechanical current calculations. We find that although the overall magnitude of current can change dramatically, the intrinsic distinguishability of the bases is not significantly affected by pore size and transverse field strength. The latter is the result of very effective stabilization of the DNA by the transverse field, $\mathbf{E}_\perp$, so long as that field is much larger than the pulling field, $\mathbf{E}_\parallel$. In addition, the ions and water together effectively screen the charge on the nucleotides, so that the electron states participating in the transport properties of nucleotides in solution resemble those of uncharged species. Finally, water in the environment has a negligible direct influence on the electrical current through the DNA.

5.1 Setup and Methods

Identical to the previous chapter, we take a two step computational approach to examine the issues described above: *1)* molecular dynamics simulations are used to sample real time atomistic coordinates of the DNA, water, and ions in a prototypical Si_3N_4 nanopore, and *2)* these coordinates are used in quantum mechanical calculations to find the current across the nanostructure. To calculate the current, we use a scattering approach with a tight-binding Hamiltonian to represent the electronic structure of the system. For each carbon, nitrogen, oxygen, and phosphorus atom $s-, p_x-, p_y-$, and p_z- orbitals are used, while s-orbitals are used for hydrogen and gold. We take the the Fermi level to be that of bulk gold, which is identical to that of the extended molecule. However, for the biases we consider, the current calculations are relatively insensitive to the exact position of the Fermi level, as it falls within the HOMO-LUMO gap.

The retarded Green's function, $\mathcal{G}_{DNA}$, can be written as

$$\mathcal{G}_{DNA}(E) = [E\mathcal{S}_{DNA} - \mathcal{H}_{DNA} - \Sigma_t - \Sigma_b]^{-1}, \tag{5.1}$$

where $\mathcal{S}_{DNA}$ and $\mathcal{H}_{DNA}$ are the overlap and the Hamiltonian matrices and $\Sigma_{t(b)}$ are the self energy terms that describe the interaction in between the leads and

the DNA. For a given $\mathcal{G}_{DNA}$ the transmission coefficient can then be calculated as

$$T(E) = \mathrm{Tr}[\Gamma_t \mathcal{G}_{DNA} \Gamma_b \mathcal{G}_{DNA}^{\dagger}], \tag{5.2}$$

where $\Gamma_{t(b)} = i(\Sigma_{t(b)} - \Sigma_{t(b)}^{\dagger})$. Finally the current in between two electrodes is given by

$$I = \frac{2e}{h} \int_{-\infty}^{\infty} dE T(E)[f_t(E) - f_b(E)] \tag{5.3}$$

where $f_{t(b)}$ is the Fermi-Dirac function of top (bottom) electrode. [128] Room temperature is assumed throughout this paper and we have assumed that the voltage drops uniformly in the space between the DNA molecule and electrodes. We will consider transverse biases small enough that we do not expect chemical reactions to occur, and definitely smaller than the electrolysis threshold for water of about 1.2V.

The justification for using a tight-binding approach is two-fold. First, the current through the junction is strongly dependent upon the coupling of the nucleotide (in the junction region) to the electrodes. Thus, the important quantity to reproduce is the molecular orbitals of the bases and backbone relative to the electrodes in order to get the DNA-electrode coupling. We find that the tight-binding calculations reproduce very well the molecular orbitals of charge-neutral nucleotides when compared to density functional theory (DFT) calculations. We have performed DFT calculations with DZVP basis set and GGA functional B88-PW91. The HOMO, LUMO, and nearby electronic levels have similar molecular wavefunctions in both the DFT and tight-binding calculations. Second, the presence of a nearby counterion (see below) in addition to the nearby water effectively brings the HOMO-LUMO gap of the nucleotide close to the one of the charge neutral case (although the positioning of the gold Fermi level may change with respect to these states), while the molecular orbitals of the bases remain nearly identical regardless of the presence of the counterion. However, the position of the counterion is not fixed, but it fluctuates around the charge on the backbone at an average distance of 6.5 Å. This will cause additional fluctuations in the current across the junction. Nonetheless, since the current value is mainly controlled by the DNA-electrode coupling, these fluctuations are less likely to contribute than those due to structural motion.

To analyze the dynamics of the DNA strand as it propagates through the pore, classical molecular dynamics simulations have been performed with the package NAMD2. [56] For the interaction in between the DNA, water, and ions the CHARMM27 force field [40, 84] was used, while UFF parameters [100] were used for interactions between the Si_3N_4 membrane and other atoms. The location of the Si_3N_4 atoms is assumed to be frozen throughout the simulation. When integrating over time, a time step of 1 fs was used and the temperature of the system was kept constant at 300K throughout the whole simulation by coupling all but the hydrogen atoms to a thermal bath with a Langevin damping constant of 0.2 ps^{-1}. The Van der Waals interactions were gradually cut off starting 10 Å from the atom until reaching zero interaction 12 Å away. The DNA strand was driven through the pore with a large electric field of 6 kcal/(mol Å e) in order to achieve feasible simulation times. This field is larger than the ones used experimentally. This results in a negligible stabilizing electric field, $\mathbf{E}_\perp$. Thus, for sampling current distributions of the nucleotides, we turn off $\mathbf{E}_\parallel$ when a base is aligned in between the electrodes. This gives an adequate representation of the structural fluctuations when $|\mathbf{E}_\perp| \gg |\mathbf{E}_\parallel|$. One of our main conclusions is that the device has to be operated in this regime for sequencing to be possible.

The pore analyzed in this chapter is made up of a 24 Å thick silicon nitride membrane in the $\beta-$phase. [45] The experimental etching of the pore is mimicked by removing the atoms inside a double conical shape with a minimum diameter of 1.4 nm located at the center of the membrane and with an outer diameter of 2.5 nm (see Figure 1 for a schematic representation of the pore). This corresponds to a cone angle of 20 degrees for each of the cones. In actual experimental realizations of nanopores such geometry may not always be realized. For the conclusions of this paper this would not matter as the calibration of the device would correct for geometrical imperfections in the pore, as discussed later in the paper. A sphere, with a radius of 6 nm, of TIP3 water [55] is placed around the pore and 1M of potassium and chlorine ions are added. Finally, a single-stranded poly-x (where x is A, T, C or G) molecule is generated by removing one strand from a helical double stranded DNA molecule. At the initial time of the simulation, this molecule

is placed parallel to the pore such that the tip of the ss-DNA is just inside the pore.

5.2 Results and Discussion

We discuss our results in three subsections: In *Setup*, we examine a larger pore diameter and weaker transverse field than in previous chapter; In *Nucleotide Stabilization*, we look at the current distribution with varying transverse field strength; In *Influence of the Environment*, we look at the role of the environment on the electronic conductance.

5.2.1 Setup

Figure 5.2a shows the current as a function of time as a ss-DNA strand made up of 15 Adenine bases propagates through the 14 Å diameter pore with embedded electrodes. A pore with a diameter smaller than 10 Å does not allow the translocation of ss-DNA, while a pore with a diameter larger than about 15 Å cause a much smaller conductance. Figure 5.2b shows the current as a function of time when $\mathbf{E}_{\|}$ has been turned off. The starting condition was taken from the simulation used for Figure 5.2a at the time indicated by the dashed line in Figure 5.2a, when a base was aligned in between the electrodes. We can see that as time progresses the base stays aligned in between the electrodes due to the interaction of the nucleotide dipole with the transverse electric field. This is discussed in further detail later on in this chapter. Similar curves have been found for all other DNA bases.

Since we envision operating the nanopore/electrode device in a regime where the transverse field is much stronger than the driving field [1], we can examine the real time structural fluctuations by sampling the current with the driving field off. The distributions of these currents, with this particular pore geometry, for all four bases are shown in the top section of Figure 5.3, assuming each sample is

[1]Note that it could be possible to operate a device in this regime as a thermal ratchet, e.g., the thermal fluctuations overcome the barrier to moving each nucleotide away from the junction region.

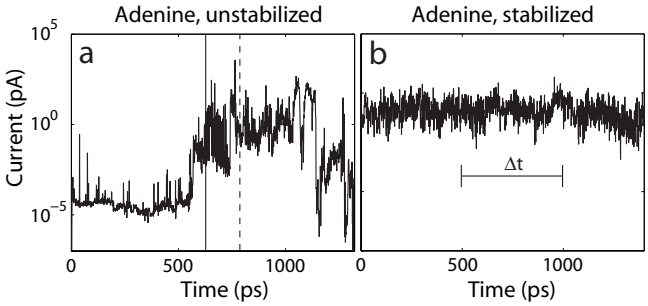


Figure 5.2: Current, at a bias of 0.1 V, as a function of time for poly$(dA)_{15}$, as (a) it is propagating through a pore with two electrodes without a stabilizing field, and (b) when the driving field is turned off at a time (indicated by the dashed line in (a)) when a base is aligned in between the electrode pair. Solid vertical line in (a) indicates the time at which the DNA starts propagating through the pore. The transverse electric field is included in the simulations for figure (b). Δt represents a finite experimental bandwidth.

measured *instantaneously*. From the molecular dynamics simulations we observe that ions fluctuate inside the pore at time scales of the order of 5 ps. As the total current sampling time per base is 1.2 ns, we effectively sample over multiple ionic configurations. We can see that these distributions are unique, but overlapping. This means that a handful of measurements of a base to be sequenced would not be enough to distinguish it from the other bases. However, in a real experiment each measurement would take a finite amount of time to be performed (finite bandwidth indicated with Δt in Figure 5.2b). In other words, the electric probes have a finite time bandwidth. Hence, a real measurement averages over a time interval, which is determined by the sampling frequency of the electrodes/probes, causing the distributions to narrow around their average current.

In order to accurately determine the new shape of the distributions when each measurement is time averaged, one would ideally need multiple ensembles, where for example one would be the current shown in Figure 5.2b. Due to numerical complexity this is however not feasible. Instead we assume that the interpolated distributions shown in the top half of Figure 5.3 are exact. Then we assume that the average current for another ensemble can be generated by sampling these interpolated distributions. By repeating this process multiple times, one can then

calculate the new distributions, where each measurement is *time averaged*. These new distributions are shown in the bottom part of Figure 5.3. Clearly, the more times one were to sample the original distributions when creating new ensembles, the sharper the new distributions would become. The number of samples that should be taken is determined by the ratio between the period of physical measurement and the time interval for two measurements to be considered independent of each other. While the sampling frequency can be determined exactly, it is hard to give an exact value of the time needed in between two instantaneous measurements for them to be considered independent. However, we can take the timescale for atomic movements in the simulation, which is about 1 ps, as a rough estimate.

Assuming no external noise, the distributions in the lower half of Figure 5.3 show that as long as one samples the instantaneous distributions at least 100 times (solid lines), the new distributions will be completely separated from each other, and if sampled 1000 times the new distributions assume much sharper shapes. Assuming that the time scale for independent sample measurements is of the order of 1 ps, one would need an apparatus sampling at a rate no faster than $\sim 1/(1000 \times 1\text{ps}) = 1\text{GHz}$ to obtain disjoint distributions. Since sampling frequencies of the order of GHz or less are relatively easy to obtain, we conclude that a *single* current measurement would be sufficient to distinguish the different bases. We would like to stress again that, in this analysis, we have assumed no other external source of noise is present (like, for instance, telegraph noise). If thermal noise is of concern, one may reduce the sampling frequency, which both reduces the thermal noise and sharpens the intrinsic current distributions. For example, at a sampling frequency of 100 kHz, the rms current thermal noise for Guanine is of the order of 40 fA[2], while the distributions due to structural fluctuations assume $\delta-$function like shapes. A larger average current can be obtained by either increasing the bias or by slightly reducing the pore size. If the distributions of the four bases were to begin overlapping due to external noise, multiple measurements per base would be needed, and a statistical analysis similar to the one presented

[2]The root mean square current thermal noise is given by $i_n = \sqrt{4k_bT\Delta f/R}$, where T is the temperature, Δf is the sampling frequency, and R is the resistance of the nucleotide in the junction.

in previous chapter could be performed. In the rest of the chapter we will keep on discussing the case where each measurement is assumed to be instantaneous, as this case contains more information; one can always transform any distribution given below into a "finite-bandwidth" one as described above.

Current distributions for a different pore diameter and transverse field were examined in the previous chapter, assuming instantaneous measurements. Although the electrode spacing is larger in this chapter, 14 Å compared to 12.5 Å, and the electrode bias is smaller, 0.1 V compared to 1.0 V, the distributions show remarkable similarities. Adenine shows the largest mode in both cases and Guanine the second largest. Notice, however, that in the previous chapter Thymine had a slightly larger mode current than Cytosine, while the results presented here are reversed. This can be attributed to the change in electrode spacing and highlights the importance of calibrating the device (see discussion below). It also demonstrates the importance of the DNA-electrode coupling: in the upright configuration for which the nucleotides are held, the Thymine nucleotide has the largest base-electrode distance, and therefore its coupling to the second electrode is most sensitive to the electrode spacing. [3] On the other hand the currents are orders of magnitude larger for the smaller pore/larger bias case. For example, the mode conductance for Adenine is roughly 1,000 times larger. This difference can be attributed to the change in the electrode spacing; a smaller pore radius will result in a larger current.

Following the discussion in the previous paragraph, we would like to emphasize that since it is highly unlikely that the exact geometry of two pores would be identical, the first step to sequence a DNA strand would be to calibrate the device by creating these distributions for the pore at hand. Then a strand can be sequenced by comparing its current, at each base location, to these target distributions.

One final comment before we go on to discuss stabilization. When $\mathbf{E}_{\|}$ is turned off, we observe a mild drift of the Thymine(T) nucleotide, which causes a slightly different form for its current distribution when assuming that each measurement

[3] For larger electrode spacing, the nucleotide conductance is strongly dependent on the base-electrode distance. As the electrode spacing gets smaller, the current depends more on the spatial character and energies of the molecular orbitals.

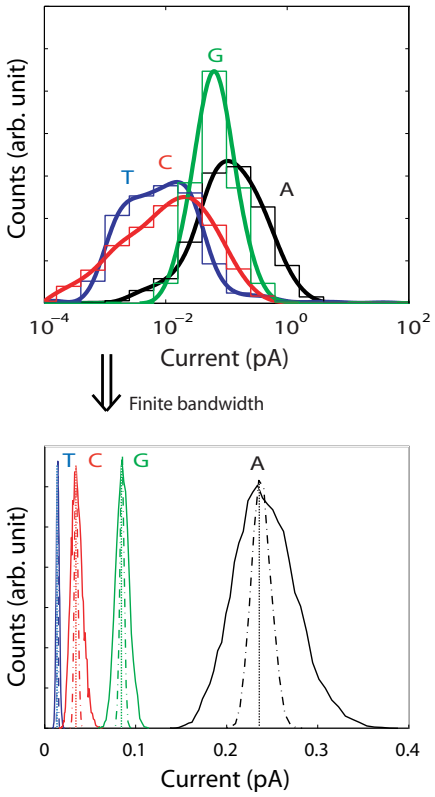


Figure 5.3: Top graph shows the probability distributions, assuming instantaneous measurements, of currents at a bias of 0.1 V for poly$(dX)_{15}$, where X is Adenine/Thymine/Cytosine/Guanine for the black/blue/red/green curves, respectively. The thin lines show the actual current intervals used for the count, while the thick lines are an interpolation. After the driving electric field is turned off, the system is left to equilibrate for 200 ps before samples are taken. Each distribution is made up of 1200 samples, each taken with a 1 ps interval. The bottom graph again shows the probability distributions, but now with the assumption that each measurement is time averaged in between each sample. The color coding is the same as for the top graph, while solid/dashed/dotted line assumes that the distributions in the top graphs are sampled $100/1{,}000/10^7$ times for each new data point.

is instantaneous. In our previous work we found nearly Gaussian distributions for A and G nucleotides but not C and T. Since C and T are smaller bases, we believe their homogeneous strands have more freedom to move within the pore. When the strand moves enough, a nearest neighbor base can come in close vicinity of the electrodes. For the same reasons, the nearest neighbor base makes a larger difference in the conductance of C and T bases. In a stretched configuration, the nearest neighbor bases do not affect the conductance very much so long as the electrode width is on the order of a single nucleotide. [128] However, the molecular dynamics simulation allows many configurations to be explored, including ones where the nucleotide is near the edge of the electrode and thus the neighboring nucleotide can make a substantial contribution to the conductance of the junction. Thus, a potential future direction of research may be to examine the role of base sequence on DNA motion within the nanopore.

5.2.2 Nucleotide Stabilization

Each phosphate group carries a negative charge in solution. In addition, as we have anticipated, we find that there is always a counterion fluctuating about the backbone charge, at an average distance of 6.5 Å. This helps neutralizing the DNA charge inside the pore as confirmed by other molecular dynamics simulations [99] and also experiment. [104, 88] However, our results show that the transverse field can still act as a very effective stabilizer on the resulting nucleotide-counterion dipole.

To better understand the effect of the stabilizing field on the current, one can compare the conductance distributions for varying transverse electric fields. In Figure 5.4 the conductance distributions for four different cases are shown. The black curve shows the conductance distribution for the completely unstabilized and unaligned case, generated by transforming the current in Figure 5.2a into a distribution starting from the time when the strand starts to translocate. The blue curve is the conductance distribution generated by turning $\mathbf{E}_{\|}$ off at a time when a base is aligned in between the electrodes, as indicated by the dashed line in Figure 5.2a, while not including any stabilizing field. This corresponds to the limiting case

in which both $\mathbf{E}_{\parallel}$ and $\mathbf{E}_{\perp}$ are allowed to approach zero with $|\mathbf{E}_{\perp}| \gg |\mathbf{E}_{\parallel}|$. Red and green distributions are generated in the same manner as the blue curve, but with both a bias and stabilizing field of 0.1 V and 1.0 V, respectively. As expected, the distribution for the unaligned case is much broader, compared to the other cases, as the bases are oriented in all possible directions while the strand propagates through the pore with a driving field much larger than the stabilizing field. When starting with a base aligned in between the two electrodes the distributions are clearly much sharper. One also notices an increase of conductance of almost an order of magnitude for a stabilizing field of 0.1 V compared to the one with no stabilizing field. Furthermore, the conductance increases by almost two orders of magnitude when increasing the stabilizing field from 0.1 V to 1.0 V. This confirms the effect of the stabilizing field: as the field increases in strength it pulls the backbone closer to one electrode, and aligns the base towards the other electrode, which increases the conductance. However, it is important to note that in the above results the fluctuations are not being reduced by the stabilizing field, but rather by the lack of pulling field.

In order to confirm that the stabilizing field can actually reduce structural fluctuations, we have analyzed a case in which the driving field is turned off as an Adenine base was aligned in the direction *normal* to the stabilizing field. Then, as a bias of 0.1 V is turned on in between the electrodes, the base starts to align with the stabilizing field and is completely aligned after about 100 picoseconds. We can thus conclude that as long as the strand is pulled through the pore at a pace slower than $\sim$100 ps per base, the stabilizing electric field induced by this bias will be sufficient for sequencing purposes. In experiments [38, 39] the typical translocation speed is much slower than the reorientation time of $\sim$100 ps, allowing the bases sufficient time to reorient with the transverse electric field.

5.2.3 Influence of the Environment

As we discussed above, water and counter-ions do influence the electronic structure of nucleotides in solution. Without these species, the nucleotides would have an unscreened charge and electronic transport would be quite different.

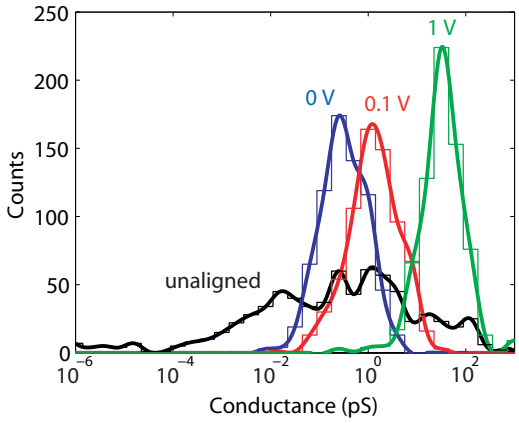


Figure 5.4: Probability distributions of conductance for varying stabilizing fields for poly$(dA)_{15}$. Black curve corresponds to the completely unstabilized case as shown in Figure 5.2a, while blue, red and green curves correspond to an increasing stabilizing field when the driving field is turned off.

Nevertheless, the fluctuation of water molecules around the nucleotides inside the pore has little direct effect on the electrical current. Figure 5.5 shows the current with and without water for a Guanine base stabilized in between the electrodes. The presence of water lowers the current on average by 18%. For the smaller pore geometry used in the previous chapter, an even smaller change of 4% was observed for Adenine as it propagates through the pore unstabilized. This is an expected result, as the smaller pore allows for fewer water molecules to enter, with a corresponding decrease of its contribution to the current. Also, the small effect of water on the current is the result of a slight modification of the nucleotide electronic states. This is opposed to an increase in conductance due to "bridging" effects, which can occur if the pore was larger.[82] Considering that structural fluctuations account for orders of magnitude change in conductance, we can conclude that the direct effect of water on conductance can be neglected.

5.3 Conclusions and Future Work

By combining molecular dynamics simulations with quantum mechanical current calculations, we examined the feasibility of DNA sequencing via transverse

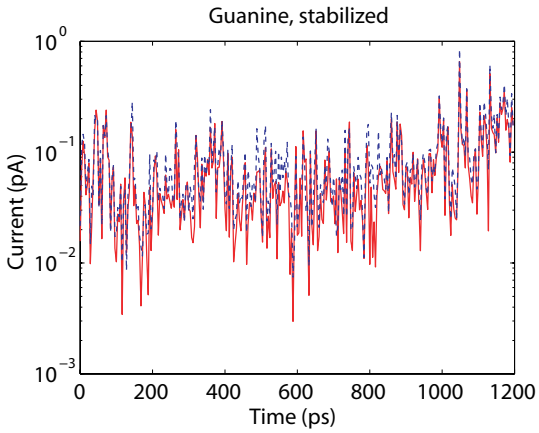


Figure 5.5: Current, at a bias of 0.1 V, as a function of time for poly(dG)$_{15}$, with a single Guanine base stabilized in between the electrodes by the transverse electric field, with (solid red curve) and without (dashed blue curve) water included in the current calculation.

electronic transport. Specifically, we have shown that unless the current is sampled with extreme frequencies, over $\sim$1 GHz, the time averaging occurring in the probe apparatus will reduce the fluctuations in the current to such a level that an individual current measurement may be sufficient to sequence the base, assuming that any external sources of noise in the current are small. We also addressed how the transverse field strength, pore diameter, and local environment affect the distinguishability of the bases. Furthermore, we have shown that the electric field induced by the electrodes will effectively stabilize the bases and hence allows for accurate sequencing when $|\mathbf{E}_\perp| \gg |\mathbf{E}_\parallel|$. In addition, we have discussed how ions and water effectively screen the charged nucleotides. We have also shown that water in the environment has a negligible direct effect on the electrical current. Our results also emphasize the importance of device calibration.

It is important to note that there are many issues left to be addressed, like DNA-surface bonding, time for the DNA to find and go through the pore (which will depend on device parameters), and the effect of ionic fluctuations on the electronic transport properties of the DNA.

The text of this chapter is in part a reprint of the material as will appear in Johan Lagerqvist, Michael Zwolak and Massimiliano Di Ventra *Influence of*

Device Operation and the Environment on Rapid DNA Sequencing via Transverse Electronic Transport, submitted to Proc. Natl. Acad. Sci. U.S.A. (2006). The dissertation author is the primary investigator of this paper.

6

Charge Screening in Nanopores

Over the last decade there has been tremendous advances in both the fabrication of nanopores and their use for molecular characterization and nucleic acid analysis. [58, 1, 91, 92, 117, 29, 90, 79, 95, 108, 2, 17, 38, 28, 81, 80, 46] Experimental characterization of molecules has so far relied on measuring changes in the ionic current through the pore. [58, 1, 91, 92, 117, 29, 90, 79, 95, 108, 2, 17, 38] The factors contributing to the magnitude of the ionic current both in the presence and absence of translocating molecules are still, however, somewhat of a mystery. In addition to the ionic current, other ways to detect and characterize single-molecules in nanopores may come from the embedding of nanoscale sensors within the pore. [66, 65, 128, 44, 43, 47] The microscopic electric field due to the ionic and aqueous environment will affect the kind of signals and noise these sensors detect. Understanding the electrostatics of ions in water at atomic length scales is thus crucial to our ability to design functional single-molecule sensors in nanopores and interpret their output, and will also give insight into the operation of biological ion channels.

In the context of the ionic current and ionic blockade, several studies have examined the electrostatics of ions in nanopores using a continuum model for the dielectric properties of water. [125, 57, 110, 9] Teber shows that the nanopore electrostatic environment looks essentially one-dimensional due to the large difference of dielectric constant of water and the surrounding pore material. [110] Due to the one-dimensionality, the electrostatic energy penalty is large to move an ion

from outside the pore into the pore. [125, 110] Zhang et *al.* then examined the effect of surface charges on the pore walls and found that even small amounts of surface charge drastically reduced the energy penalty to move an ion into the pore. [125] In light of these previous studies, one is lead to the following question: does a continuum dielectric picture accurately portray the physics of the ion in the nanopore?

In this chapter we examine the microscopic details of an ion in an aqueous environment both in and out of a pore using all-atom molecular dynamics simulations. We calculate the bare electric field due to the ion and water molecules, that is the electric field without any spatial averaging. These calculations show that even in "bulk" water, the bare field is very different than one would expect from a continuum dielectric. However, the bare field is the one of interest due to the short length scales of the nanopore geometry and the large local field gradient of a single ion. We show that as long as the pore allows the first hydration shell to stay intact, e.g., ∼6 nearby water molecules, the electric field of the ion can be well screened. We also discuss the consequences of the formation of hydration layers and the discrete nature of polarization at atomic length scales for the applicability of continuum dielectric models.

We examine two cases in this work: *(1)* we first study a single anion inside a sphere of water and then *(2)* we study a single anion in different size nanopores. Both cases are studied by using molecular dynamics simulations. [1] The simulations allow for the rotation of the water molecules and the deformation of its internal bonds. With these two contributions, molecular dynamics is known to give an adequate representation of the dielectric properties of water for weak, constant external fields. [107] On the other hand, the electronic distributions around the molecules are not allowed to be polarized by the electric field nor is charge transfer allowed to occur. [2] The main contribution to the low frequency dielectric constant

[1] The molecular dynamics simulations are performed with the program NAMD2. [56] The interactions in between the DNA, water, and ions are described with the CHARMM27 force field [40, 84], while UFF parameters [100] are used to describe the interactions between the Si_3N_4 membrane and other atoms. The TIP3 [55] model is used for the water molecules, which is known to reproduce the dielectric properties of bulk water. [107] The details of the molecular dynamics simulations are identical to the ones of Chapter 4 and 5, unless stated otherwise.

[2] We have checked that the latter effect is small by performing DFT calculations on the anion

of water, though, is from the reorientation of the water molecules. [53] Thus, to first approximation we can neglect those two additional effects.

Within the molecular dynamics simulations we freeze a single chlorine ion [3] in the center of the water sphere/nanopore system. Since we have the atomic structure of the whole system, the electric field at any given point can be calculated by integrating over the electron clouds of all species and summing the fields from the nuclei. However, as each water molecule is charge neutral, the dipole contribution will be the dominant contributor to the electric field. To calculate the field a water molecule at any given point in space feels, the total electric then is taken as the sum of the electric fields from the dipole moments of all water molecules in the system plus the electric field from the ion.

6.1 Water Sphere

As the first case to study, we look at a single anion within a sphere of water with a radius of 30 Å. This is large enough such that the system can be taken as a single ion in "bulk" water. Figure 6.1 shows the time averaged[4] total electric field a species would feel from the dipole moment of all other water molecules and the ion (solid black curve). The unscreened electric field from the ion only is also shown(dashed red curve).

In close vicinity of the ion, the total electric field is fairly close in magnitude to that of the electric field of the ion only. As the electric field for an ion decays as a function of one over the square of the distance from the ion, the electric field induced in close vicinity of the ion is extremely strong. This large field is forcing the dipoles to reorient themselves close to perfectly against the field induced by the ion, such that an even larger field to screen would not force any further reorientation of the dipoles. A typical snapshot of the ion and the first layer of water molecules,

with its first hydration layer, $\sim$ 6 nearby water molecules, using a DZVP basis set and GGA functional B88-PW91. These calculation show on average only a $\sim$ 5% change in partial charges on the atoms in the water molecules. This also indicates that the change in polarization is probably of the same order.

[3]The thermal wave length of a chlorine ion at room temperature is is $\sim$ 0.2Å, which allows for the approximation of an immobile ion.

[4]The electric field is time averaged over 1,000 snapshots, each taken 1 ps apart.

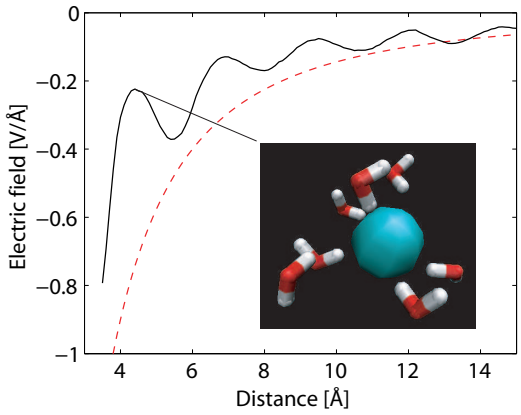


Figure 6.1: Time averaged radial electric field, E_r, a species would feel at a distance, r, from for a single negatively charged chlorine ion inside a large water sphere. The red dashed curve is the unscreened electric field of the ion itself, while the black curve is the total electric field from both the ion and all other water molecules. The electric field is calculated by averaging over 1,000 snapshots, each taken 1 ps apart and by averaging over all water molecules within a spherical shell with an inner, outer radius of $r \pm 0.5$Å. The inset shows a typical snapshot of the ion (cyan sphere) and all water molecules (red and white) within the first local maxima in the total electric field, as indicated by the guide line.

as visualized in the inset of Figure 6.1, clearly shows how a positively charged hydrogen always is oriented towards the negatively charged ion. We see that this causes the water to screen the electric field of the ion with no more than a factor of 1 to 4 at any local point in space, which is much lower than the value found when bulk water is screening a weak field. This is similar to the physics involved when water is screening a high frequency field. Up to a frequency of 10 GHz, the water molecules have time to reorient themselves against the external field, however for an even higher frequency, there is not sufficient time for the water molecules to reorient themselves to counteract the field, and the dielectric constant radically drops [53].

As expected, the total electric field decays as a function of distance from the ion, however the decay is not monotonous. Oscillations with a wave length of ~ 2.5 Å can clearly be seen in the total field. The oscillations are schematically explained in Figure 6.2. The anion is located in the center of the figure. If a surface is drawn around the anion, surface 1 in the figure, the field looks to be the one of the anion only. Further from the ion there is a hydration layer (the region in between the solid lines). If a surface 2 is drawn, the electric field is that from the anion plus a positive charged sphere-like surface. This corresponds to the first minimum in electric field in Figure 6.1. This picture is confirmed by that the density of oxygen atoms shows a maximum at a radius 0.3 Å larger than the radius of the first minimum in the electric field. Even further away from the anion, a surface 3 can be drawn outside the first hydration layer. Then the electric field is that from the anion, the positively charged sphere and the negatively charged sphere. The latter two have identical charge magnitudes, and thus cancel each other by Gauss's law. This surface corresponds to a maximum in electric field. This schematic view is of course not perfect, resulting in the non-perfect cancelations seen at each minimum in Figure 6.1.

At a distance of 4 Å away from the ion, at the first local maxima of the total electric field, we see that the ion is very effectively screened. Within this radius there is only on average 6 water molecules, indicating that the number number of water molecules needed to screen an ion indeed is very low. In a nanopore, one

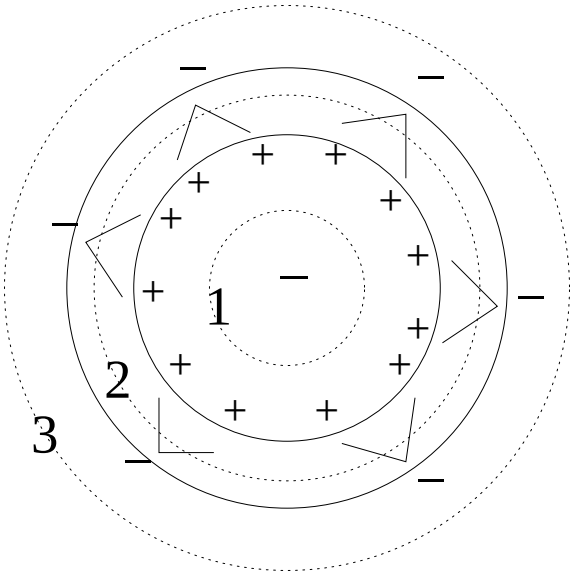


Figure 6.2: Schematic view of oscillations in the electric field, as described in the main text.

would hence expect that as long as the radius of the pore allows for at least 6 water molecules to be in close vicinity of the ion, the ion can be well screened. Clearly, these water molecules must not strongly interact with the surface of the pore, such that they are effected more by the surface than the ion. In the next section we will take a closer look at exactly what this means. First, however, some comments regarding why our results are drastically different from the continuum dielectric picture.

We know that in the continuum picture, water screens a weak external field with a dielectric constant close to 80 [53]. The unusually high value of the dielectric constant is a result of the intrinsic dipole moment of each water molecule reorienting itself against the external electric field. It has however long been known that in the close vicinity of an ion this is not the case; [24, 89] that is, close to the ion, the screening is much weaker than the screening seen for a weak external field. This arises from the fact that all dipoles already are aligned against the electric field induced by the ion. Hence, as the dimensions of the system in question are decreased to the size of a small number of water molecules, one may question the validity of the dielectric picture as treated in a continuum model. Specifically,

due to the variability of the dielectric medium on atomic length scales and the strength of the electric field close to a single ion, the electrostatic environment observed is not one that is averaged over space, but rather one that is averaged over time. Spatially averaging on length scales of about 100 Å is required to obtain the continuum picture. [53]

6.2 Nanopores

With the understanding of the screening of a single ion in bulk water, we now turn our attention towards the case of a single anion located in the center of a cylindrical nanopore. Similarly to before, we have performed molecular dynamics simulations of a single frozen chlorine ion in an aquatic atmosphere; however, now the chlorine ion is confined within a nanopore made out of silicon nitride. In order to avoid interference effects in between the ion and the ends of the pore, a long pore with length 8 nm is chosen. At this length any effect the ion has on water outside the pore is completely screened. In similar fashion as for the water sphere we can now calculate the time averaged[5] total electric field a water molecule would feel, at any point inside the pore, as the sum of the electric field from the ion, water and any field resulting from the membrane (the material the pore is etched out of).

For electrostatic purposes, the dielectric properties of the membrane are treated as bulk-like [6]. At any given time, the electric field from the ion and the water induces dipoles within the membrane, resulting in effective surface charges at the wall of the pore. While this surface charge, in theory, can be calculated for all snapshots, it results in a numerically extremely challenging problem. Instead we treat the problem with a mean field approach by assuming the induced surface charge is a function of the time-averaged electric field only. This is however a self-consistent problem; as a water molecule moves, the surface charge induced by

[5]The electric field is time averaged over 5,000 snapshots, each taken 100 fs apart.

[6]For all pores analyzed in this chapter, multiple hydration layers are present in between the ion and walls of the pore. This causes the electric field of the ion to be well screened at the wall of the pore, which allows for the approximation of bulk-like dielectric properties of the membrane.

this water molecule changes, resulting in a change of the dynamics of the water molecule. To recast the problem into a non-self-consistent problem, we further assume the surface charge is induced by the electric field of bulk water, at the same distance from the ion. Finally, also for numerical reasons, we assume the surface charge is averaged evenly over the surface of the entire pore surface[7].

Figure 6.3 shows the electric field in the radial direction as a function of distance from the origin, at $z = 0$. Standard cylindrical coordinates are used, where the ion and center of pore both are located at the origin. The dashed lines correspond to pore radiuses varying from 8 to 15 Å, as indicated in the figure caption. The total electric field of an ion in bulk water (from Figure 6.1) is overlayed as a black thick line for comparison. We can see that for large pores, the electric field in close vicinity of the ion is very similar to that of bulk water. Close to the edge we however see that interactions between the water and wall clearly affect the electric field. For all but the narrowest pore, a clear local maximum in the electric field at around 4 Å exists, indicating that the majority of the edge effects are screened in the center of the pore. Thus, for all but the narrowest pore, the first hydration layer around the ion is screening the electric field of the ion only. Figure 6.3 similarly shows the z component of the electric field at the center of the pore, as a function of distance from the ion. Again we see similar behavior of the electric field of an ion in bulk water and the electric field of an ion in all but the narrowest pores.

These two figures combined show us that despite the long and narrow shape of the pore, the pore can not be treated as a one dimensional system. The first hydration layer alone effectively screens the ionic charge such that the system has to be treated as a full three-dimensional system. Thus, as long as the pore is wide enough to allow for just one layer of water molecules to surround the ion, the one dimensional approximation (as used in [125] and [126], for example) is not valid.

[7]We have tested these assumptions by repeating the calculations for an 8 Å radius pore, assuming both no surface charge and by assuming that the uniform charge is equal to the maximum surface charge occurring at $z = 0$. The first case corresponds to an underestimation of the induced charge, while the second case is an overestimation of the charge. For both cases the total electric field changes by no more than 6% at any point in space. A vast majority of space, however, shows a much smaller change in electric field.

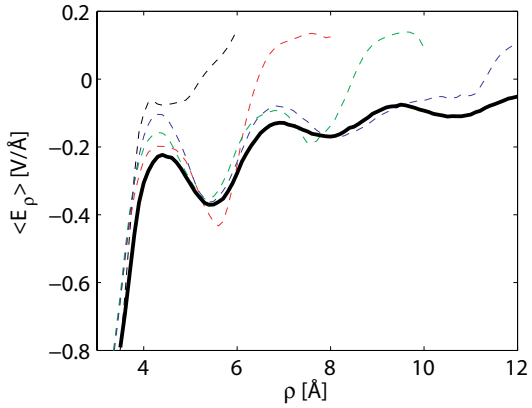


Figure 6.3: Total electric field in the radial direction,E_ρ, as a function of distance, ρ, from a negatively charged chlorine ion, in the plane perpendicular to the pore. The dashed black/red/green/blue line shows the electric field for an ion in a nanopore with a radius of 8/10/12/15 Å, while the thick black line is the total electric field of an ion in bulk water, as shown in Figure 6.1. The electric field is calculated by averaging over 5,000 snapshots, each taken 100 fs apart and by averaging over all water molecules within a window shaped as a cylindrical shell, centered around the ion, with an inner(outer) radius 0.5 Å smaller(larger) than ρ and with $|z| < 2$Å. Standard cylindrical coordinates are used, where the ion and center of the pore both are located at the origin.

We would however like to stress that the biological pores used in these papers are narrower than ours, such that there may not be sufficient space for a hydration layer around the ion. We conclude that a continuum dielectric picture does not accurately portray the physics of the ion in the nanopore.

6.3 Conclusions and Future Work

In this chapter we have highlighted the importance of utilizing all atom models in nanoscale systems. Despite that, at first sight, a solid state nanopore may appear to be a one dimensional structure, we have here shown that this is not the case; a full three dimensional treatment is necessary. We have found that as long as the pore allows for the first hydration layer, ∼6 water molecules, to surround the ion, the electric field of the ion is well screened.

Finally, due to the oscillations seen in the electric field, there may be an os-

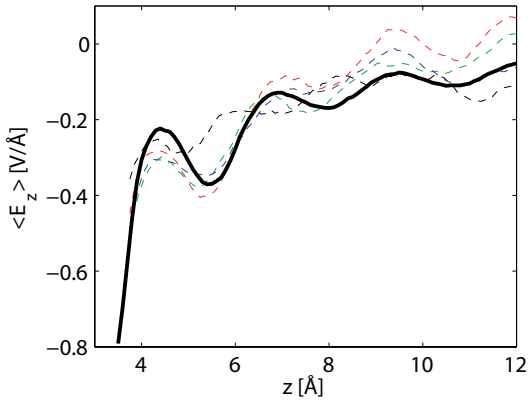


Figure 6.4: Total electric field in the z-direction,E_z, as a function of distance, z, from a negatively charged chlorine, in the center of the pore. The dashed black/red/green/blue line shows the electric field for an ion in a nanopore with a radius of 8/10/12/15 Å, while the thick black line is the total electric field of an ion in bulk water, as shown in Figure 6.1. The electric field is calculated by averaging over 5,000 snapshots, each taken 100 fs apart and by averaging over all water molecules within a cylindrical window located at the center of the pore with a radius of 2 Å, starting and ending at $z - 0.75$Å and $z + 0.75$Å, respectively. Standard cylindrical coordinates are used, where the ion and center of the pore both are located at the origin.

cillation of the energy penalty, as function of pore radius, for moving an ion into the pore. Thus, the ionic current may display oscillations as the pore radius is increased. Future work consists of estimating this energy penalty and confirming the existence of oscillations in the ionic current.

The text of this chapter is in part a reprint of the material as will appear in Johan Lagerqvist, Michael Zwolak and Massimiliano Di Ventra *Ion Electronics in Nanopores*, in preparation (2006). The dissertation author is the primary investigator of this paper.

Bibliography

[1] M. Akeson, D. Branton, J. J. Kasianowicz, E. Brandin, and D. W. Deamer. Microsecond time-scale discrimination among polycytidylic acid, polyadenylic acid, and polyuridylic acid as homopolymers or as segments within single rna molecules. *Biophys. J.*, 77:3227–3233, 1999.

[2] A. Aksimentiev, J. B. Heng, G. Timp, and K. Schulten. Microscopic kinetics of dna translocation through synthetic nanopores. *Biophys. J.*, 87(3):2086–2097, 2004.

[3] D. Arovas. Solid state physics - lecture notes, chapter 2. *Available at http://physics.ucsd.edu/students/courses/winter2004/physics211b/*, 2004.

[4] N. W. Ashcroft and N. D. Mermin. *Solid State Physics*. Harcourt, 1976.

[5] G. B. Bachelet, D. R. Hamann, and M. Schluter. Pseudopotentials that work - from h to pu. *Phys. Rev. B*, 26(8):4199–4228, 1982.

[6] A. L. Biance, J. Gierak, E. Bourhis, A. Madouri, X. Lafosse, G. Patriarche, G. Oukhaled, C. Ulysse, J. C. Galas, Y. Chen, and L. Auvray. Focused ion beam sculpted membranes for nanoscience tooling. *Microelectron. Eng.*, 83(4-9):1474–1477, 2006.

[7] Y. M. Blanter and M. Bttiker. Transition from sub-poissonian to super-poissonian shot noise in resonant quantum wells. *Phys. Rev. B*, 59(15):10217, 1999. Copyright (C) 2006 The American Physical Society Please report any problems to prola@aps.org PRB.

[8] Y. M. Blanter and M. Buttiker. Shot noise in mesoscopic conductors. *Physics Reports-Review Section of Physics Letters*, 336(1-2):2–166, 2000.

[9] D. J. Bonthuis, J. Zhang, B. Hornblower, J. Mathé, B. I. Shklovskii, and A. Meller. Self-energy limited ion transport in sub-nanometer channels. *cond-mat/0604148*, 2006.

[10] I. Braslavsky, B. Hebert, E. Kartalov, and S. R. Quake. Sequence information can be obtained from single dna molecules. *Proc. Natl. Acad. Sci. U. S. A.*, 100(7):3960–3964, 2003.

[11] O. M. Bulashenko and J. M. Rubi. Shot noise as a tool to probe an electron energy distribution. *Physica E-Low-Dimensional Systems & Nanostructures*, 12(1-4):857–860, 2002.

[12] N. Bushong and M. Di Ventra. Current-induced effects in nanoscale conductors. In G. C. Richter, G. Fagas, and Klaus, editors, *Introducing Molecular Electronics*. Springer Verlag, Berlin, 2005.

[13] N. Bushong, N. Sai, and M. Di Ventra. Approach to steady-state transport in nanoscale conductors. *Nano Lett.*, 5(12):2569–2572, 2005.

[14] M. Buttiker, Y. Imry, R. Landauer, and S. Pinhas. Generalized many-channel conductance formula with application to small rings. *Phys. Rev. B*, 31(10):6207–6215, 1985.

[15] E. Y. Chan. Advances in sequencing technology. *Mutat. Res.*, 573:13–40, 2005.

[16] J. Chen, M. A. Reed, A. M. Rawlett, and J. M. Tour. Large on-off ratios and negative differential resistance in a molecular electronic device. *Science*, 286(5444):1550–1552, 1999.

[17] P. Chen, J. Gu, E. Brandin, Y.-R. Kim, Q. Wang, and D. Branton. Probing single dna molecule transport using fabricated nanopores. *Nano Lett.*, 4(11):2293–2298, 2004.

[18] Y. C. Chen and M. Di Ventra. Shot noise in nanoscale conductors from first principles. *Phys. Rev. B*, 67(15), 2003. 153304.

[19] Y. C. Chen and M. Di Ventra. Effect of electron-phonon scattering on shot noise in nanoscale junctions. *Phys. Rev. Lett.*, 95(16), 2005. 166802.

[20] Y. C. Chen, M. Zwolak, and M. Di Ventra. Local heating in nanoscale conductors. *Nano Lett.*, 3(12):1691–1694, 2003.

[21] Y. C. Chen, M. Zwolak, and M. Di Ventra. Inelastic current-voltage characteristics of atomic and molecular junctions. *Nano Lett.*, 4(9):1709–1712, 2004.

[22] Y. C. Chen, M. Zwolak, and M. Di Ventra. Inelastic effects on the transport properties of alkanethiols. *Nano Lett.*, 5(4):621–624, 2005.

[23] F. S. Collins, E. D. Green, A. E. Guttmacher, and M. S. Guyer. A vision for the future of genomics research. *Nature*, 422(6934):835–847, 2003.

[24] B. E. Conway, J. O. Bockris, and A. I. A. The dielectrif constant of the solution in the diffuse and helmholtz double layers at a charged interface in aqueous solution. *Transaction of the Faraday Society*, 47:756–766, 1951.

[25] X. D. Cui, A. Primak, X. Zarate, J. Tomfohr, O. F. Sankey, A. L. Moore, T. A. Moore, D. Gust, G. Harris, and S. M. Lindsay. Reproducible measurement of single-molecule conductivity. *Science*, 294(5542):571–574, 2001.

[26] S. Datta. *Electronic Transport in Mesoscopic Systems*. Cambridge University Press, 1995.

[27] S. Datta, W. D. Tian, S. H. Hong, R. Reifenberger, J. I. Henderson, and C. P. Kubiak. Current-voltage characteristics of self-assembled monolayers by scanning tunneling microscopy. *Phys. Rev. Lett.*, 79(13):2530–2533, 1997.

[28] D. W. Deamer and M. Akeson. Nanopores and nucleic acids: prospects for ultrarapid sequencing. *Trends Biotechnol.*, 18:147–151, 2000.

[29] D. W. Deamer and D. Branton. Characterization of nucleic acids by nanopore analysis. *Acc. Chem. Res.*, 35:817–825, 2002.

[30] M. Di Ventra, Y. C. Chen, and T. N. Todorov. Are current-induced forces conservative? *Phys. Rev. Lett.*, 92(17), 2004. 176803.

[31] M. Di Ventra and N. D. Lang. Transport in nanoscale conductors from first principles. *Phys. Rev. B*, 65(4), 2002. 045402.

[32] M. Di Ventra, N. D. Lang, and S. T. Pantelides. Electronic transport in single molecules. *Chem. Phys.*, 281(2-3):189–198, 2002. Sp. Iss. SI.

[33] M. Di Ventra, S. T. Pantelides, and N. D. Lang. First-principles calculation of transport properties of a molecular device. *Phys. Rev. Lett.*, 84(5):979–982, 2000.

[34] M. Di Ventra and T. N. Todorov. Transport in nanoscale systems: the microcanonical versus grand-canonical picture. *Journal of Physics-Condensed Matter*, 16(45):8025–8034, 2004.

[35] M. Di Ventra and M. Zwolak. Dna electronics. In S.-N. H., editor, *Encyclopedia of Nanoscience and Nanotechnology*, volume 2, page 475. American Scientific Publishers, 2004.

[36] Z. J. Donhauser, B. A. Mantooth, K. F. Kelly, L. A. Bumm, J. D. Monnell, J. J. Stapleton, D. W. Price, A. M. Rawlett, D. L. Allara, J. M. Tour, and P. S. Weiss. Conductance switching in single molecules through conformational changes. *Science*, 292(5525):2303–2307, 2001.

[37] E. G. Emberly and G. Kirczenow. Comment on "first-principles calculation of transport properties of a molecular device". *Phys. Rev. Lett.*, 87(26), 2001. 269701.

[38] D. Fologea, M. Gershow, B. Ledden, D. S. McNabb, J. A. Golovchenko, and J. Li. Detecting single stranded dna with a solid state nanopore. *Nano Lett.*, 5(10):1905–1909, 2005.

[39] D. Fologea, J. Uplinger, B. Thomas, D. S. McNabb, and J. Li. Slowing dna translocation in a solid-state nanopore. *Nano Lett.*, 5(9):1734–1737, 2005.

[40] N. Foloppe and A. D. MacKerell. All-atom empirical force field for nucleic acids: I. parameter optimization based on small molecule and condensed phase macromolecular target data. *J. Comput. Chem.*, 21(2):86–104, 2000.

[41] M. Gattobigio, G. Iannaccone, and M. Macucci. Enhancement and suppression of shot noise in capacitively coupled metallic double dots. *Phys. Rev. B*, 65(11), 2002. 115337.

[42] J. K. Gimzewski and C. Joachim. Nanoscale science of single molecules using local probes. *Science*, 283(5408):1683–1688, 1999.

[43] M. E. Gracheva, A. Aksimentiev, and J.-P. Leburton. Electrical signatures of single-stranded dna with single base mutations in a nanopore capacitor. *Nanotechnology*, 17:3160–3165, 2006.

[44] M. E. Gracheva, A. Xiong, A. Aksimentiev, K. Schulten, G. Timp, and J.-P. Leburton. Simulation of the electric response of dna translocation through a semiconductor nanoporecapacitor. *Nanotechnology*, 17(3):622–633, 2006.

[45] R. Grun. Crystal-structure of beta-si3n4 - structural and stability considerations between alpha-si3n4 and beta-si3n4. *Acta Crystallographica Section B-Structural Science*, 35(APR):800–804, 1979.

[46] C. C. Harrell, S. B. Lee, and C. R. Martin. Synthetic single-nanopore and nanotube membranes. *Anal. Chem.*, 75(24):6861–6867, 2003.

[47] J. B. Heng, A. Aksimentiev, C. Ho, V. Dimitrov, T. W. Sorsch, J. F. Miner, W. M. Mansfield, K. Schulten, and G. Timp. Beyond the gene chip. *Bell Labs Tech. J.*, 10(3):5–22, 2005.

[48] J. B. Heng, A. Aksimentiev, C. Ho, P. Marks, Y. V. Grinkova, S. Sligar, K. Schulten, and G. Timp. The electromechanics of dna in a synthetic nanopore. *Biophys. J.*, 90(3):1098–1106, 2006.

[49] P. Hohenberg and W. Kohn. Inhomogeneous electron gas. *Physical Review*, 136(3B):B864, 1964. Copyright (C) 2006 The American Physical Society Please report any problems to prola@aps.org PR.

[50] G. Iannaccone, M. Macucci, and B. Pellegrini. Theory of conductance and noise additivity in parallel mesoscopic conductors. *Phys. Rev. B*, 56(19):12104–12107, 1997.

[51] Y. Imry. *Introduction to Mesoscopic Physics*. Oxford University Press, 1997.

[52] Y. Imry and R. Landauer. Conductance viewed as transmission. *Reviews of Modern Physics*, 71(2):S306–S312, 1999. Sp. Iss. SI.

[53] J. D. Jackson. *Classical Electrodynamics*. Wiley, 3rd edition, 1998.

[54] Q. Ji, Y. Chen, L. L. Ji, X. M. Jiang, and K. N. Leung. Ion beam imprinting system for nanofabrication. *Microelectron. Eng.*, 83(4-9):796–799, 2006.

[55] W. L. Jorgensen. Quantum and statistical mechanical studies of liquids .19. pressure-dependence of the structure and properties of liquid normal-butane. *J. Am. Chem. Soc.*, 103(16):4721–4726, 1981.

[56] L. Kale, R. Skeel, M. Bhandarkar, R. Brunner, A. Gursoy, N. Krawetz, J. Phillips, A. Shinozaki, K. Varadarajan, and K. Schulten. Namd2: Greater scalability for parallel molecular dynamics. *J. Comput. Phys.*, 151(1):283–312, 1999.

[57] A. Kamenev, J. Zhang, A. Larkin, and B. Shklovskii. Transport in one-dimensional coulombgases: From ion channels to nanopores. *Physica A (Amsterdam)*, 359:129–161, 2006.

[58] J. J. Kasianowicz, E. Brandin, D. Branton, and D. W. Deamer. Characterization of individual polynucleotide molecules using a membrane channel. *Proc. Natl. Acad. Sci. U. S. A.*, 93:13770–13773, 1996.

[59] G. Kiesslich, A. Wacker, and E. Scholl. Shot noise of coupled semiconductor quantum dots. *Phys. Rev. B*, 68(12), 2003. 125320.

[60] C. Kittel. *Introduction to Solid State Physics, 7th edition*. Wiley, 1996.

[61] W. Kohn and L. J. Sham. Self-consistent equations including exchange and correlation effects. *Physical Review*, 140(4A):A1133, 1965. Copyright (C) 2006 The American Physical Society Please report any problems to prola@aps.org PR.

[62] R. Kubo, M. Toda, and N. Hashitsume. *Statistical Physics II. Nonequilibrium Statistical Mechanics*. Springer-Verlag, Berlin, 1985.

[63] J. G. Kushmerick, D. B. Holt, S. K. Pollack, M. A. Ratner, J. C. Yang, T. L. Schull, J. Naciri, M. H. Moore, and R. Shashidhar. Effect of bond-length alternation in molecular wires. *J. Am. Chem. Soc.*, 124(36):10654–10655, 2002.

[64] J. Lagerqvist, Y. C. Chen, and M. Di Ventra. Shot noise in parallel wires. *Nanotechnology*, 15(7):S459–S464, 2004.

[65] J. Lagerqvist, M. Zwolak, and M. Di Ventra. *In preparation*, 2006.

[66] J. Lagerqvist, M. Zwolak, and M. Di Ventra. Fast dna sequencing via transverse electronic transport. *Nano Lett.*, 6(4):779–782, 2006.

[67] R. Landauer. Spatial variation of currents and fields due to localized scatterers in metallic conduction. *Ibm Journal of Research and Development*, 1(3):223–231, 1957.

[68] R. Landauer. Electrical resistance of disordered one-dimensional lattices. *Philos. Mag.*, 21(172):863–867, 1970.

[69] R. Landauer. Residual resistivity dipoles. *Zeitschrift Fur Physik B-Condensed Matter*, 21(3):247–254, 1975.

[70] R. Landauer. Spatial variation of currents and fields due to localized scatterers in metallic conduction. *Ibm Journal of Research and Development*, 32(3):306–316, 1988.

[71] R. Landauer. Conductance from transmission - common-sense points. *Phys. Scr.*, T42:110–114, 1992.

[72] R. Landauer. Condensed-matter physics - the noise is the signal. *Nature*, 392(6677):658–659, 1998.

[73] E. S. Lander et al. Initial sequencing and analysis of the human genome. *Nature (London, U. K.)*, 409:860921, 2001.

[74] N. D. Lang. Resistance of atomic wires. *Phys. Rev. B*, 52(7):5335–5342, 1995.

[75] N. D. Lang and P. Avouris. Electrical conductance of parallel atomic wires. *Phys. Rev. B*, 62(11):7325–7329, 2000.

[76] N. D. Lang and M. Di Ventra. Comment on "first-principles treatments of electron transport properties for nanoscale junctions". *Phys. Rev. B*, 68(15), 2003. 157301.

[77] N. D. Lang and A. R. Williams. Theory of atomic chemisorption on simple metals. *Phys. Rev. B*, 18(2):616–636, 1978.

[78] S. G. Lemay, D. M. van den Broek, A. J. Storm, D. Krapf, R. M. M. Smeets, H. A. Heering, and C. Dekker. Lithographically fabricated nanopore-based electrodes for electrochemistry. *Anal. Chem.*, 77(6):1911–1915, 2005.

[79] J. Li, M. Gershow, D. Stein, E. Brandin, and J. A. Golovchenko. Dna molecules and configurations in a solid-state nanopore microscope. *Nat. Mater.*, 2:611–615, 2003.

[80] J. Li, D. Stein, C. McMullan, D. Branton, M. J. Aziz, and J. A. Golovchenko. Ion-beam sculpting at nanometre length scales. *Nature (London, U. K.)*, 412:166–169, 2001.

[81] N. C. Li, S. F. Yu, C. C. Harrell, and C. R. Martin. Conical nanopore membranes. preparation and transport properties. *Anal. Chem.*, 76(7):2025–2030, 2004.

[82] J. P. Lin, I. A. Balabin, and D. N. Beratan. The nature of aqueous tunneling pathways between electron-transfer proteins. *Science*, 310(5752):1311–1313, 2005.

[83] R. C. Liu, B. Odom, Y. Yamamoto, and S. Tarucha. Quantum interference in electron collision. *Nature*, 391(6664):263–265, 1998.

[84] A. D. MacKerell and N. K. Banavali. All-atom empirical force field for nucleic acids: Ii. application to molecular dynamics simulations of dna and rna in solution. *J. Comput. Chem.*, 21(2):105–120, 2000.

[85] M. Magoga and C. Joachim. Conductance of molecular wires connected or bonded in parallel. *Phys. Rev. B*, 59(24):16011–16021, 1999.

[86] J. T. Mannion, C. H. Reccius, J. D. Cross, and H. G. Craighead. Conformational analysis of single dna molecules undergoing entropically induced motion in nanochannels. *Biophys. J.*, 90(12):4538–4545, 2006.

[87] M. Margulies, M. Egholm, W. E. Altman, S. Attiya, J. S. Bader, L. A. Bemben, J. Berka, M. S. Braverman, Y. J. Chen, Z. T. Chen, S. B. Dewell, L. Du, J. M. Fierro, X. V. Gomes, B. C. Godwin, W. He, S. Helgesen, C. H. Ho, G. P. Irzyk, S. C. Jando, M. L. I. Alenquer, T. P. Jarvie, K. B. Jirage, J. B. Kim, J. R. Knight, J. R. Lanza, J. H. Leamon, S. M. Lefkowitz, M. Lei, J. Li, K. L. Lohman, H. Lu, V. B. Makhijani, K. E. McDade, M. P. McKenna, E. W. Myers, E. Nickerson, J. R. Nobile, R. Plant, B. P. Puc, M. T. Ronan, G. T. Roth, G. J. Sarkis, J. F. Simons, J. W. Simpson, M. Srinivasan, K. R. Tartaro, A. Tomasz, K. A. Vogt, G. A. Volkmer, S. H. Wang, Y. Wang, M. P. Weiner, P. G. Yu, R. F. Begley, and J. M. Rothberg. Genome sequencing in microfabricated high-density picolitre reactors. *Nature*, 437(7057):376–380, 2005.

[88] J. Mathe, H. Visram, V. Viasnoff, Y. Rabin, and A. Meller. Nanopore unzipping of individual dna hairpin molecules. *Biophys. J.*, 87(5):3205–3212, 2004.

[89] E. L. Mehler and G. Eichele. Electrostatic effects in water-accessible regions of proteins. *Biochemistry*, 23(17):3887–3891, 1984.

[90] A. Meller and D. Branton. Single molecule measurements of dna transport through a nanopore. *Electrophoresis*, 23(16):2583–2591, 2002.

[91] A. Meller, L. Nivon, E. Brandin, J. Golovchenko, and D. Branton. Rapid nanopore discrimination between single polynucleotide molecules. *Proc. Natl. Acad. Sci. U. S. A.*, 97(3):1079–1084, 2000.

[92] A. Meller, L. Nivon, and D. Branton. Voltage-driven dna translocations through a nanopore. *Phys. Rev. Lett.*, 86:34353438, 2001.

[93] R. M. Metzger, B. Chen, U. Hopfner, M. V. Lakshmikantham, D. Vuillaume, T. Kawai, X. L. Wu, H. Tachibana, T. V. Hughes, H. Sakurai, J. W. Baldwin, C. Hosch, M. P. Cava, L. Brehmer, and G. J. Ashwell. Unimolecular electrical rectification in hexadecylquinolinium tricyanoquinodimethanide. *J. Am. Chem. Soc.*, 119(43):10455–10466, 1997.

[94] A. Montanari, R. Rosso, and M. S. Taqqu. A seasonal fractionally differenced arima model: an application to the nile river monthly flows at aswan. *Water Resour. Res.*, 36:1249–1259, 2000.

[95] J. J. Nakane, M. Akeson, and A. Marziali. Nanopore sensors for nucleic acid analysis. *J. Phys.: Condens. Matter*, 15:R1365R1393, 2003.

[96] A. Nitzan and M. A. Ratner. Electron transport in molecular wire junctions. *Science*, 300(5624):1384–1389, 2003.

[97] G. S. Ohm. Die galvanische kette, mathematisch bearbeitet, 1827.

[98] R. K. Pathria. *Statistical Mechanics, 2nd ed.* Butterworth-Heinemann, Oxford, MA, 1996.

[99] Y. Rabin and M. Tanaka. Dna in nanopores: Counterion condensation and coion depletion. *Phys. Rev. Lett.*, 94(14), 2005. 148103.

[100] A. K. Rappe, C. J. Casewit, K. S. Colwell, W. A. Goddard, and W. M. Skiff. Uff, a full periodic-table force-field for molecular mechanics and molecular-dynamics simulations. *J. Am. Chem. Soc.*, 114(25):10024–10035, 1992.

[101] M. A. Reed, J. Chen, A. M. Rawlett, D. W. Price, and J. M. Tour. Molecular random access memory cell. *Appl. Phys. Lett.*, 78(23):3735–3737, 2001.

[102] M. A. Reed, C. Zhou, C. J. Muller, T. P. Burgin, and J. M. Tour. Conductance of a molecular junction. *Science*, 278(5336):252–254, 1997.

[103] N. Sai, M. Zwolak, G. Vignale, and M. Di Ventra. Dynamical corrections to the dft-lda electron conductance in nanoscale systems. *Phys. Rev. Lett.*, 94(18), 2005. 186810.

[104] A. F. Sauer-Budge, J. A. Nyamwanda, D. K. Lubensky, and D. Branton. Unzipping kinetics of double-stranded dna in a nanopore. *Phys. Rev. Lett.*, 90(23), 2003. 238101.

[105] W. Schottky. ber spontane stromschwankungen in verschiedenen elektrizittsleitern. *Annalen der Physik*, 362:541–567, 1918.

[106] J. Shendure, R. D. Mitra, C. Varma, and G. M. Church. Advanced sequencing technologies: Methods and goals. *Nat. Rev. Genet.*, 5(5):335–344, 2004.

[107] T. Simonson. Accurate calculation of the dielectric constant of water from simulations of a microscopic droplet in vacuum. *Chem. Phys. Lett.*, 250:450–454, 1996.

[108] A. J. Storm, J. H. Chen, X. S. Ling, H. Zandbergen, and C. Dekker. Fabrication of solid-state nanopores with single-nanometre precision. *Nat. Mater.*, 2(8):537540, 2003.

[109] N. J. Tao, J. A. DeRose, and S. M. Lindsay. Self-assembly of molecular superstructures studied by in situ scanning tunneling microscopy: Dna bases on gold (111). *J. Phys. Chem.*, 97(4):910–919, 1993.

[110] S. Teber. Translocation energy of ions in nano-channels of cell membranes. *Journal of Statistical Mechanics - Theory and Experiment*, page P07001, 2005.

[111] W. D. Tian, S. Datta, S. H. Hong, R. Reifenberger, J. I. Henderson, and C. P. Kubiak. Conductance spectra of molecular wires. *J. Chem. Phys.*, 109(7):2874–2882, 1998.

[112] H. E. van den Brom. *Noise properties of atomic-size contacts*. PhD thesis, Leiden University, 2000.

[113] H. E. van den Brom and J. M. van Ruitenbeek. Quantum suppression of shot noise in atom-size metallic contacts. *Phys. Rev. Lett.*, 82(7):1526–1529, 1999.

[114] H. van Houten and C. Beenakker. Quantum point contacts. *Physics Today*, 49(7):22–27, 1996.

[115] B. J. van Wees, H. van Houten, C. W. J. Beenakker, J. G. Williamson, L. P. Kouwenhoven, D. Vandermarel, and C. T. Foxon. Quantized conductance of point contacts in a two-dimensional electron-gas. *Phys. Rev. Lett.*, 60(9):848–850, 1988.

[116] J. C. Venter et al. The sequence of the human genome. *Science (Washington, DC, U. S.)*, 291:13041351, 2001.

[117] W. Vercoutere, S. Winters-Hilt, H. Olsen, D. Deamer, D. Haussler, and M. Akeson. Rapid discrimination among individual dna hairpin molecules at single-nucleotide resolution using an ion channel. *Nat. Biotechnol.*, 19:248–252, 2001.

[118] D. J. Wold and C. D. Frisbie. Fabrication and characterization of metal-molecule-metal junctions by conducting probe atomic force microscopy. *J. Am. Chem. Soc.*, 123(23):5549–5556, 2001.

[119] B. Q. Xu and N. J. J. Tao. Measurement of single-molecule resistance by repeated formation of molecular junctions. *Science*, 301(5637):1221–1223, 2003.

[120] S. N. Yaliraki and M. A. Ratner. Molecule-interface coupling effects on electronic transport in molecular wires. *J. Chem. Phys.*, 109(12):5036–5043, 1998.

[121] Z. Yang, M. Chshiev, M. Zwolak, Y. C. Chen, and M. Di Ventra. Role of heating and current-induced forces in the stability of atomic wires. *Phys. Rev. B*, 71(4), 2005. 041402.

[122] Z. Q. Yang and M. Di Ventra. Nonlinear current-induced forces in si atomic wires. *Phys. Rev. B*, 67(16), 2003. 161311.

[123] Z. Q. Yang, A. Tackett, and M. Di Ventra. Variational and nonvariational principles in quantum transport calculations. *Phys. Rev. B*, 66(4), 2002. 041405.

[124] A. I. Yanson, G. R. Bollinger, H. E. van den Brom, N. Agrait, and J. M. van Ruitenbeek. Formation and manipulation of a metallic wire of single gold atoms. *Nature*, 395(6704):783–785, 1998.

[125] J. Zhang, A. Kamenev, and B. I. Shklovskii. Conductance of ion channels and nanopores with charged walls: A toy model. *Phys. Rev. Lett.*, 95:148101, 2005.

[126] X.-G. Zhang, P. S. Krstić, R. Zikic, J. C. Wells, and M. Fuentes-Cabrera. Deconstructing the dna nucleotide conductance. *In reviewing process*, 2006.

[127] C. Zhou, M. R. Deshpande, M. A. Reed, L. Jones, and J. M. Tour. Nanoscale metal self-assembled monolayer metal heterostructures. *Appl. Phys. Lett.*, 71(5):611–613, 1997.

[128] M. Zwolak and M. Di Ventra. Electronic signature of dna nucleotides via transverse transport. *Nano Lett.*, 5:421–424, 2005.